

UC Berkeley

UC Berkeley Electronic Theses and Dissertations

Title

A physiological and genomic investigation of dissimilatory phosphite oxidation in *Desulfotignum phosphitoxidans* strain FiPS-3 and in microbial enrichment cultures from wastewater treatment sludge

Permalink

<https://escholarship.org/uc/item/4w8938g4>

Author

Figueroa, Israel Antonio

Publication Date

2016

Peer reviewed|Thesis/dissertation

A physiological and genomic investigation of dissimilatory phosphite oxidation in
Desulfotignum phosphitoxidans strain FiPS-3 and in microbial enrichment cultures from
wastewater treatment sludge

By

Israel Antonio Figueroa

A dissertation submitted in partial satisfaction of the

requirements for the degree of

Doctor of Philosophy

in

Microbiology

in the

Graduate Division

of the

University of California, Berkeley

Committee in charge:

Professor John D. Coates, Chair

Professor Arash Komeili

Professor David F. Savage

Fall 2016

Abstract

A physiological and genomic investigation of dissimilatory phosphite oxidation in *Desulfotignum phosphitoxidans* strain FiPS-3 and in microbial enrichment cultures from wastewater treatment sludge

by

Israel Antonio Figueroa

Doctor of Philosophy in Microbiology

University of California, Berkeley

Professor John D. Coates, Chair

Phosphite (HPO_3^{2-}) is a highly soluble, reduced phosphorus compound that is often overlooked in biogeochemical analyses. Although the oxidation of phosphite to phosphate is a highly exergonic process ($E^{\circ} = -650 \text{ mV}$), phosphite is kinetically stable and can account for 10-30% of the total dissolved P in various environments. Its role as a phosphorus source for a variety of extant microorganisms has been known since the 1950s and the pathways involved in assimilatory phosphite oxidation (APO) have been well characterized. More recently it was demonstrated that phosphite could also act as an electron donor for energy metabolism in a process known as dissimilatory phosphite oxidation (DPO). The bacterium described in this study, *Desulfotignum phosphitoxidans* strain FiPS-3, was isolated from brackish sediments and is capable of growing by coupling phosphite oxidation to the reduction of either sulfate or carbon dioxide. FiPS-3 remains the only isolated organism capable of DPO and the prevalence of this metabolism in the environment is still unclear. This study, therefore, sought to investigate the genetic and physiological factors associated with DPO in FiPS-3 as well as to expand our understanding of this metabolism by enriching for novel environmental microorganisms capable of DPO.

The first chapter of this dissertation is a published review paper (Figueroa & Coates 2016) that examines the current state of knowledge regarding the geochemistry of phosphite and the biology of phosphite oxidation. The chapter presents evidence suggesting that phosphite may have been involved in the development of early life and that it may be more prevalent on modern Earth than previously thought. Potential natural and anthropogenic sources of phosphite in the environment are discussed and the genetic and physiological properties thought to distinguish DPO from APO are explored.

The second chapter of this dissertation (unpublished work) deals with my work using pure cultures of FiPS-3 to investigate DPO metabolism. Genomic analysis of FiPS-3 combined with physiological experiments led to improved growth of this strain and revealed its ability to grow aerobically. RNAseq analysis confirmed the importance of the *ptx-ptd* gene cluster under DPO conditions and suggested that the *ptx* and *ptd* portions of the cluster may constitute separate

modules that are differentially regulated. Additionally, DPO-dependent biomineralization in FiPS-3 cultures was examined.

The third chapter of this dissertation (unpublished work) documents my efforts to enrich for novel organisms capable of DPO from anaerobic wastewater treatment sludge. Enrichments with phosphite as the sole electron donor and carbon dioxide as the sole electron acceptor showed a decrease in phosphite with a concomitant increase in phosphate, which was not seen in killed controls. Phosphite oxidation was coupled to cellular growth and was enhanced by rumen fluid addition, while molybdate and sulfite were inhibitory. Community analysis revealed significant changes in the microbial population due to the presence of phosphite and identified a single bacterial operational taxonomic unit (OTU) whose abundance strongly correlated with phosphite oxidation. Phylogenetic analysis indicated that this OTU (designated Phox-21) belonged to a candidate order within the *Deltaprotobacteria* with no known cultured isolates.

The fourth chapter of this dissertation (unpublished work) is a metagenomic analysis of the enrichment communities described in Chapter 3, focusing on the putative DPO-capable bacterium Phox-21. This analysis revealed the presence of a *ptx-ptd* cluster in Phox-21, similar to the one found in FiPS-3, which further supports the hypothesis that this organism is capable of DPO. The investigation also uncovered that Phox-21 has an incomplete Wood-Ljungdahl Pathway, which suggests it is capable of reducing carbon dioxide to formate as part of its energy metabolism but not of assimilating carbon dioxide into biomass. Furthermore, the metagenomic dataset provided insights on the metabolic capabilities of other community members, thus offering a wider ecological context for the role of DPO in this system.

The fifth chapter of this dissertation summarizes the conclusions of this study and discusses the implications of this research for future investigations regarding the biology and geochemistry of DPO and other forms of reduced phosphorus metabolism.

ACKNOWLEDGEMENTS

I would like to thank my Ph.D. advisor, John D. Coates, for his intellectual guidance and financial support, as well as my senior colleagues, Anna Engelbrektson and Hans Carlson, for their mentorship and logistical support throughout my doctoral research. I am also grateful to my undergraduate research assistants, Pranav Somasekhar, Carmence Ho, and Annette Liao, for their help throughout the years with making media, growing and sampling cultures, analyzing samples, prepping experiments, extracting DNA, and countless other tasks essential to the completion of this research. Additionally, I extend my sincerest gratitude to all the people who contributed to this body of work: Iain Clark and Ryan Melnyk for their help with RNAseq data analysis, Shirley Zhu and Adam Williamson for their work on DPO-dependent biomineralization, Martin Musabyimana of the East Bay Municipal Utilities District for providing the wastewater sludge samples used in this study, Kenny Mok of the Taga Laboratory at UC Berkeley for providing the rumen fluid samples used in this study, Charlotte Carlström and Robert Rhode for their help with microbial community analysis, Tyler Barnum for his involvement in the development of a metagenomics analysis pipeline, and Ke Bi of the Computational Genomics Resource Laboratory for his aid in troubleshooting computational issues.

I would also like to thank the National Science Foundation's Graduate Research Fellowship Program, the UC Berkeley Chancellor's Fellowship, and the Energy Biosciences Institute for their financial support. Last, but not least, I am grateful to everyone in the Plant & Microbial Biology Department at UC Berkeley and to Rocío Sánchez and Dana Jantz, in particular, for all their help and support throughout the years.

CHAPTER 1

Microbial phosphite oxidation and its potential role in the global phosphorus and carbon cycles

Israel A. Figueroa & John D. Coates

Department of Plant and Microbial Biology, University of California, Berkeley, CA, USA

INTRODUCTION

Phosphite (HPO_3^{2-}) is a bioaccessible, reduced phosphorus compound that is present in a variety of environments throughout the world and yet its role in biogeochemistry is often overlooked. Phosphate (PO_4^{3-}) is the dominant inorganic P species on Earth and it is in this oxidation state (P^{5+}) that phosphorus is incorporated into biological molecules (Pasek 2008; Pasek et al. 2014) (Figure 1.1). However, it has been known since the 1950s that certain microorganisms are capable of utilizing phosphite (which has a P^{3+} oxidation state) as a P source by oxidizing it to phosphate, which they then incorporate into their cells (Adams & Conrad 1953) (Figure 1.1). This process is known as assimilatory phosphite oxidation (APO) and its genetic basis and biochemical mechanisms have been extensively studied (Casida 1960; Malacinski & Konetzka 1966; Foster et al. 1978; Metcalf & Wolfe 1998; Costas et al. 2001; K. Yang et al. 2004; White & Metcalf 2004b; Wilson & Metcalf 2005). More recently, it was shown that phosphite could also act as an electron donor and energy source for microbial growth and carbon fixation in a process known as dissimilatory phosphite oxidation (DPO) (Schink & Friedrich 2000). The existence of DPO is perhaps not surprising when one considers the chemical properties of phosphite: it is about 1,000 times more soluble than phosphate under similar conditions, it is kinetically stable and thus unlikely to participate in unwanted reactions, and its oxidation is very thermodynamically favorable due to the low redox potential (-650 mV) of the phosphate/phosphite couple (Pasek 2008; White & Metcalf 2007; Roels & Verstraete 2001).

Given the benefits of utilizing phosphite both as a phosphorus source and as an electron donor, it is likely that many more phosphite-oxidizing microbes remain to be discovered. Such a prospect raises several questions about the characteristics of microbial phosphite oxidation and its potential impact on the environment. What distinguishes DPO from APO in terms of genetics, physiology, and bioenergetics? In which kinds of environments would we expect to find each of these metabolisms? How prevalent are these metabolisms and what are their phylogenetic distributions? How might phosphite-oxidizing microbes affect global cycling of phosphorus and carbon? In this chapter, I will address these questions by reviewing the current state of knowledge regarding the geochemistry of phosphite and the biology of phosphite oxidation and discuss the role that microbial phosphite-oxidizing processes might play in the global biogeochemical context.

PHOSPHITE GEOCHEMISTRY FROM THE ARCHEAN TO THE ANTHROPOCENE

Evidence for the prevalence of phosphite on early Earth

Although conditions on early Earth are still a matter of much debate, Pasek and co-workers have argued that reduced phosphorus compounds, in particular phosphite, were abundant when life first emerged during the Archean period (4-2.5 Gya) (Pasek 2008; Pasek & Kee 2011; Pasek et al. 2013). They note the fact that most meteorites contain phosphide minerals (P^{3-} oxidation state), such as schreibersite ($[Fe,Ni]_3P$), which can abiotically corrode in the presence of water to release reduced P compounds such as phosphite, hypophosphite ($H_2PO_2^-$, P^{1+} oxidation state), and phosphine gas (PH_3 , P^{3-} oxidation state) (Pasek & Kee 2011; Pasek & Lauretta 2005; Bryant & Kee 2006) (Figure 1.1). Due to the heavy bombardment believed to have occurred 4.5-3.8 Gya, up to 1018 kg (i.e. 10% of the total P on the surface of the Earth) may have been derived from meteorite impacts (Pasek 2008; Pasek & Lauretta 2008; Pasek & Kee 2011). Given that schreibersite corrosion occurs fairly rapidly at geological timescales ($1-10^4$ years) and phosphite can account for >50% of the total soluble reduced P produced, meteoritic impacts would have deposited a substantial quantity of phosphite on the early Earth (Pasek 2008). Some additional phosphite could also have been derived from lightning discharges associated with volcanic activity since phosphite is known to occur when lightning strikes phosphate-containing minerals and volcanic ash (Glindemann et al. 1999; Pasek & Block 2009). Since phosphite is very kinetically stable (due to the 370 kJ of activation energy needed to break the P-H bond) it would have had a half-life of 10^8-10^{10} years under the reducing conditions of the Archean and could therefore have accumulated in the early ocean to concentrations of up to 10 mM (Pasek 2008). The recent detection of phosphite at relatively high proportions in 3.5 billion-year-old marine carbonate rocks appears to support this scenario (Pasek et al. 2013).

The idea that reduced phosphorus compounds may have been involved in the development of early life was first proposed by Gulick in the 1950s (Gulick 1955). He reasoned that phosphate would have been a poor substrate for the phosphorylation of prebiotic organic molecules due to its low solubility and reactivity, whereas reduced P species such as phosphite and hypophosphite, which are significantly more soluble and more reactive towards organic carbon and nitrogen compounds, could have facilitated the emergence of phosphorylated biomolecules (Gulick 1955). Gulick's theory was dismissed at the time because there was no known source of reduced P that could account for the proposed reactions, but in light of recent evidence for the prevalence of phosphite on early Earth, Pasek and co-workers have revisited this idea (Pasek & Kee 2011). In a series of experiments, they showed that schreibersite corrosion in water not only produces phosphite and hypophosphite but can also lead to the phosphorylation of simple organic molecules like acetate and ethanol (Pasek & Lauretta 2005; Pasek et al. 2007). Based on these findings it seems plausible that phosphite could have played a key role in the emergence of life, although further work is needed in order to establish the relevance of these reactions within the context of protobiotic chemistry.

Phosphite on modern Earth: Where does it come from?

It had been previously assumed that reduced P compounds present on early Earth would have been gradually oxidized to phosphate after the Great Oxygenation Event (~2.5 Gya) and therefore phosphite should be a negligible component of modern environments (Pasek 2008). However, phosphite has recently been detected in various environments including rivers, lakes, swamps, and geothermal pools (Pasek et al. 2014; Han et al. 2013; Pech et al. 2009). The phosphite concentrations measured in these studies ranged from 0.1 to 1.3 μM and accounted for 1 to 33% of the total dissolved P in the systems. Although phosphite tended to be more abundant under more reducing conditions, concentrations of up to 1 μM were observed even in some surface water samples (Pasek et al. 2014). The presence of micromolar amounts of phosphite in oxygen-exposed environments is unexpected given that phosphite reacts with oxygen fairly rapidly at geologically timescales (Pasek 2008). As noted by Pasek and coworkers, meteorite strikes and lightning discharges are relatively rare on modern Earth, making it unlikely that these processes by themselves can account for the amounts of phosphite detected in surface waters (Pasek & Kee 2011; Pasek et al. 2014). Some of this observed phosphite might be of anthropogenic origin since it can be a byproduct of the industrial production of phosphonates (compounds with C-P bonds), which are used as herbicides, detergents, and chelating agents (Yu et al. 2015; Ternan et al. 1998; Nowack 2003). Additionally, phosphite itself is used as a reducing agent in some industrial metal electroplating processes (Nagaosa & Aoyama 2001) and as a fungicide in agriculture (Thi Bich Thao et al. 2009). Phosphite can therefore be a component of industrial waste as well as agricultural runoff and has in fact been detected in the influent of wastewater treatment plants (Figure 1.2) (Yu et al. 2015). Han and coworkers have also observed higher phosphite concentrations at heavily polluted lake sites compared to less impacted areas (Han et al. 2013).

In pristine environments, geothermal activity may potentially serve as an alternate source of phosphite via the formation and subsequent corrosion of metal phosphides (Figure 1.2). Like other reduced P compounds, phosphide minerals are unstable in the presence of oxygen at geological timescales and are therefore rare on the Earth's surface (Britvin et al. 2015). The deposition of extraterrestrial schreibersite by meteorites and the reduction of phosphorus impurities in iron ore during industrial smelting are typically cited as the only significant sources of phosphides on Earth (Britvin et al. 2015; Pasek 2008; Glindemann et al. 1998). Nonetheless, natural terrestrially produced schreibersite has been found in iron-rich basalts in Greenland (Pauly 1969; Pedersen 1981), in ultramafic rocks uncovered during continental drilling in China (Yang et al. 2005), and in pyrometamorphic rocks in the Levant (Britvin et al. 2015). Britvin and coworkers cite these findings as evidence for "the occurrence of geologically juvenile terrestrial phosphides" and outline the four conditions necessary for the formation of these compounds: (1) the presence of phosphorus, (2) the presence of transition metals such as Fe or Ni, (3) a highly reducing geochemical environment, and (4) temperatures high enough to sustain the reduction process (Britvin et al. 2015). Based on these criteria it is likely that metal phosphide formation occurs in the subsurface due to the geothermal reduction of phosphate. Indeed, Glindemann and colleagues have noted that the strong reducing conditions observed within the Earth's crust should be conducive to the reduction of phosphate minerals to phosphides (Glindemann et al. 1998). The average elemental proportion of phosphorus in the Earth's crust is thought to be about 0.1% although it may be higher in the oceanic crust due to phosphate deposition into porous

subseafloor basalts during hydrothermal circulation of seawater along mid-ocean ridge flanks (Wheat et al. 1996; Clarke & Washington 1924). Subseafloor basalts are also rich in Fe(II) and other reduced chemical species such as H₂, H₂S, and CH₄ (Edwards et al. 2005). Furthermore, temperatures at the contact zone between mantle-derived magma and seawater at mid ocean ridge spreading zones can be as high as 400°C (Kelley et al. 2003). Reduction of phosphate in the presence of metal salts to produce metal phosphides is known to occur within hours at temperatures as low as 400°C in the presence of hydrogen gas (Prins & Bussell 2012). The subseafloor crust therefore appears to satisfy all the requirements for the formation of metal phosphides, which would subsequently react with seawater at short geological timescales to release phosphite and other reduced P compounds. Since phosphite is highly soluble and kinetically stable it would likely diffuse up through the porous basalt into the cooler upper layers of the subseafloor and possibly into the water column before being re-oxidized by dissolved oxygen in the ocean.

Phosphite may also be derived from biological processes, such as phosphonate degradation (Figure 1.2). Phosphonates are organic compounds with C-P bonds, as opposed to the C-O-P esters found in organophosphate compounds, and they have a P oxidation state of +3, as in phosphite (Metcalf & Wanner 1991; White & Metcalf 2007) (Figure 1.1). They can account for up to 25% of the dissolved organic P in some marine environments (Clark et al. 1999; Kolowitz et al. 2001). Some of this environmental phosphonate may be derived from industrial processes, but there are also biological routes for phosphonate production. Various organisms can incorporate phosphonates into their cell membranes as phosphonolipids or secrete antibiotic phosphonate compounds such as fosfomycin (White & Metcalf 2007; Martinez et al. 2011). Although the biosynthetic pathways for these compounds have not been well characterized, the conversion of phosphoenolpyruvate (PEP) to phosphonopyruvate (PnPy) by the enzyme PEP mutase is thought to be a common initial step in the production of phosphonates (White & Metcalf 2007). Phosphonates can also serve as a source of phosphorus or carbon for a variety of microorganisms and several pathways for phosphonate degradation have been characterized (White & Metcalf 2007). For example, some bacteria can use methylphosphonate as a P source in a process that releases methane and inorganic phosphate (Karl et al. 2008). This process is catalyzed by the C-P lyase enzyme and involves a phosphate radical intermediate (Kamat et al. 2013; Buckel 2013). Under mildly reducing conditions phosphate radicals can rearrange to form phosphite, making it a possible byproduct of methylphosphonate degradation in anaerobic environments (Pasek 2008; Pasek et al. 2014). Moreover, phosphonates with carbonyl or hydroxyl groups at the α -carbon, such as phosphonoformic acid, tend to form phosphite rather than phosphate as the product of C-P cleavage even under oxidizing conditions (Freeman et al. 1991). Given that C-P lyase enzymes are involved in the degradation of a variety of phosphonates, it is possible that these reactions are a significant source of environmental phosphite.

Biological phosphate reduction has also been posited as a possible source of environmental phosphite. Devai and colleagues detected phosphine gas production in wastewater and marsh soils and showed that phosphine production was stimulated by the addition of inorganic phosphate and organic matter, leading them to conclude that phosphate was being reduced to phosphine by microorganisms present in their samples (Dévai et al. 1988; Dévai & Delaune 1995). Some of this phosphine could subsequently be oxidized to phosphite in the presence of O₂

or UV radiation (Zhu et al. 2006; Stone & White 2012). However, the conclusion by Devai et al. that the phosphine they observed was derived from biological phosphate reduction has since been questioned by several researchers (Glindemann et al. 1998; Roels & Verstraete 2001; Roels & Verstraete 2004; Siyuan C Morton et al. 2005). Roels and coworkers have noted that biological phosphate reduction is problematic from a thermodynamic standpoint, since there is no known biological electron donor with a low enough redox potential to make the reaction exergonic (Roels & Verstraete 2001). Glindemann and coworkers have shown that phosphine can be produced during the corrosion of iron, even under sterile conditions (Glindemann et al. 1998). This is due to the fact that iron minerals often contain phosphorus impurities that can be abiotically reduced to iron phosphides during the industrial smelting process and these phosphides can then be released as phosphine gas during corrosion (Glindemann et al. 1998). Subsequent studies have likewise concluded that phosphine is released due to iron corrosion and that the higher rates of phosphine production observed in the presence of microorganisms is likely due to the microbial production of organic acids and hydrogen sulfide, which accelerate the corrosion process (Roels & Verstraete 2004; Siyuan C Morton et al. 2005).

Although evidence of biological phosphate reduction remains inconclusive, several theoretical mechanisms by which this process could occur have been proposed. Pasek and colleagues have suggested that in addition to being produced during phosphonate degradation, phosphite could also be formed as a byproduct of phosphonate biosynthesis in reducing environments (Pasek et al. 2014). They determined that the reductive cleavage of phosphoenolpyruvate by H_2 to form phosphite and pyruvate is thermodynamically feasible under standard cellular conditions (Pasek et al. 2014). Given that phosphoenolpyruvate is a key intermediate in the production of phosphonates from inorganic phosphate, such a mechanism would be a way of indirectly converting phosphate to phosphite. A more direct mechanism of phosphate reduction has been proposed by Roels and colleagues, who note that the reduced molybdoferredoxin cofactor of the nitrogenase complex has a redox potential of -1.0 V, which is low enough to reduce phosphate to phosphite (Roels & Verstraete 2001). However, they question the usefulness of such a reaction since energy from ATP hydrolysis must be expended in order to achieve such a low reduction potential and the organism would gain nothing from the production of phosphite. Nevertheless, it is possible that phosphite may be formed as an unwanted product of nitrogenase function in the presence of phosphate. This sort of inadvertent phosphate reduction might also occur in photosynthetic organisms, since the redox potentials of excited reaction center chlorophyll molecules range from -0.8 V (P680) to -1.26 V (P700) (Blankenship & Prince 1985). Environments dominated by anoxygenic phototrophs may therefore be potential hotspots of biological phosphite production since the absence of strong oxidants in these systems would favor the accumulation of reduced phosphorus species.

PHOSPHITE OXIDATION IN BIOLOGY

Phosphite as a microbial phosphorus source

The process of assimilatory phosphite oxidation (APO), which allows certain microorganisms to use phosphite as a phosphorus source, has been fairly well studied. At least twenty microbial isolates have so far been shown to carry out APO under laboratory conditions, including proteobacteria, firmicutes, and cyanobacteria (Adams & Conrad 1953; Malacinski & Konetzka 1966; Foster et al. 1978; Metcalf & Wolfe 1998; Schink & Friedrich 2000; K. Yang et al. 2004; Wilson & Metcalf 2005; Martinez et al. 2011). Genetic and biochemical studies of some of these organisms have revealed several enzymes capable of oxidizing phosphite (White & Metcalf 2007). Some C-P lyases, such as the one found in *E. coli*, are able to metabolize phosphite in addition to phosphonates, although the exact mechanism of the reaction has not been determined (Metcalf & Wanner 1991). Based on what is known about the mechanism of methylphosphonate degradation by C-P lyase, phosphite oxidation to phosphate most likely proceeds through a radical cleavage of the P-H bond (Frost et al. 2002; Kamat et al. 2013; Buckel 2013). It is not clear what determines the substrate specificity of these enzymes, since not all C-P lyases are capable of oxidizing phosphite (White & Metcalf 2007). *Pseudomonas stutzeri*, for example, has two distinct C-P lyase operons, only one of which confers the ability to carry out APO (White & Metcalf 2004b). Another enzyme known to oxidize phosphite is the bacterial alkaline phosphatase (BAP) of *E. coli*, which is a periplasmic protein encoded by the *phoA* gene that is normally involved in the hydrolysis of organophosphates for P uptake during phosphate starvation (K. Yang et al. 2004). In addition to its phosphatase activity, however, *E. coli* BAP has also been shown to oxidize phosphite to phosphate in vitro in a reaction that yields molecular hydrogen (K. Yang et al. 2004). This reaction is thought to proceed in a similar manner to a typical phosphate ester hydrolysis reaction, except that instead of an alkoxide (RO-) leaving group, the hydride (H-) from phosphite serves as a leaving group and reacts with a proton to form H₂ (K. Yang et al. 2004). The ability to oxidize phosphite appears to be a unique property of the *E. coli* BAP, since various other alkaline phosphatases from bacteria as well as eukaryotes have been tested for phosphite-oxidizing activity and so far none have yielded positive results (K. Yang et al. 2004).

The third known APO enzyme is the phosphite dehydrogenase encoded by the *ptxD* gene (Costas et al. 2001; White & Metcalf 2007). The PtxD enzyme from *P. stutzeri* is capable of oxidizing phosphite in vitro with NAD⁺ as its sole cofactor, yielding phosphate and NADH (Costas et al. 2001). The *P. stutzeri* PtxD has a high affinity for both phosphite ($K_m = 53.1 \mu\text{M}$) and NAD⁺ ($K_m = 54.6 \mu\text{M}$), but no activity has so far been detected in the presence of various potential alternative substrates including hypophosphite, thiophosphite, methylphosphonate, aminoethylphosphonate, D-3-phosphoglycerate, glycerate, lactate, formate, nitrite, arsenite, and sulfite (Costas et al. 2001; Relyea & van der Donk 2005). PtxD belongs to the NAD⁺-dependent D-hydroxy acid dehydrogenase protein family, but is the only member known to have an inorganic substrate (Relyea & van der Donk 2005). None of the other members of this family tested to date (D-3-phosphoglycerate dehydrogenase, lactate dehydrogenase, glycerate dehydrogenase, and formate dehydrogenase) are capable of phosphite oxidation (Relyea & van der Donk 2005). The specificity of this enzyme therefore sets it apart from C-P lyase and BAP and suggests that its biological role is limited to phosphite oxidation. Although no crystal

structure of PtxD is currently available, Relyea & van der Donk have used protein alignments, homology models and site-directed mutagenesis to identify four key residues (Lys76, Arg237, Glu266, and His292) likely to be involved in substrate binding and catalysis (Relyea & van der Donk 2005). However, further work is needed in order to elucidate the exact enzymatic mechanism by which phosphite oxidation occurs. In addition to *ptxD*, four other genes are found in the *ptxABCDE* operon of *P. stutzeri* (Metcalf & Wolfe 1998; White & Metcalf 2004a; White & Metcalf 2007) (Figure 1.3). The *ptxABC* gene cluster encode a phosphite ABC transporter, while *ptxE* encodes a transcription factor belonging to the LysR family (Metcalf & Wolfe 1998). However, deletion of *ptxE* appears to have no effect on the expression of the *ptx* operon or on the ability of *P. stutzeri* to grow on phosphite as its sole P source, so its role remains a mystery (White & Metcalf 2004a; White & Metcalf 2007). Expression of the *ptx* operon in *P. stutzeri* is induced by phosphate starvation and regulated by the PhoBR two-component system common to other phosphate starvation inducible (Psi) genes (White & Metcalf 2004a). Interestingly, the presence of phosphite does not induce the *ptx* operon when excess phosphate is present, which confirms that the only role of this operon is to provide phosphorus for the cell (White & Metcalf 2004a).

There are currently 601 genomes with predicted *ptxD* homologs in the Integrated Microbial Genomes (IMG) database, which represents roughly 1.5% of the total bacterial and archaeal genomes in the database. Since PtxD appears to be a dedicated phosphite dehydrogenase it is likely that most, if not all, of these organisms are capable of APO. However, only 5 of these candidates have so far been tested for their ability to oxidize phosphite and very little work has been done to document the prevalence of APO in the environment (Metcalf & Wolfe 1998; Simeonova et al. 2010; Wilson & Metcalf 2005; Martinez et al. 2011). Stone and White surveyed 12 different soil and freshwater sediment samples and found that 10-67% of bacteria were capable of growth with phosphite as the sole P source based on most probable number counts (Stone & White 2012). Interestingly, they did not find a significant difference in the proportion of APO-capable bacteria when they compared pristine sites to those impacted by human activity (Stone & White 2012). Martinez and coworkers identified a strain of the globally abundant cyanobacterium *Prochlorococcus* that is capable of APO and confirmed the presence of the *ptxABCD* gene cluster in its genome (Martinez et al. 2011). They also noted the presence of *ptx* clusters in the genomes of other marine bacteria such as *Cyanothece* sp., *Trichodesmium erythraeum*, *Nodularia spumigea*, and *Marinobacter aquaeolei*, and concluded that APO may be an important strategy for P acquisition in the world's oceans (Martinez et al. 2011). Furthermore, several researchers have found evidence indicating lateral acquisition of *ptx* genes (Metcalf & Wolfe 1998; Wilson & Metcalf 2005; Martinez et al. 2011; White & Metcalf 2007). Taken together, these observations suggest that the capacity for APO is widespread among microorganisms from a variety of environments and phylogenetic lineages, which makes sense given the competitive advantage that this ability confers, particularly under phosphate-limited conditions.

Phosphite as a microbial energy source and electron donor

Desulfotignum phosphitoxidans strain FiPS-3 is currently the only known isolate capable of dissimilatory phosphite oxidation (DPO) (Schink & Friedrich 2000; Schink et al. 2002). This bacterium was isolated from brackish canal sediments in Venice, Italy and is able to grow by

coupling phosphite oxidation to the reduction of either sulfate to sulfide, carbon dioxide to acetate, or nitrate to ammonia (Schink & Friedrich 2000; Schink et al. 2002)). As seen in equations 1-3 (Table 1.1), the oxidation of phosphite coupled to either sulfate, carbon dioxide, or nitrate reduction is exergonic and yields enough energy to drive ATP formation, which requires approximately 40 - 50 kJ.mol⁻¹ ATP under typical intracellular conditions (Thauer et al. 1977). The ability to conserve this energy and grow with phosphite as the sole electron donor is what distinguishes a DPO-capable organism from one that merely uses phosphite as a P source by means of APO. Still, one would expect any organism capable of DPO to also be capable of APO, since the phosphate produced by this metabolism could be subsequently incorporated into biomass. This is the case with FiPS-3, which can use phosphite as its sole P source in the presence of an alternative electron donor such as fumarate (Simeonova et al. 2010). However, the amount of phosphite needed to drive the growth of FiPS-3 to high cell densities (~10 mM) is two orders of magnitude greater than that required for use as a P source (~0.1 mM), which leads to the accumulation of phosphate in the medium during DPO (Schink et al. 2002, (Simeonova et al. 2010). No other APO-capable organism tested so far has been able to grow with phosphite as its sole electron donor or to accumulate phosphate in the medium, which indicates that DPO is a distinct metabolic process (White & Metcalf 2007).

FiPS-3 belongs to the *Desulfobacterales*, an order within the Deltaproteobacteria comprised of sulfate reducing bacteria (Schink et al. 2002). Interestingly, the closest known relative of FiPS-3, *Desulfotignum balticum* strain SaxT, is not capable of either DPO or APO even though the two strains have 99% 16S rDNA identity (Schink et al. 2002). One salient difference between the two strains is that homologs of *ptxD* and *ptxE* are present in the genome of FiPS-3 but not in that of SaxT or other members of the *Desulfobacterales* (Poehlein et al. 2013). In FiPS-3, *ptxDE* are part of a seven gene operon distinct from the *ptx* operon of *P. stutzeri* (Simeonova et al. 2010; Poehlein et al. 2013) (Figure 1.3). The FiPS-3 operon lacks the *ptxABC* genes, which encode an ATP-dependent phosphite transporter and are typically found in APO gene clusters (Simeonova et al. 2010; White & Metcalf 2007). Although the PtxD enzyme from FiPS-3 has not yet been purified and characterized in vitro, its sequence indicates that it is the most divergent of known PtxD homologs yet still retains the predicted catalytic residues and NAD binding site (Martinez et al. 2011; Simeonova et al. 2010).

In addition to *ptxDE*, there are five other genes in the operon, *ptdFCGHI*, that show no homology to genes found in known APO gene clusters (Simeonova et al. 2010) (Figure 1.3). Furthermore, the presence of transposase genes flanking the *ptx-ptd* cluster in FiPS-3, as well as the fact that this cluster has not been found in SaxT or other members of the *Desulfobacterales*, are strong indicators that these genes were horizontally acquired (Poehlein et al. 2013). Although the functions of all the *ptd* genes have not yet been experimentally determined, their annotations in the IMG database offer some insight into their possible roles. PtdC (IMG locus tag: Dpo_11c01230) is annotated as a glycerol-3-phosphate transporter belonging to the major facilitator superfamily. The glycerol-3-phosphate transporter from *E. coli*, GlpT, functions as an antiporter, which couples the export of inorganic phosphate from the cell to the import of glycerol-3-phosphate (Lemieux et al. 2005). PtdF (IMG locus tag: Dpo_11c01240) is annotated as an UDP-glucose 4-epimerase, an enzyme that in *E. coli* converts UDP-galactose to UDP-glucose and uses NAD⁺ as a cofactor (Bauer et al. 1992). PtdG (IMG locus tag: Dpo_11c01220) is annotated as a nucleotide-binding universal stress protein from the UspA family. In *E. coli*,

UspA is a phosphoprotein that is expressed in response to a wide variety of stresses including growth arrest during stationary phase, exposure to heat, and carbon, nitrogen, phosphorus, and sulfur starvation (Kvint et al. 2003). UspA can autophosphorylate with ATP or GTP as phosphate donors, but its exact biochemical function in cellular stress response remains unknown (Kvint et al. 2003). PtdH (IMG locus tag: Dpo_11c01210) is predicted to be a B12-dependent radical SAM family protein. Members of this protein family are characterized by the presence of both an S-adenosylmethionine (SAM)-binding domain and a cobalamin-binding domain and are able to generate radical intermediates that may be involved in a variety of reactions such as methylations, dehydrogenations, bond cleavages, molecular rearrangements, and substrate activations (Broderick et al. 2014). PtdI (IMG locus tag: Dpo_11c01200) is a hypothetical protein with no homologs of known function in the IMG database.

Simeonova and coworkers have shown that expression of the PtdF protein is increased in the presence of phosphite (Simeonova et al. 2009). However, when they heterologously expressed the *ptxD-ptdFCG* cluster in SaxT they found that, although it gained the ability to use phosphite as a P source, it was still unable to grow with phosphite as an electron donor (Simeonova et al. 2010). Furthermore, when they transformed SaxT with different versions of the *ptxD-ptdFCG* plasmid containing single deletions of each of the genes, they found that deleting either *ptxD* or *ptdC* abolished the ability of transformants to grow with phosphite as sole P source but deleting *ptdF* and *ptdG* did not (Simeonova et al. 2010). These results indicate that *ptxD* and *ptdC* are necessary and sufficient for phosphite uptake and oxidation, but additional genes are needed in order to couple phosphite oxidation to cell growth. Presumably, PtxD carries out the phosphite-oxidizing step via an NAD-dependent mechanism similar to that described in *P. stutzeri*. Based on its homology to GlpT, Simeonova and colleagues have posited that PtdC acts as a phosphite/phosphate antiporter in lieu of the ATP-dependent transporter typically encoded by *ptxABC* in APO-capable bacteria (Simeonova et al. 2010). What role the other four *ptd* genes may play in DPO remains unclear. It is likely that *ptdH* and *ptdI*, which were not included in the expression plasmid, are required for energy conservation along with *ptdF* and *ptdG*. However, it is also possible that additional genes outside of the *ptx-ptd* operon are involved in the metabolism. Future work is needed in order to conclusively answer this question, but based on the available evidence it appears that the *ptx-ptd* operon harbors the genes responsible for DPO in FiPS-3.

Bioenergetics of phosphite oxidation

The fact that PtxD alone does not confer the ability to grow with phosphite as an electron donor raises an intriguing question: Why are other genes besides PtxD required for DPO? The PtxD of *P. stutzeri* is known to produce NADH during phosphite oxidation and *P. stutzeri* carries out APO under aerobic conditions, meaning it should be capable of generating about 2 mol ATP per mol NADH oxidized by the electron transport chain (Rich 2003). Why, then, is this organism not capable of growing by DPO? The answer probably has to do with the way phosphite is transported into the cell. Recent work has shown that ABC transporters hydrolyze 2 molecules of ATP for each molecule of substrate they import (Patzlaff et al. 2003). Since *P. stutzeri* uses the ABC transporter PtxABC to bring phosphite into the cell, the cost of transport would consume the 2 ATP produced from phosphite oxidation. Furthermore, the expected ATP yield of phosphite oxidation would actually be lower during active growth since some of the NADH

produced would have to be diverted for use in anabolic reactions. APO in *P. stutzeri* would therefore be an energy neutral or net energy-consuming process (Figure 1.4a). FiPS-3, on the other hand, uses PtdC as its phosphite transporter instead of PtxABC. If PtdC does, in fact, function as a phosphite/phosphate antiporter as has been proposed, then there would be no energy cost associated with phosphite uptake in FiPS-3 (Figure 1.4b).

However, when both PtxD and PtdC were expressed in SaxT, it still did not gain the ability to grow by DPO, which indicates that an additional mechanism of energy conservation, possibly mediated by the *ptdFGHI* genes, is required in this organism. In contrast to *P. stutzeri*, FiPS-3 and SaxT growing by sulfate reduction would gain substantially less energy from NADH oxidation. During sulfate reduction 2 ATP must be initially expended in order to activate and reduce sulfate to sulfite, which can then be further reduced to sulfide in an exergonic reaction (Badziong & Thauer 1978). Sulfate reducing bacteria growing on H₂ typically generate 3 ATP from the sulfite reduction step for a net overall production of 1 mol ATP per mol sulfate reduced, which corresponds to the expected yield based on equation 4 (Table 1.1) (Badziong & Thauer 1978). However, if sulfite reduction were instead coupled to NADH oxidation according to equation 5 (Table 1.1), the expected yield would only be 2 mol ATP per mol sulfite reduced, which would result in no net ATP production from the overall reduction of sulfate (Figure 1.4b). In order to grow by DPO, therefore, FiPS-3 and SaxT would not only need to save energy on phosphite uptake, but also conserve more of the free energy available from the oxidation of phosphite. The NAD⁺/NADH couple has a redox potential of -320 mV under standard physiological conditions (Thauer et al. 1977), which means that the reduction of NAD⁺ coupled to phosphite oxidation ($E^{\circ\prime} = -650$ mV) releases 63.7 kJ.mol⁻¹ phosphite.

This additional energy is presumably lost in traditional APO-capable organisms, but there is evidence that it is conserved in FiPS-3. Schink and coworkers observed substantially higher cell yields when FiPS-3 was grown on phosphite and sulfate (12.1 g.mol⁻¹ phosphite) versus formate and sulfate (4.85 g.mol⁻¹) (Schink et al. 2002). Since phosphite and formate both donate 2 electrons and the redox potential of the CO₂/formate couple ($E^{\circ\prime} = -432$ mV) is actually higher than that of NAD⁺/NADH (Thauer et al. 1977), the higher yields seen on phosphite are not consistent with NADH oxidation being the sole means of ATP production during DPO. Furthermore, the growth yield of FiPS-3 on phosphite and CO₂ via the Wood-Ljungdahl pathway (12.8 g.mol⁻¹ phosphite) was about 10 times higher than the yields typically observed for other Wood-Ljungdahl acetogens growing on H₂ ($E^{\circ\prime} = -414$ mV) and CO₂, such as *Acetobacterium woodii* (1.1 g.mol⁻¹ H₂) and *Acetogenium kivui* (1.3 g.mol⁻¹ H₂) (Schink et al. 2002; Thauer et al. 1977; Tschech & Pfennig 1984; H. C. Yang & Drake 1990). These results suggest that FiPS-3 can in fact take advantage of the extremely electronegative redox potential of phosphite, although it is unclear how this is accomplished since there are no known biological redox carriers that can accept electrons at such a low potential (Schink et al. 2002). Schink and coworkers have proposed that ATP is generated from phosphite oxidation by means of substrate level phosphorylation in addition to the reduction of NAD⁺, thus yielding both energy and reducing equivalents for each molecule of substrate utilized (Schink et al. 2002). Such a reaction would be thermodynamically feasible according to equation 6 (Table 1.1). Therefore, the function of the *ptdFGHI* genes may be to facilitate substrate level phosphorylation during phosphite oxidation (Figure 1.4b). Relyea and van der Donk have suggested that one of the possible mechanisms of phosphite oxidation by PtxD may involve the creation of a

phosphorylated enzyme intermediate that is subsequently hydrolyzed to release phosphate (Relyea & van der Donk 2005). PtdFGHI might interact with PtxD in order to facilitate the transfer of this phosphoryl group to ADP, either directly or by means of additional phosphorylated intermediates. This is a promising avenue for future inquiry but more work is currently necessary in order to determine whether phosphite acts as a phosphoryl donor for ATP synthesis during DPO and what role, if any, the *ptdFGHI* genes play in this process.

CONCLUDING REMARKS

Over the last 20 years, the study of reduced phosphorus compounds and their role in nature has grown from a series of curious observations and intriguing theories into an exciting new frontier in biogeochemistry. In particular, recent discoveries regarding the geochemistry and biology of phosphite have highlighted the potential significance of this compound both as a facilitator for the emergence of life on ancient Earth and as a modern driver of microbial processes that continue to shape the global biosphere. Phosphite has been detected in several environments at concentrations that suggest the current existence of a phosphorus redox cycle occurring at short geological timescales. Several anthropogenic sources of phosphite have been identified, and there is evidence that phosphite may also be produced by natural processes such as biological phosphonate metabolism and geothermal phosphate reduction. The presence of the genes responsible for assimilatory phosphite oxidation (APO) in hundreds of microbial isolates from a variety of environments indicates that this process is widespread and may have a substantial impact on the global P cycle. Furthermore, the discovery of dissimilatory phosphite oxidation (DPO) and its ability to sustain carbon fixation while providing an energetic benefit raises the possibility of phosphite as a key, though hitherto unrecognized, driver of primary productivity in the environment.

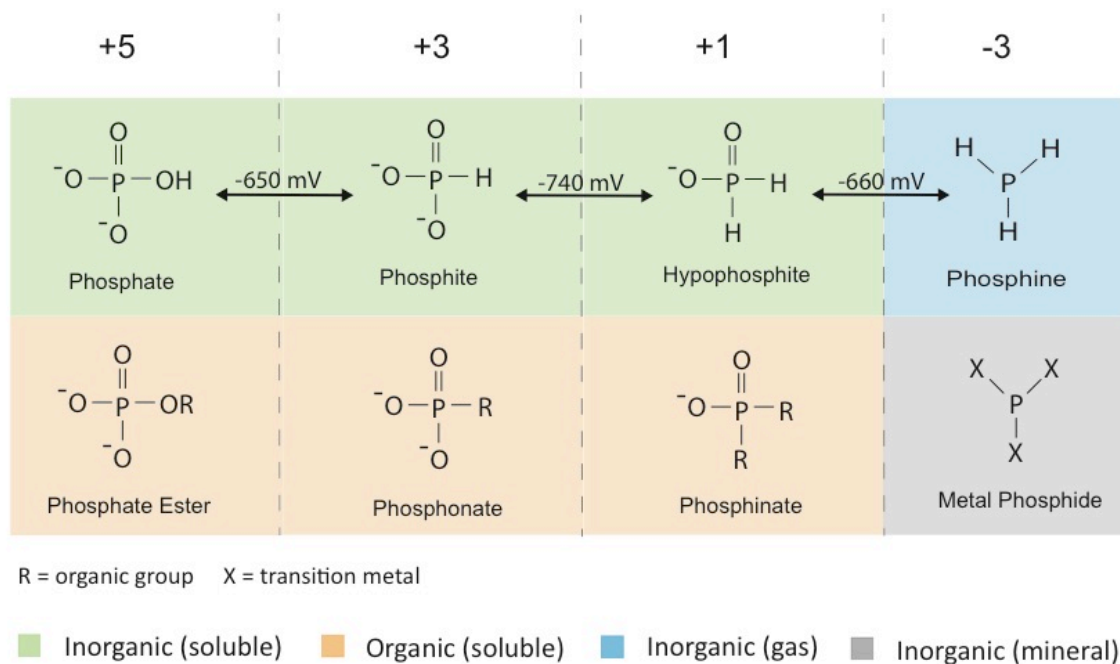


Figure 1.1. Chemical structures and redox properties of phosphorus compounds discussed in the text. The number above each column indicates the P oxidation state of the compounds below. Arrows indicate the standard reduction potential at pH 7 of each redox couple based on Roels & Verstraete (2001).

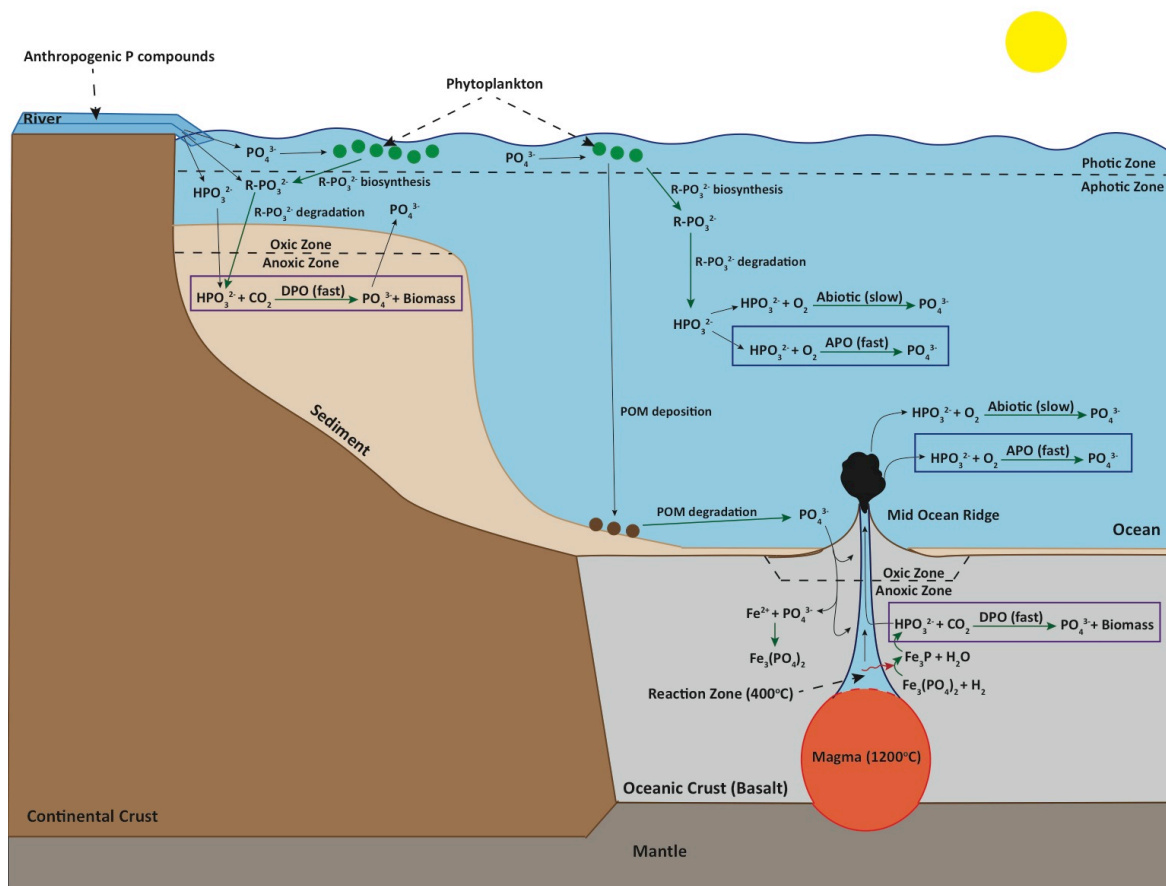


Figure 1.2. Potential sources and sinks of phosphite in marine environments and proposed role of microbial phosphite oxidation in phosphorus and carbon cycling. APO = assimilatory phosphite oxidation, DPO = dissimilatory phosphite oxidation, POM = particulate organic matter. Solid black arrows indicate transport, green arrows indicate chemical reactions, red arrows indicate heat, dotted black arrows indicate labels.

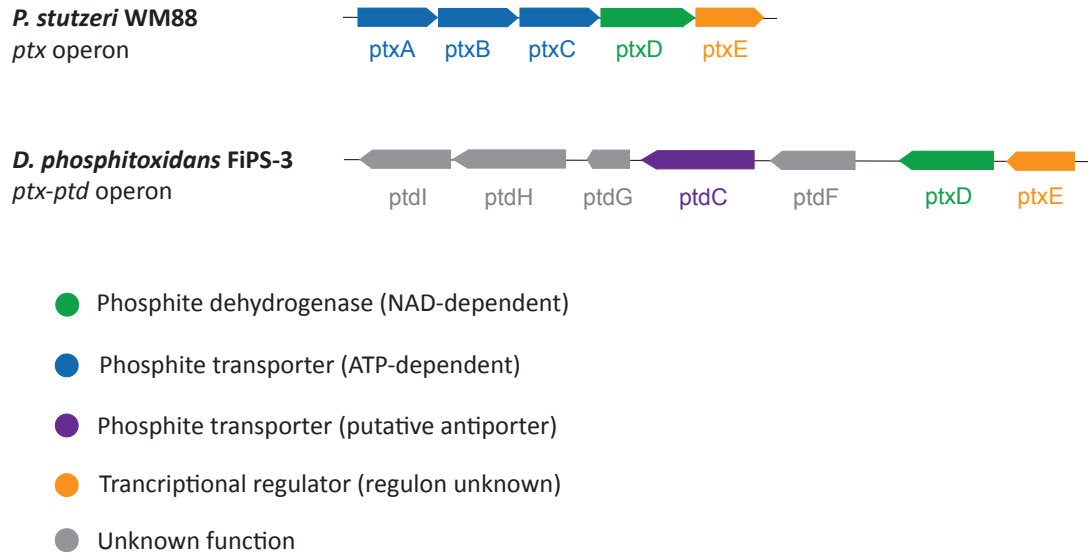
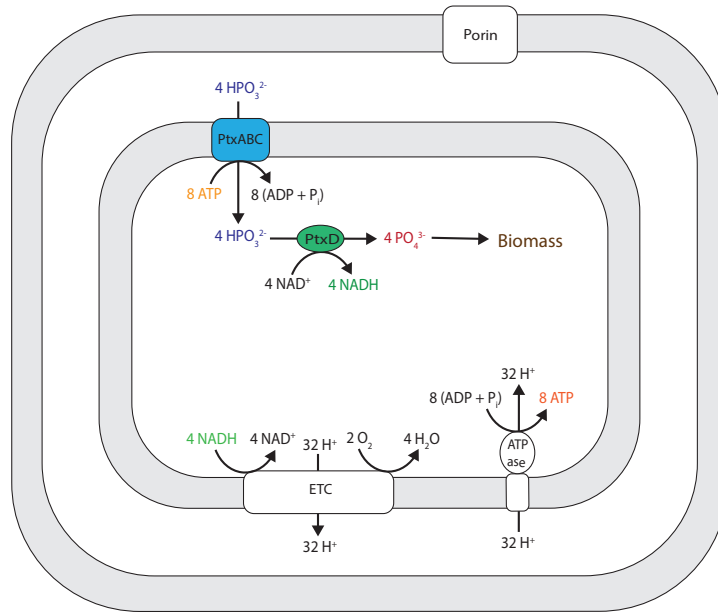


Figure 1.3. Phosphite oxidation operons of *Pseudomonas stutzeri* WM88 and *Desulfotignum phosphitoxidans* FiPS-3. WM88 is only capable of assimilatory phosphite oxidation, whereas FiPS-3 can carry out both assimilatory and dissimilatory phosphite oxidation.

A) Assimilatory phosphite oxidation in *P. stutzeri* WM88



B) Dissimilatory phosphite oxidation in *D. phosphitoxidans* FiPS-3

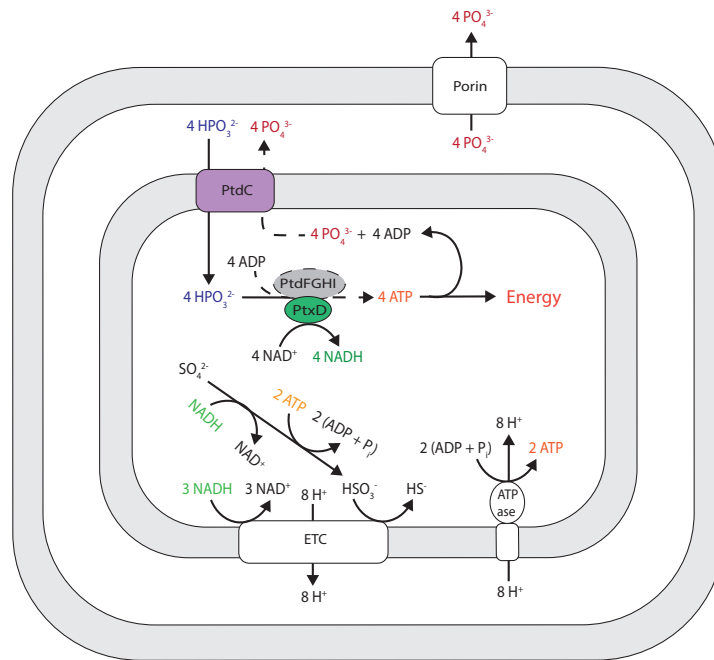


Figure 1.4. Cellular energetics and transport during aerobic assimilatory phosphite oxidation in *Pseudomonas stutzeri* WM88 (**A**) and dissimilatory phosphite oxidation coupled to sulfate reduction in *Desulfotignum phosphitoxidans* FiPS-3 (**B**). Dotted lines denote putative mechanisms based on physiological and genomic observations that have yet to be confirmed by direct biochemical evidence.

Table 1.1. Chemical equations and free energy values for reactions discussed in the text. ΔG° = Gibbs free energy under standard conditions at pH 7. Equations and values were taken from the studies cited under references or calculated based on data from these studies.

Reactions	ΔG° (kJ.mol ⁻¹)	References
(1) $4\text{HPO}_3^{2-} + \text{SO}_4^{2-} + \text{H}^+ \rightarrow 4\text{HPO}_4^{2-} + \text{HS}^-$	-91	Schink et al. 2002
(2) $4\text{HPO}_3^{2-} + 2\text{CO}_2 + 2\text{H}_2\text{O} \rightarrow 4\text{HPO}_4^{2-} + \text{CH}_3\text{COO}^- + \text{H}^+$	-77	Schink et al. 2002
(3) $4\text{HPO}_3^{2-} + \text{NO}_3^- + \text{H}_2\text{O} + \text{H}^+ \rightarrow 4\text{HPO}_4^{2-} + \text{NH}_3$	-89	This review (based on Poehlein et al. 2013, Thauer et al. 1977)
(4) $\text{HSO}_3^- + 3\text{H}_2 \rightarrow \text{SH}^- + 3\text{H}_2\text{O}$	-172	Badziong & Thauer 1978
(5) $\text{HSO}_3^- + 3\text{NADH} + 3\text{H}^+ \rightarrow \text{SH}^- + 3\text{NAD}^+ + 3\text{H}_2\text{O}$	-118	This review (based on Badziong & Thauer 1978, Thauer et al. 1977)
(6) $\text{HPO}_3^{2-} + \text{NAD}^+ + \text{ADP}^{3-} \rightarrow \text{NADH} + \text{ATP}^{4-}$	-14	This review (based on Schink et al. 2002, Thauer et al. 1977)

CHAPTER 2

Observations regarding the physiology and genetics of dissimilatory phosphite oxidation in *Desulfotignum phosphitoxidans* strain FiPS-3

(Unpublished data)

INTRODUCTION

As discussed in Chapter 1, *Desulfotignum phosphitoxidans* strain FiPS-3 is currently the only organism known to carry out dissimilatory phosphite oxidation (DPO). This chapter documents my work using pure cultures of FiPS-3 to investigate the physiological and genetic factors associated with this metabolism. There was no genome sequence available for FiPS-3 when I first started this project, so one of my early endeavors was to have its genome sequenced in order to better understand its genetic capabilities. However, while I was in the process of analyzing this genome, another research group published their own genomic analysis of FiPS-3, which touched upon many of the same findings that my own work had revealed (Poehlein et al. 2013). Nonetheless, I present here several observations regarding amino acid biosynthesis as well as aerobic metabolism that were not explored by Poehlein et al. and which led to a substantial improvement in the growth of FiPS-3 as well as to the discovery of its ability to grow in the presence of oxygen. The availability of a genome sequence for FiPS-3 also allowed me to perform an RNAseq analysis, which confirmed that the *ptx-ptd* genes are upregulated under phosphite-oxidizing conditions. Furthermore, I noticed that DPO in my FiPS-3 cultures was accompanied by the precipitation of phosphate minerals, a phenomenon that has been previously observed by Schink et al. (2002). Subsequent investigations demonstrated that this biomineralization process could be used to cement an unconsolidated calcium carbonate matrix and that different types of minerals could be formed depending on the media composition.

MATERIALS & METHODS

FiPS-3 culturing and growth curves

A culture of *Desulfotignum phosphitoxidans*, strain FiPS-3 (DSMZ 13687) was obtained from the German Collection of Microorganisms and Cell Cultures. Cells were grown anaerobically at 30°C on minimal media in 120 mL serum bottles or in 22 mL screw cap tubes. The composition of the minimal medium per liter of distilled water was as follows: 20 g NaCl, 5 g NaHCO₃, 12 g HEPES buffer, 1 g NH₄Cl, 0.77 g KCl, 1.5 g MgCl₂, 0.14 g CaCl₂, and 0.5 g L-cysteine HCl. The medium also contained vitamins, trace minerals, and resazurin. The final pH of the medium was 7.2 and it was degassed and transferred to bottles and tubes under a N₂/CO₂ (80:20) headspace and autoclaved. Phosphite, fumarate, sulfate, phosphate, and amino acids (Sigma Aldrich) were added to the media from sterile, anaerobic stock solutions prior to inoculation as needed. Samples for ion chromatography (IC) analysis were filtered and stored at 4°C, while samples for DNA extraction were stored at -80°C. Cell growth was assessed by measuring optical density at 600 nm (OD₆₀₀) using a Cary 50 Bio Spectrophotometer.

Ionic metabolite analysis

Phosphite, phosphate, and sulfate concentrations were measured via ion chromatography using a Dionex ICS 2100 instrument with a Dionex IonPac AS 16 (4 × 250 mm) column (Thermo Fisher Scientific) maintained at 30°C. To improve the separation of the phosphite, phosphate, and sulfate peaks, a gradient elution program was developed in which the mobile phase concentration increased from 12 mM to 35 mM NaOH after 10 minutes. The total run time of the program was 20 minutes with a constant mobile phase flow rate of 1.2 mL/min and a sample injection volume of 25 µL. Background conductivity was suppressed with a Dionex ASRS suppressor set at 100 mA and operating in recycle mode.

Scanning electron microscopy (SEM) and x-ray diffraction (XRD) analysis

Several milligrams of mineral precipitates were sampled from FiPS-3 cultures grown on phosphite with either calcium or magnesium in the media and mineral samples were ground into a powder. For SEM, a sample of the powdered mineral was suspended in several milliliters of distilled water to create a mineral slurry. Silicon wafers were washed with ethanol for 30 s and air dried. A 20-µl poly-L-lysine drop was placed on the silicon wafers for 1 min and then withdrawn. The wafers were then rinsed with ultraclean water. A drop of the mineral slurry was fixed with 2% glutaraldehyde in 0.1 M sodium cacodylate buffer, added to the silicon wafers, and allowed to settle for 1 h. Samples were then dehydrated for 10 min in 35%, 50%, 70%, 80%, 95%, and 100% ethanol, followed by critical point drying. Dehydrated samples were mounted onto stubs, sputter coated with palladium/gold, and visualized using a Hitachi S-5000 scanning electron microscope at 20 kV. For XRD, a sample of the powdered mineral was suspended in a few drops of amyl acetate to create a mineral slurry. The mineral slurry was then analyzed with a PANalytical X'Pert Pro diffractometer equipped with a Co x-ray tube and an X'Celerator detector.

RNA extraction and RNAseq

Cells were grown to mid-logarithmic phase ($OD_{600} = 0.3-0.4$) with either 10 mM phosphite or 10 mM fumarate as sole electron donor and then harvested by centrifugation. RNA was extracted according to the TRI Reagent Solution protocol (Thermo Fisher Scientific) and DNAase treated using the Turbo DNA-free Kit (Thermo Fisher Scientific). RNA was submitted to the QB3 Vincent J. Coates Genomics Sequencing Laboratory at UC Berkeley for cDNA library preparation and sequencing using an Illumina HiSeq 2000 (50 bp single reads). RNA counts for each gene were normalized by gene length and by total number of reads per sample and the statistical significance of differential expression between the two conditions was assessed using the DESeq software package (Anders & Huber 2010).

RESULTS

Growth of FiPS-3 is improved by addition of phenylalanine and histidine

Analysis of the FiPS-3 genome revealed that it lacks *pheA* (prephenate dehydratase) and *pheC* (cyclohexadienyl dehydratase), which are involved in phenylalanine biosynthesis, as well as *hisE* (phosphoribosyl-ATP pyrophospho-hydrolase), which is involved in histidine biosynthesis. When phenylalanine and histidine were added to the growth media, the doubling time decreased from 192 hours to 48 hours and the maximum OD increased from 0.25 to 0.5 (Figure 2.1). A similar effect was observed when yeast extract or casamino acids were added to the media (data not shown). The rate of DPO in the amino acid supplemented media increased concomitantly with the increased rate of growth and under these improved growth conditions cells were able to completely oxidize 8 mM phosphite in 8 days (Figure 2.1).

FiPS-3 is capable of growing under aerobic conditions

Surprisingly for a supposedly strict anaerobe, the genome of FiPS-3 contains the full *coxABCD* gene cluster predicted to encode the oxygen-respiring cytochrome c oxidase (complex IV). Based on this finding, I decide to test whether FiPS-3 could grow with phosphite as its sole electron donor in the presence of oxygen. Initial attempts to grow it under well-aerated conditions in a shaking incubator proved unsuccessful. However, when oxygen was added to the headspace of sealed, anaerobic culture tubes and the cultures were incubated without shaking, FiPS-3 was able to grow and oxidize phosphite (Figure 2.2). FiPS-3 grew better with 20% O₂ compared to 5% O₂ in the headspace and no growth was seen in control cultures lacking O₂ and having no other electron acceptor (Figure 2.2a). Growth rates with 20% O₂ were comparable to those seen with sulfate as the electron acceptor (Figure 2.2a). Furthermore, aerobic growth of FiPS-3 resulted in substantially faster rates of phosphite oxidation than in aerobic abiotic controls, in which no phosphite oxidation was observed during the course of the experiment (Figure 2.2b).

DPO by FiPS-3 leads to precipitation of phosphate minerals in the presence of magnesium and calcium

In accordance with previous observations, DPO-dependent growth of FiPS-3 was accompanied by the appearance of mineral precipitates in the medium several days after the onset of phosphite oxidation (Figure 2.3a). The precipitates appeared to be crystalline and varied in size from several millimeters to several centimeters in length. Typically, some of the crystals would adhere to the bottom and sides of the glass culture tubes, although most would remain suspended in the medium. No precipitates were observed in cultures grown with fumarate as the electron donor instead of phosphite (Figure 2.3a). Subsequent tests showed that DPO-dependent biomineralization could be used to consolidate a fine-grained calcium carbonate matrix at standard temperature and pressure and circumneutral pH. When FiPS-3 was grown in the presence of phosphite, all of the calcium carbonate present in the media was consolidated into a hardened mineral phase that adhered to the bottom of the glass culture bottles, whereas in FiPS-3 cultures grown on fumarate or in sterile phosphite-containing media the calcium carbonate

particles remained suspended in the liquid phase (Figure 2.3b). SEM imaging of precipitates from FiPS-3 cultures amended with either calcium or magnesium showed different mineral morphologies depending on which cation was present in the media (Figure 2.4). Analysis of the precipitates using XRD confirmed that they were crystalline phosphate minerals and that their chemical compositions varied based on the cation present. Hydroxyapatite ($\text{Ca}_{10}(\text{OH})_2(\text{PO}_4)_6$) was produced in the presence of calcium, whereas struvite ($\text{MgNH}_4\text{PO}_4 \cdot 6\text{H}_2\text{O}$) was produced in the presence of magnesium. The SEM images also appeared to show that some of the cells involved in the biomineralization process became embedded in the mineral phase (Figure 2.4).

The *ptx-ptd* gene cluster of FiPS-3 is upregulated in the presence of phosphite

RNAseq analysis of FiPS-3 cultures grown on either phosphite or fumarate as sole electron donors showed that all of the *ptx-ptd* genes had significantly higher expression levels ($p < 0.05$) on phosphite compared to the control (Table 2.1). In fact, *ptdF* was the most upregulated gene in the entire genome under phosphite-oxidizing conditions, with an ~100-fold increase in expression compared to the control (Table 2.1, Appendix 2.1). The other four *ptd* genes were all among the top 25 most upregulated genes on phosphite, having an ~10-fold increase in expression (Table 2.1, Appendix 2.1). Interestingly, *ptxDE*, which are directly upstream of *ptdFCGHI*, had only about a 2-fold increase in expression on phosphite. Other genes that were significantly upregulated on phosphite (\log_2 fold change > 2 , $p < 0.05$) are predicted to be involved in molybdenum, cobalt, nickel, acetate, and glutathione transport as well as in queuosine biosynthesis (Appendix 2.1). In addition, there were a number of ambiguously annotated genes as well as genes predicted to encode hypothetical proteins that had increased expression in the presence of phosphite.

DISCUSSION

Genomic analysis suggested that FiPS-3 was incapable of synthesizing phenylalanine and histidine, and addition of these amino acids to the growth media did indeed result in a drastic reduction in cell doubling time and increase in maximum OD. However, FiPS-3 was still able to grow, albeit poorly, in the absence of phenylalanine and histidine, indicating that it is still able to make these amino acids even though it appears to be missing genes in both biosynthetic pathways. This discrepancy could be due to misannotations in the genome or to the existence of alternative biosynthetic pathways. In any case, the addition of phenylalanine and histidine greatly improved the growth and phosphite oxidation rate of FiPS-3 cultures. The growth benefit conferred by these two amino acids was similar to that of yeast extract or casamino acids and was probably due to their ability to serve as organic carbon and nitrogen sources.

FiPS-3 has previously been characterized as a strict anaerobe, and the presence of cytochrome c oxidase (*cox*) genes in its genome has been attributed to an uncharacterized mechanism of nitrite resistance, although this hypothesis was never tested (Schink et al. 2002; Poehlein et al. 2013). Here I show that FiPS-3 is not only capable of growing under aerobic conditions, but indeed grows better in the presence of oxygen than in controls containing no electron acceptor. This observation, coupled with the presence of *cox* genes in its genome, suggests that FiPS-3 is capable of oxygen respiration. This is an unexpected result given that oxygen tolerance is rare among sulfate reducing bacteria and that the capacity for aerobic respiration is rarer still, with only a handful of oxygen-respiring sulfate reducers having been documented so far (Dilling & Cypionka 1990; Sigalevich & Cohen 2000). However, the fact that FiPS-3 grew at a similar rate in the presence of oxygen as it did under sulfate-reducing conditions is puzzling, since oxygen is a substantially more favorable electron acceptor from a thermodynamic point of view and should, therefore, allow for faster growth. This may be indicative of a failure on the part of FiPS-3 to adequately cope with oxidative stress, which imposes a growth cost under aerobic conditions. Its inability to grow in a well-aerated culture lends support to this hypothesis and highlights the fact that the actual dissolved oxygen concentrations it was exposed to in unmixed cultures were likely well below the concentrations present in the headspace. As such, it may be more accurate to regard FiPS-3 as a microaerophile rather than a true facultative aerobe. Furthermore, it is also possible that FiPS-3 was not actually growing by aerobic respiration in oxygen-containing cultures but rather growing by sulfate reduction with the oxygen serving to re-oxidize any sulfide produced back to sulfate. Even though sulfate was not added to the aerobic cultures, even a small amount carried over from the inoculum could have supported the observed growth if the sulfide produced was continuously reacting with oxygen to replenish the sulfate pool available to the cells. Further experiments, such as quantification of *cox* gene expression levels during aerobic growth or assessment of aerobic growth in the presence of complex IV inhibitors, are needed in order to distinguish between these two scenarios.

In my FiPS-3 cultures, growth by DPO led to the precipitation of struvite or hydroxyapatite crystals when magnesium or calcium were added to the media. Schink et al. (2002) have previously observed the formation of struvite crystals during phosphite oxidation by FiPS-3 cultures. They attributed this phenomenon to the accumulation of inorganic phosphate to high

concentrations in the extracellular milieu and the subsequent reaction of this phosphate with magnesium ions present in the medium to form crystalline mineral precipitates. This process of DPO-dependent biomineralization exploits the large difference in solubility between phosphite and phosphate and could potentially be applied to the development of bioconcrete. Bioconcrete refers to ‘self-healing’ concrete that incorporates biomineralizing microorganisms in order to help seal cracks that develop over time and thus improve durability and strength (Seifan et al. 2016). Most of the research conducted in this area has so far focused on the precipitation of calcium carbonates by heterotrophic bacteria (Seifan et al. 2016). However, the precipitation of calcium and magnesium phosphate minerals by means of a chemolithoautotrophic DPO-capable bacterium may present an alternate approach for the advancement of this technology.

Although upregulation of the PtdF protein in the presence of phosphite has been previously reported (Simeonova et al. 2009), this is the first evidence of increased expression of the entire *ptx-ptd* gene cluster under phosphite-oxidizing conditions. This finding affirms the connection between the *ptd* genes and DPO and lends further support to the hypothesis that these genes are necessary for growth by means of phosphite oxidation. It is important to note that 1 mM phosphate was present in both growth conditions, so that the increased expression of these genes was not due to phosphate starvation, which is known to induce expression of *ptx* genes in APO-capable organisms (White & Metcalf 2004a). However, the substantial difference in expression levels seen between the *ptx* and *ptd* genes was unexpected and implies that *ptxDE* and *ptdFCGHI* may represent two distinct functional modules that are differentially regulated. The fact that *ptxDE* are also present in APO-capable organisms in combination with an alternate phosphite transporter (*ptxABC*) also supports the notion that the *ptx* and *ptd* genes represent separate modules.

As discussed in Chapter 1, PtxD is known to be the enzyme responsible for phosphite oxidation both in APO organisms and in FiPS-3, while the function of the predicted transcriptional regulator *ptxE* remains a mystery. It is possible that the role of *ptxE* is actually to promote transcription of *ptdFCGHI* in the presence of phosphite, which could explain the higher levels of expression seen for these genes. The *ptd* module is involved in phosphite transport and possibly also in energy conservation. Given that PtxD is highly efficient at turning over phosphite (Costas et al. 2001; Relyea & van der Donk 2005), the transport and energy conservation steps may in fact represent the bottlenecks for growth by DPO. Increased expression of the *ptd* genes could, therefore, be a way to compensate for the relative inefficiency of these processes compared to the phosphite oxidation step itself. Furthermore, the exceptionally high level of *ptdF* expression compared to the other *ptd* genes suggests that this enzyme may catalyze the rate-limiting step in the pathway.

Overall, my RNAseq results highlight the importance of the *ptd* genes during DPO-dependent growth of FiPS-3, but exactly what their functional roles are and how they are regulated remains to be elucidated. It is essential, going forward, to determine the minimal set of genes that are necessary and sufficient for growth by DPO, either through targeted knockouts in FiPS-3 or through expression of candidate genes in heterologous hosts. DPO enzymes could then be purified and characterized in vitro in order to determine their mechanisms of action. Unfortunately, my attempts to carry out targeted gene deletions in FiPS-3 as well as to heterologously express the full *ptx-ptd* gene cluster in *D. balticum* SaxT and in *E. coli* have so

far proven unsuccessful. Nonetheless, I hope that my efforts to improve the growth of FiPS-3 under both anaerobic and aerobic conditions will aid in the development of genetic tools in this organism that will allow future researchers to address some of these unanswered questions. Furthermore, the ability of FiPS-3 to precipitate phosphate minerals as a byproduct of DPO holds great promise as a potential mechanism for bioconcrete production. However, before this process can be applied on an industrial scale, further research must be undertaken in order to establish the optimal conditions for biomineralization by FiPS-3 as well as to assess the material properties of the different mineral products.

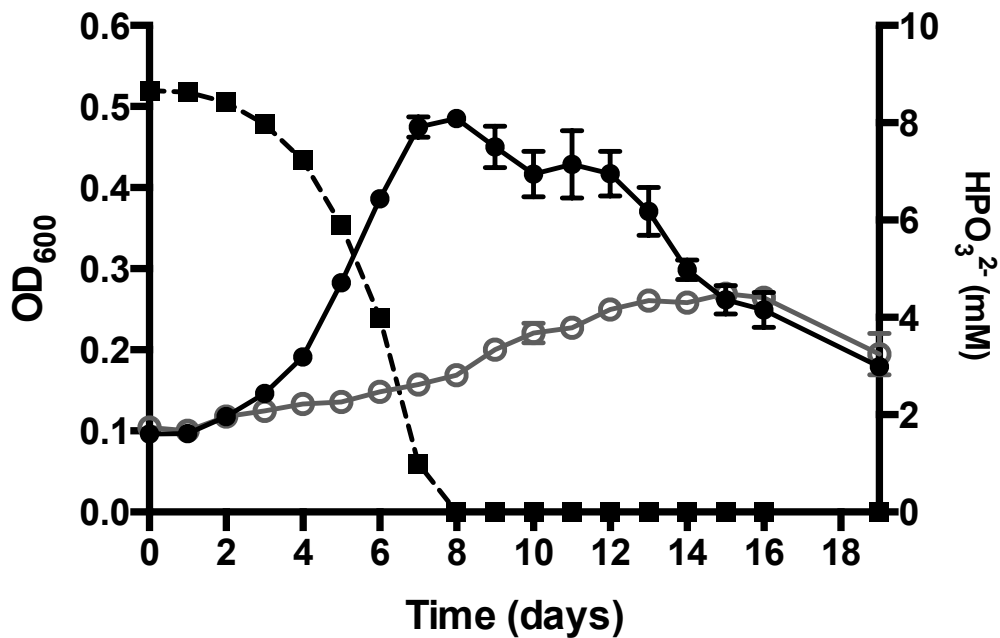


Figure 2.1. Improved growth and phosphite oxidation by *D. phosphitoxidans* FiPS-3 in the presence of 1 mM phenylalanine and 1 mM histidine (closed black circles) compared to control cultures lacking amino acids (open gray circles). Black squares with dotted lines indicate phosphite concentrations in amino acid amended cultures. All cultures were grown at 30°C on minimal media with 10 mM phosphite and 10 mM sulfate. Data points represent the average of triplicate cultures, with error bars denoting the standard error of the mean.

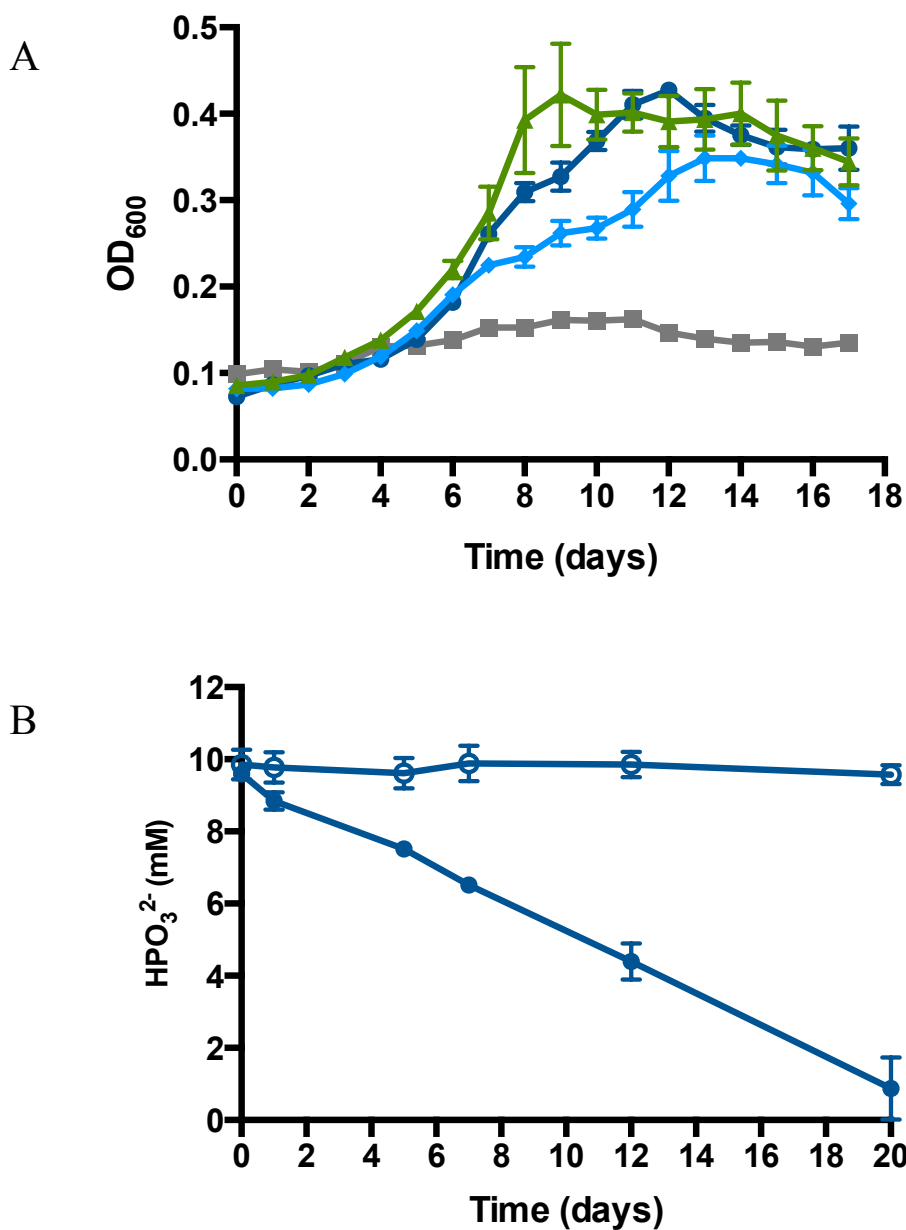
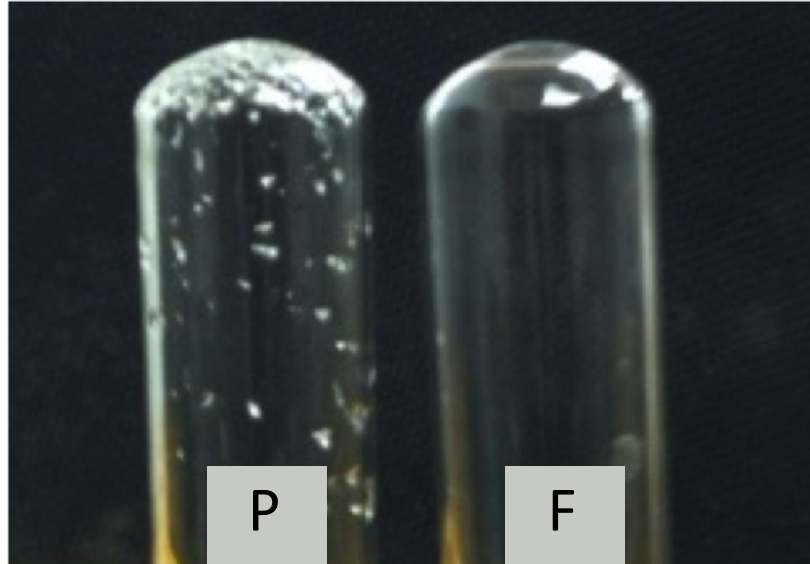


Figure 2.2. Growth (A) and phosphite oxidation (B) by *D. phosphitoxidans* FiPS-3 in the presence of 20% oxygen (closed dark blue circles), 5% oxygen (light blue diamonds), 10 mM sulfate (green triangles), and no acceptor (gray squares). Open dark blue circles indicate phosphite concentrations in abiotic controls in the presence of 20% oxygen. All cultures were grown in sealed tubes without shaking at 30°C on minimal media with 1 mM phenylalanine and histidine, and 10 mM phosphite. For oxygen-containing cultures, air was injected into the headspaces at the appropriate concentrations. Data points represent the average of triplicate cultures, with error bars denoting the standard error of the mean.

A



B

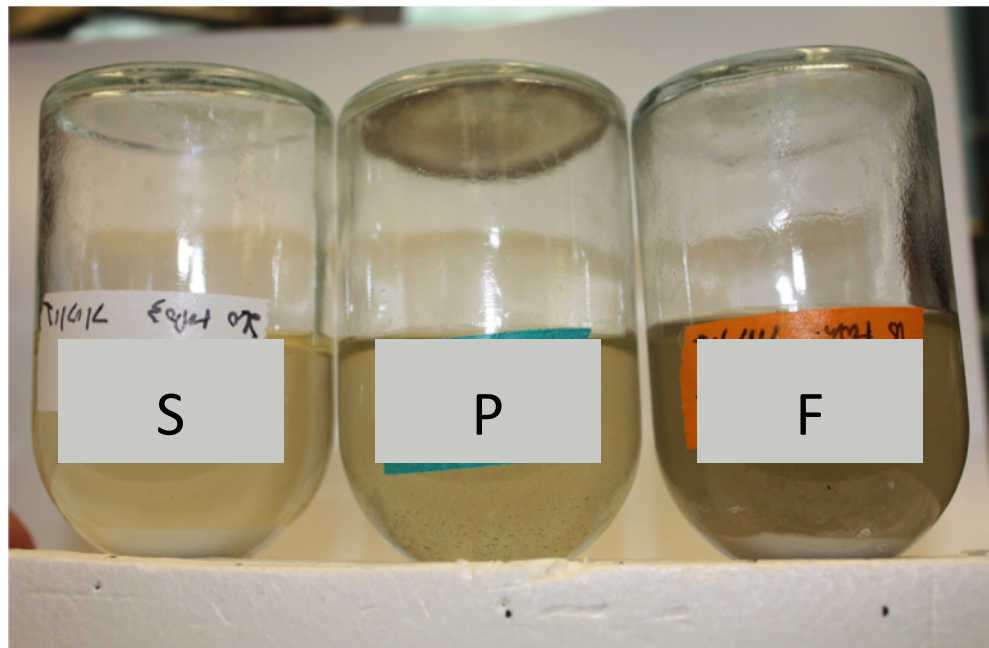
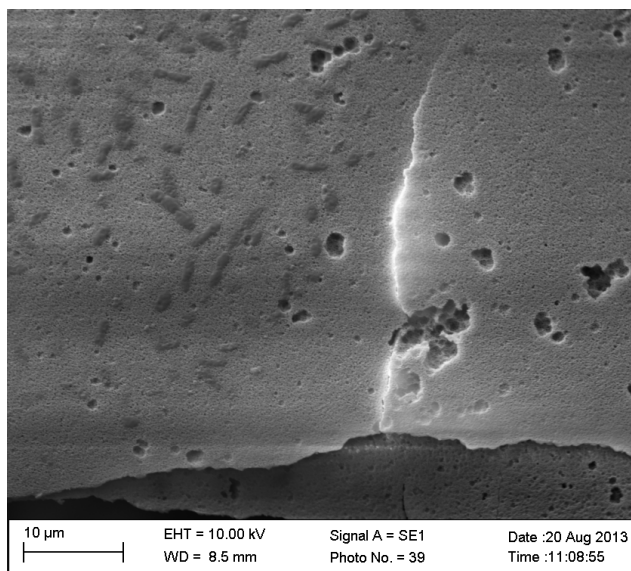


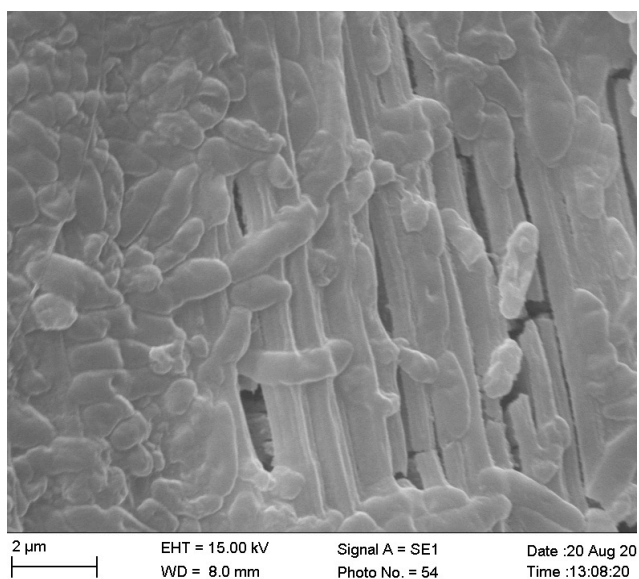
Figure 2.3. DPO-dependent biomineralization by *D. phosphitoxidans* FiPS-3 in minimal media (A) and minimal media plus 50 mM CaCO₃ (B). P = 20 mM phosphite added, F = 20 mM fumarate added, S = sterile control with 20 mM phosphite added. All cultures were grown anaerobically at 30°C with 1 mM phenylalanine and histidine and 10 mM sulfate.

A



Hydroxyapatite - $\text{Ca}_{10}(\text{OH})_2(\text{PO}_4)_6$

B



Struvite - $\text{MgNH}_4\text{PO}_4 \cdot 6\text{H}_2\text{O}$

Figure 2.4. SEM images of phosphate minerals produced during DPO-dependent growth by *D. phosphitoxidans* FiPS-3 in minimal media containing 20 mM CaCl_2 (A) or 20 mM MgCl_2 (B). All cultures were grown anaerobically at 30°C with 1 mM phenylalanine and histidine, 20 mM phosphite, and 10 mM sulfate. Mineral compositions were determined by XRD.

Table 2.1. Expression of *ptx-ptd* genes in *D. phosphitoxidans* FiPS-3 in the presence of phosphite (P) and fumarate (F). RNA counts for each gene were determined by RNAseq and values shown are the average normalized counts of triplicate biological samples for each treatment. Statistical significance of differential expression between the two conditions for each gene was assessed using the DESeq software package. All cultures were grown in minimal media at 30°C with 1 mM phenylalanine and histidine, 10 mM sulfate, and 1 mM phosphate. All cultures were sampled for RNA extraction at mid-logarithmic growth phase (OD₆₀₀ = 0.3-0.4).

Gene	RNA counts (F)	RNA counts (P)	P/F fold change	p-value
<i>ptxE</i>	1.67 ± 0.15 *10 ³	2.88 ± 0.57 *10 ³	1.70	2.03E-05
<i>ptxD</i>	2.11 ± 0.16 *10 ³	3.73 ± 0.32 *10 ³	1.77	1.38E-09
<i>ptdF</i>	1.10 ± 0.17 *10 ⁴	1.32 ± 0.39 *10 ⁶	119.43	3.62E-174
<i>ptdC</i>	3.13 ± 0.04 *10 ³	3.75 ± 0.25 *10 ⁴	11.96	8.15E-231
<i>ptdG</i>	7.20 ± 0.04 *10 ²	5.30 ± 0.58 *10 ³	7.36	3.16E-90
<i>ptdH</i>	1.28 ± 0.10 *10 ³	1.12 ± 0.19 *10 ⁴	8.75	3.54E-76
<i>ptdI</i>	7.90 ± 0.15 *10 ²	6.21 ± 0.90 *10 ³	7.8	3.95E-52

CHAPTER 3

Microbial community analysis and physiological characterization of dissimilatory phosphite-oxidizing wastewater enrichments

(Unpublished data)

INTRODUCTION

Given that *D. phosphitoxidans* strain FiPS-3 was the only known organism capable of DPO, I set out to identify additional organisms capable of this metabolism in order to expand our understanding of this process. I added phosphite to various environmental samples as the sole electron donor and energy source in an effort to enrich for DPO-capable microbes and to analyze the effect of this compound on the microbial communities. Furthermore, in an effort to identify novel organisms capable of coupling phosphite oxidation to carbon fixation, I included CO₂ as the sole electron acceptor in the enrichments. I monitored various enrichments from freshwater sediments, marine sediments, and wastewater treatment digesters for phosphite consumption over the course of a year. Of these, only the enrichments from anaerobic wastewater treatment sludge demonstrated consumption of phosphite and were therefore chosen for community analysis and physiological characterization.

MATERIALS & METHODS

Sampling, media composition, and growth conditions

Sludge samples were obtained from an anaerobic digester operating at 37°C at the East Bay Municipal Utilities District wastewater treatment facility in Oakland, CA. Anaerobic bottles (Bellco, Wineland, NJ) containing 45 mL of basal media were each inoculated with 5 mL of sludge and incubated at 37 °C. The composition of the basal medium (pH = 7) was as follows (per 1 L of distilled water): 5 g NaHCO₃, 12 g HEPES, 1 g NH₄Cl, 0.5 g KCl, 0.5 g L-cysteine HCl, 0.001 g resazurin, and 10 mL each of vitamins and trace minerals (Balch et al. 1979). The media were prepared and dispensed into individual bottles under an N₂/CO₂ (80:20, v/v) headspace, sealed with butyl rubber stoppers, and autoclaved. Bicarbonate-free controls were prepared by omitting NaHCO₃ from the basal media and degassing it with 100% N₂. Phosphite, sulfate, sulfite, and molybdate (Sigma Aldrich) were added from sterile, anaerobic stocks to the basal media as needed. Rumen fluid from fistulated cows fed a high forage diet was obtained from the UC Davis Department of Animal Science (Crofts et al. 2014). Rumen fluid stocks were prepared anaerobically, autoclaved at 121°C for 20 minutes, and added to the basal media as needed. Killed controls were autoclaved at 121°C for 1 hour. Samples for ion chromatography (IC) analysis were filtered and stored at 4°C, while samples for DNA extraction were stored at -80°C. Cell growth was assessed by measuring optical density at 600 nm (OD₆₀₀) using a Cary 50 Bio Spectrophotometer.

Ionic metabolite analysis

Phosphite, phosphate, and sulfate concentrations were measured via ion chromatography using a Dionex ICS 2100 instrument with a Dionex IonPac AS 16 (4 × 250 mm) column (Thermo Fisher Scientific) maintained at 30°C. To improve the separation of the phosphite, phosphate, and sulfate peaks, a gradient elution program was developed in which the mobile phase concentration increased from 12 mM to 35 mM NaOH after 10 minutes. The total run time of the program was 20 minutes with a constant mobile phase flow rate of 1.2 mL/min and a sample injection volume of 25 µL. Background conductivity was suppressed with a Dionex ASRS suppressor set at 100 mA and operating in recycle mode.

DNA Extraction, 16S rDNA Amplicon Library Preparation, and Sequencing

DNA was isolated using the MoBio DNA PowerSoil Kit (MoBio Laboratories). The archaeal and bacterial primer set MiSeq 16S F (5' TCGTCGGCAGC GTCAGATGTGTATAAGAGACAGCAGCAGCMGCCGCGGTAA 3') and MiSeq 16S R (5' GTCTCGTGGGCTCGGAGATGTGTATAAGAGACAGGACTACHVGGGTATCTAATCC 3') was used to amplify a 287 bp segment of the 16S rRNA gene that spans HV region four. These primers were based on primers S-D-Arch-0519-a-S-15 (A519F) and S-D-Bact-0785-a-A-21 (Bakt_805R) (Klindworth et al. 2012) but include the necessary Illumina adapters. PCR amplification and library preparation were carried out as described previously (Carlström et al., 2016). Samples were sent to the UC Davis Genome Center for sequencing on an Illumina MiSeq using the MiSeq V2 reagent kit (2 x 250 bp) and software version MiSeq 2.4.1.

Community Analysis

Illumina amplicon reads were analyzed as described previously (Carlström et al., 2016). Briefly, Mothur v. 1.3.3 (Schloss et al. 2009) was used to cluster reads into OTUs based on a 3% dissimilarity threshold and then generate a table of relative abundances and taxonomic identities for each OTU. Abundance data were normalized by the total number of reads in each sample and analyzed using the statistical program PRIMER 7 (PRIMER-E Ltd, Plymouth, UK) (Clarke et al. 2008). The data were square root transformed and Bray-Curtis similarity matrices were created. Clustering amongst samples was assessed using group average hierarchical clustering and nonmetric multidimensional scaling (NMDS) (Clarke 1993). Similarity profile analysis (SIMPROF) (Clarke et al. 2008) was used as a statistical measure to determine significance of the groupings identified in the NMDS. Similarity percentage (SIMPER) (Clarke 1993) was used to determine the OTUs contributing to the top 10% of differences between the groups. Permutational analysis of variance (PERMANOVA) (Anderson 2001) was used to determine significance of differences in community composition between different treatments.

OTU 21-specific 16S rRNA gene qPCR

Full-length 16S rRNA gene sequences were PCR amplified from genomic DNA extracted from enrichments grown on phosphite and rumen fluid using the universal primers 27F and 1525R (Weisburg et al. 1991). A clone library of these sequences was prepared using the TOPO TA Cloning Kit (Invitrogen) and 16S rRNA gene inserts from 20 clones were PCR amplified using primers M13 F and M13 R. The inserts were Sanger sequenced at the UC Berkeley DNA Sequencing Facility and compared to the partial 16S rRNA gene of OTU 21 using BLAST in order to identify a matching full sequence (Appendix 3.1a). The full OTU 21 16S rRNA gene was then used to design 16S rDNA qPCR primers specific to OTU 21 using the selective primer design software tool PRISE2 (Huang et al. 2014). The primer set F4 (5' ACGTAGGCGGATTGGTAAGT 3') and R2 (5' TACTCATCGTTACGGCGTG 3') was experimentally validated by running a conventional PCR using genomic DNA from phosphite-oxidizing enrichments. Sanger sequencing of PCR products from this test reaction confirmed that only the Phox-21 16S rRNA gene was amplified. Real time PCR assays were then performed using the Thermo Scientific Maxima SYBR Green/ROX qPCR kit. Template DNA (5 uL) was used in a reaction mixture containing 12.5 uL 2X Master Mix, 0.6 uL of each forward and reverse Phox-21 16S primer, and water to a final volume of 25 uL. Reaction conditions were 95 °C, 15 min; 35 cycles of 95 °C, 15 s; 60°C, 30 s; and 72°C, 30 s; and a final extension of 72°C, 10 min. Standard curves were generated using purified plasmids containing Phox-21 16S rDNA serially diluted to cover a range of DNA concentrations from 4.5×10^9 copies to 4.5×10^2 copies. All samples and standards were run in duplicate.

Phylogenetic Analysis of OTU 21

The full OTU 21 16S rRNA gene sequence from the clone library described above was designated as clone Phox-21 and compared to the NCBI nucleotide database using BLAST in order to identify the top 100 hits among cultured isolates as well as uncultured clones. Representative 16S rRNA gene sequences from top BLAST hits as well as other taxa of interest were chosen for phylogenetic analysis (Appendix 3.2). The Silva aligner (Pruesse et al. 2007)

was used to align selected sequences, and a maximum likelihood phylogenetic tree was constructed with 1,000 bootstrap resamplings using RAxML-HPC (Stamatakis 2006). Taxa represented in the Silva reference database were classified based on their Greengenes taxonomic assignments (McDonald et al. 2012).

Nucleotide Sequence Accession Numbers

The 16S rRNA gene sequence of clone Phox-21 is available on GenBank under accession number KU898264. MiSeq sequencing reads from all samples are deposited in the NCBI Sequencing Read Archive (SRA) under accession number SRP071909.

RESULTS

Phosphite oxidation occurred in enrichments and affected the microbial community composition

Wastewater sludge enrichments were able to completely oxidize 10 mM phosphite after 29 weeks of incubation (Figure 3.1a). The average overall rate of phosphite oxidation in the cultures was 50 ± 1 $\mu\text{M}/\text{day}$. However, the rate of phosphite oxidation increased over time from 14 ± 3 $\mu\text{M}/\text{day}$ during the first 8 weeks, to 32 ± 4 $\mu\text{M}/\text{day}$ from weeks 8 to 15, then to 70 ± 23 $\mu\text{M}/\text{day}$ from weeks 15 to 22, and finally to 90 ± 23 $\mu\text{M}/\text{day}$ from weeks 22 to 29. The oxidation of phosphite was accompanied by a stoichiometric increase in the phosphate concentration in the media, from 2 ± 0.03 mM initially to 12 ± 1.59 mM after 29 weeks. No oxidation of phosphite or accumulation of phosphate was seen in the autoclaved controls over the same time period (Figure 3.1a).

DNA samples were collected at 0, 20, and 29 weeks after inoculation (Figure 3.1a) and analyzed for microbial community composition. Hierarchical clustering analysis based on 16S rRNA taxonomic identities indicated that the initial, phosphite fed, and no donor cultures each formed distinct clusters at a 75% similarity threshold (Figure 3.1b). The compositions of phosphite-oxidizing communities were significantly different from those of the no donor communities ($p = 0.002$, pairwise PERMANOVA). Since the samples collected at 20 and 29 weeks grouped together by treatment, reads from both time points were pooled together and average OTU abundances (normalized by total reads per sample) were calculated for each treatment (Figure 3.2a). There were 20 OTUs with abundances of 1% or more under both conditions, which combined made up $63.2 \pm 25.8\%$ of the phosphite fed population and $64.4 \pm 37.1\%$ of the no donor population. Additionally, there were 3 OTUs that were prevalent ($\geq 1\%$) only in the phosphite fed cultures and 4 OTUs that were prevalent only in the no donor controls. The OTUs prevalent only in the phosphite cultures were OTU 21 (*Proteobacteria*, $4.4 \pm 2.4\%$), OTU 28 (*Thermovirga*, $1.3 \pm 0.7\%$), and OTU 33 (*Desulfomonile*, $1.0 \pm 1.0\%$). The OTUs prevalent only in the absence of phosphite were OTU 34 (*Blastopirellula*, $2.9 \pm 2.2\%$), OTU 35 (*Methanosaeta*, $2.1 \pm 0.9\%$), OTU 36 (*Syntrophorhabdus*, $1.3 \pm 0.8\%$), and OTU 37 (*Bellilinea*, $1.1 \pm 0.6\%$).

SIMPER analysis revealed 12 OTUs contributing to the top 10% of dissimilarity between the phosphite and no donor samples. Of these, 6 OTUs had higher abundances in the presence of phosphite and were also prevalent under one or both treatments (Figure 3.2b). The 3 OTUs that were prevalent only on phosphite were also the most highly enriched, with OTU 33 being enriched by $1,891.5 \pm 1.7$ fold, OTU 21 by 15.2 ± 0.4 fold, and OTU 28 by 5.9 ± 0.5 fold. The 3 OTUs that were prevalent under both treatments had lower fold differences, with OTU 10 (*Bacteria*) being enriched by 2.3 ± 0.2 fold, OTU 6 (*Anaerobaculum*) by 1.7 ± 0.5 fold, and OTU 4 (*Firmicutes*) by 1.6 ± 0.7 fold.

Phosphite oxidation rates and community composition were affected by rumen fluid and molybdate

Although OTU 33 (*Desulfomonile*) constituted a lower percentage of the final phosphite-oxidizing community compared to OTUs 21 and 28, it demonstrated the highest degree of

enrichment (fold change) on phosphite. The best studied member of the *Desulfomonile* genus, *D. tiedjei* strain DCB-1, was isolated from mesophilic wastewater sludge enrichments grown on 3-chlorobenzoate and sulfate in media containing 5% rumen fluid (Shelton & Tiedje 1984; Deweerdt et al. 1990). We therefore decided to passage our enrichments into media amended with 5% rumen fluid and after several transfers we saw a substantial increase in phosphite oxidation rates. Cultures containing rumen fluid oxidized phosphite at an average rate of $480 \pm 10 \mu\text{M/day}$ compared to $79 \pm 36 \mu\text{M/day}$ in cultures with no rumen fluid (Figure 3.3a) (t test, $p < 0.0001$). Compared to the original enrichments (Figure 3.1a), the rumen fluid amended cultures showed approximately a 10-fold increase in the rate of phosphite oxidation (t test, $p < 0.0001$). Additionally, we decided to test the effect of molybdate on our enrichments, since growth of the sulfate reducing DCB-1 was inhibited by molybdate concentrations as low as 2 mM (Deweerdt et al. 1990). Indeed, when 5 mM molybdate was added to cultures containing 5% rumen fluid, the average phosphite oxidation rate dropped to $35 \pm 12 \mu\text{M/day}$ (Figure 3.3a), indicating a strong inhibitory effect compared to the cultures with no molybdate (t test, $p < 0.0001$).

Samples were collected at 0, 5, 11, 16, and 19 days (Figure 3.3a) and a 16S rRNA community analysis was performed as previously described. NMDS based on Bray Curtis dissimilarity showed that the samples grouped into 9 distinct clusters at an 87% similarity threshold (Figure 3.3b), which was the highest similarity level at which all the initial samples grouped together. After 5 days, all of the cultures had diverged from the initial community. Most of the cultures containing rumen fluid converged towards similar community compositions, although those containing molybdate formed a distinct cluster. The cultures containing phosphite but no rumen fluid, however, moved towards a very different composition early on. Over time, the cultures containing phosphite in addition to rumen fluid began separating from the other cultures, forming a distinct cluster by day 11, which then further diverged and appeared to stabilize by day 16. The phosphite only cultures likewise continued to diverge after the first 5 days, although they appeared to stabilize by day 11. In contrast, the majority of the rumen fluid only and the molybdate containing cultures stabilized after the first 5 days, although there were several outliers that continued to diverge. Overall, it appears that rumen fluid was the main determinant of community composition early on, but phosphite caused a major shift in composition between days 5 and 16. However, the presence of molybdate was enough to prevent this phosphite-induced shift.

The changes in taxonomic composition that underlie these trends can be seen in Figure 3.4. Only 11 OTUs were prevalent under one or more treatments and together they accounted for 96-98% of the total community under all treatments. Interestingly, no reads belonging to OTU 33 or OTU 28 were detected in any of the cultures derived from the rumen fluid amended enrichments, even though these taxa had shown large increases in abundance in the original enrichments. Instead, the initial cultures were dominated by two OTUs, which together made up approximately 75% of the total community. One of these was OTU 21 ($39.1 \pm 2.5\%$) and the other was OTU 38 (*Tepidanaerobacter*, $33.7 \pm 2.2\%$). Under all treatments OTU 21 decreased initially, with a concomitant increase in OTU 19 (*Thermotogaceae*), OTU 40 (*Bacteria*), and OTU 41 (*Petrimonas*). However, only when both phosphite and rumen fluid were present and active phosphite oxidation was observed did the abundance of OTU 21 rise to $34.8 \pm 2.3\%$ by day 19 (Figure 3.4a). In all other conditions, OTU 21 continued to decline and ended up accounting for only $6.7 \pm 4.0\%$ of the final communities (Figure 3.4b-d). Not surprisingly, OTU 21 was the

taxon with the greatest increase in abundance on phosphite and rumen fluid compared to rumen fluid only at day 19 (Figure 3.5a). Three other taxa also increased significantly on phosphite and rumen fluid compared to rumen fluid only, but the \log_2 fold difference of OTU 21 (2.09 ± 0.10) was twice as high as that of OTU 39 (*Petrimonas*, 1.01 ± 0.16) and OTU 25 (*Coprothermobacter*, 1.01 ± 0.05), and five times higher than that of OTU 42 (*Aminobacterium*, 0.42 ± 0.12). On the other hand, only OTUs 21 and 42 showed significant decreases in abundance in the presence of molybdate, with a \log_2 fold difference of -3.68 ± 1.24 for OTU 21 and of -3.23 ± 0.31 for OTU 42 (Figure 3.5b). In fact, several OTUs actually had higher relative abundances in the presence of molybdate, suggesting that susceptibility to molybdate inhibition varied widely within the community.

Phosphite oxidation in our enrichments drives growth of OTU 21 and requires carbon dioxide but cannot be coupled to sulfate reduction

In order to determine if phosphite oxidation was coupled to microbial growth in our enrichments, we inoculated a new set of rumen fluid amended cultures and measured optical density (ODU = optical density unit) and phosphite concentration over time (Figure 3.6a). Significantly higher growth rates were observed in cultures containing phosphite (0.0093 ± 0.0012 ODU/day) compared to the no phosphite controls (0.0030 ± 0.0015 ODU/day) (t test, $p = 0.0012$) (Figure 3.6a). The enhanced growth of phosphite-fed cultures closely mirrored the trend observed for phosphite oxidation, indicating that although rumen fluid alone was capable of sustaining some limited growth, phosphite oxidation accounted for the majority of the growth observed in our cultures. Furthermore, we performed quantitative PCR (qPCR) using 16S rDNA primers specific to OTU 21 in order to assess the absolute abundance of this organism during phosphite-dependent growth (Figure 3.6b). Significantly higher growth rates were observed for OTU 21 in the presence of phosphite (1.2×10^9 16S rDNA copies / mL*day) compared to the no phosphite controls (7.3×10^2 16S rDNA copies / mL*day) (t test, $p = 0.0008$) and its growth co-occurred with the oxidation of phosphite (Figure 3.6b).

Given that carbon dioxide was the sole electron acceptor in the growth media, we surmised that phosphite oxidation was being coupled to carbon dioxide reduction in our system. In support of this hypothesis, cultures grown in bicarbonate-free media under an 80% N₂ / 20% CO₂ headspace readily oxidized 8 mM phosphite within 21 days, whereas no phosphite oxidation was seen during the same period in cultures grown under a 100% N₂ headspace (Figure 3.7a). Since *D. phosphitoxidans* FiPS-3 is able to couple DPO to sulfate reduction and our culture was sensitive to molybdate, a known specific inhibitor of sulfate reduction (Peck 1959; Taylor & Oremland 1979; Carlson et al. 2015), we thought that the addition of sulfate to our cultures would further enhance phosphite oxidation and growth. However, there was no significant difference in phosphite oxidation rates between enrichments containing phosphite and 2 mM sulfate (659 ± 28 μ M/day) and those containing phosphite only (635 ± 17 μ M/day) (t test, $p = 0.2458$) (Figure 3.7b). Additionally, sulfate concentrations remained constant throughout the growth period, demonstrating that sulfate reduction did not occur in the cultures. We also tested the effect of sulfite, since sulfate reducers should be capable of alternatively reducing sulfite (Barton & Fauque 2009). Interestingly, complete inhibition of phosphite oxidation was seen in the presence of 2 mM sulfite (Figure 3.7b).

The putative phosphite-oxidizing bacterium in our enrichments belongs to a candidate order within the Deltaproteobacteria

The community dynamics and growth data discussed above (Figures 3.4-3.6) strongly suggested that OTU 21 was the organism responsible for phosphite oxidation in our enrichments. In order to get a better sense of the phylogenetic identity of OTU 21, we obtained its full 16S rRNA gene sequence, confirmed that it matched the partial 16S rRNA sequence from our community analysis (Appendix 3.1a), and constructed a maximum likelihood phylogenetic tree (Figure 3.8). Our tree placed OTU 21 (henceforth designated as clone Phox-21) within the GW-28 clade, which is a candidate order within the *Deltaproteobacteria*, according to the Greengenes taxonomy (McDonald et al. 2012). Its closest relatives were all uncultured clones from engineered environments similar to the one sampled in this study, such as anaerobic wastewater and food waste digesters. However, several clones from natural environments, such as estuarine sediments (Er-LAYS-74), peat wetlands (BSN045), and sinkhole biomats (CAR8MG52) also claded within the GW-28 (Figure 3.8). All the taxa within this clade had at least 92% 16S rRNA sequence identity to OTU 21, including four clones with $\geq 97\%$ identity: POMEbac42 (98%), De3155 (97%), GW-28 (97%), and QEEB2BG06 (97%). Additionally, there were five clones with 90-91% identity to OTU 21 that were unclassified at the order level and whose placement within the GW-28 was uncertain. Interestingly, this unclassified group included clones from hydrothermal vents (GUAY_37enr_Bac71, BAC2_26, and MS12-1-F09), deep sinkhole biomats (Z273MBM77), and hydrocarbon-degrading sediments (E32) (Figure 3.8). Based on their placement within our tree, several taxa from the *Desulfovibrionales* (84-85% 16S rRNA identity) appeared to be the closest relatives of Phox-21 among cultured isolates. However, isolates with 84-85% identity were also found within the *Desulfuromonadales*, *Desulfobacterales*, *Syntrophobacterales*, and *Myxococcales*. FiPS-3, a member of the *Desulfobacterales*, had only 83% identity to Phox-21.

DISCUSSION

The oxidation of phosphite in our enrichments was clearly a biologically mediated process. Killed controls showed no phosphite oxidation even after 29 weeks and the rate of phosphite oxidation increased over time. The persistence of phosphite under abiotic conditions is congruent with its kinetic stability resulting from the high activation energy needed to break the P-H bond in the phosphite molecule (Pasek 2008). Moreover, the extent of phosphite oxidation observed in our enrichments is evidence of a dissimilatory process involved in energy metabolism as opposed to a purely assimilatory process. Phosphate accumulated in the media over time at a rate that corresponded to that of phosphite depletion and reached a final concentration that matched the amount of phosphite consumed (~10 mM). Assuming a phosphorus content of ~30 fg/cell (Fagerbakke et al. 1996), a bacterial culture would have to assimilate only about 300 μM phosphate in order to reach a density of $\sim 1 \times 10^9$ cells/mL. This means that the phosphite consumed in our enrichments far exceeded what would have been required for use as a phosphorus source. In fact, there was more than enough phosphate initially present in the cultures (~2 mM) to fulfill the phosphorus needs of growing cells in the absence of phosphite supplementation.

The fact that microbial growth rates were significantly higher in phosphite-oxidizing cultures compared to no-phosphite controls provides further evidence that phosphite was acting as an electron donor and energy source for cellular metabolism. Phosphite oxidation and growth only occurred in media amended with CO_2 and/or HCO_3^- indicating that DPO was coupled to CO_2 reduction, as has been shown for FiPS-3 (Schink et al. 2002). The rates of phosphite oxidation seen in our rumen fluid amended enrichments are comparable to those seen in cultures of FiPS-3 (Figure 2.1). However, our enrichments were incubated at 37°C and FiPS-3 can only grow at temperatures between 15 and 30°C (Schink et al. 2002). Indeed, our microbial community analysis confirmed the absence of any 16S rDNA reads belonging to the *Desulfotignum* genus in our enrichments. There was, however, a clear shift in community composition in the presence of phosphite, with OTU 33 (*Desulfomonile*), OTU 21 (*Proteobacteria*), and OTU 28 (*Thermovirga*) being the most enriched taxa.

Addition of rumen fluid to the enrichments greatly enhanced the rate of phosphite oxidation and also substantially altered the microbial community composition. Interestingly, OTUs 33 and 28 were no longer observed in the community. Instead, OTU 21 (subsequently renamed Phox-21) was further enriched to about 40% of the total community. The tight correlation seen between phosphite oxidation and Phox-21 abundance strongly supports its functional role in DPO. It remains unclear why OTUs 33 and 28 were enriched in our original cultures but not in the presence of rumen fluid. Given that rumen fluid was added to the cultures in an attempt to enhance the growth of OTU 33, its decline was particularly surprising. It is possible that these organisms benefited from the presence of phosphite under low-nutrient conditions, but were then outcompeted when nutrient-rich rumen fluid was added. Also, the fact that these taxa had very low initial abundances means that even moderate amounts of growth would have led to large increases in fold change, which would have magnified the effect of any ancillary growth benefits that these organisms may have received. In any case, the addition of rumen fluid did enhance the growth of Phox-21, which was an unexpected outcome, but perhaps not too surprising given the rich variety of nutrients and cofactors present in rumen fluid (Saleem et al. 2013).

The strong inhibitory effect of molybdate on phosphite oxidation and Phox-21 abundance in a culture not dependent on sulfate reduction was likewise unexpected, since molybdate is known to be a potent and selective inhibitor of sulfate reduction. It acts as a futile substrate for the enzyme ATP sulfurylase, resulting in depletion of the cell's ATP pool (Peck 1959; Taylor & Oremland 1979; Carlson et al. 2015). However, the addition of sulfate did not enhance phosphite oxidation, stimulate sulfidogenesis, or enhance the growth of Phox-21. It is possible that molybdate is targeting the phosphite oxidation pathway directly or affecting some other unrelated pathway, but further work is needed in order to confirm the mechanism of inhibition. Sulfite also appears to inhibit phosphite oxidation, which is further evidence of a potential incompatibility of the sulfate reduction pathway and phosphite oxidation in our enrichment. It is not clear whether the inhibition by sulfite was due to a direct interaction with the phosphite oxidation pathway or to a broader toxicity. PtxD, the phosphite oxidase found in FiPS-3 as well as in most APO-capable bacteria, is known to be inhibited by sulfite in vitro (Costas et al. 2001; Relyea & van der Donk 2005). This enzyme, if present in Phox-21, would be a likely target of sulfite inhibition. However, sulfite is also known to have a broad antimicrobial activity at concentrations as low as 600 μM (Gould & Russell 2003), which may have also played a role in its inhibition.

Phox-21 belongs to the GW-28 candidate order, a poorly studied clade within the *Deltaproteobacteria* with no known cultured representatives. Its closest relatives (16S rRNA sequence identities $\geq 97\%$) are all uncultured clones from different anaerobic waste treatment sites. Clone GW-28 was found in a household biogas digester in China (unpublished), clone POMEbac42 was found in a food waste digester in Singapore (unpublished), clone De3155 was found in alkaline landfill leachate sediment in China (Liu et al. 2011), and clone QEEB2BG06 was found in a mesophilic wastewater digester in Germany (Rivière et al. 2009). Other related taxa (16S rRNA sequence identities 90-95%) include uncultured clones from a variety of engineered and natural environments, including: wastewater digesters in France and the United States, estuarine sediments in Taiwan, peat wetlands in Japan, sinkholes in Mexico, and hydrothermal vents in the Pacific Ocean (Appendix 3.2). Whether or not the capacity for DPO is a common feature of this clade remains to be seen, as there is evidence of lateral acquisition of phosphite oxidation genes in FiPS-3 (Poehlein et al. 2013) as well as in several APO-capable bacteria (White & Metcalf 2007; Martinez et al. 2011). Indeed, whether Phox-21 itself is capable of growth by DPO coupled to CO_2 reduction in pure culture has yet to be confirmed, since efforts to isolate this organism have so far proven unsuccessful.

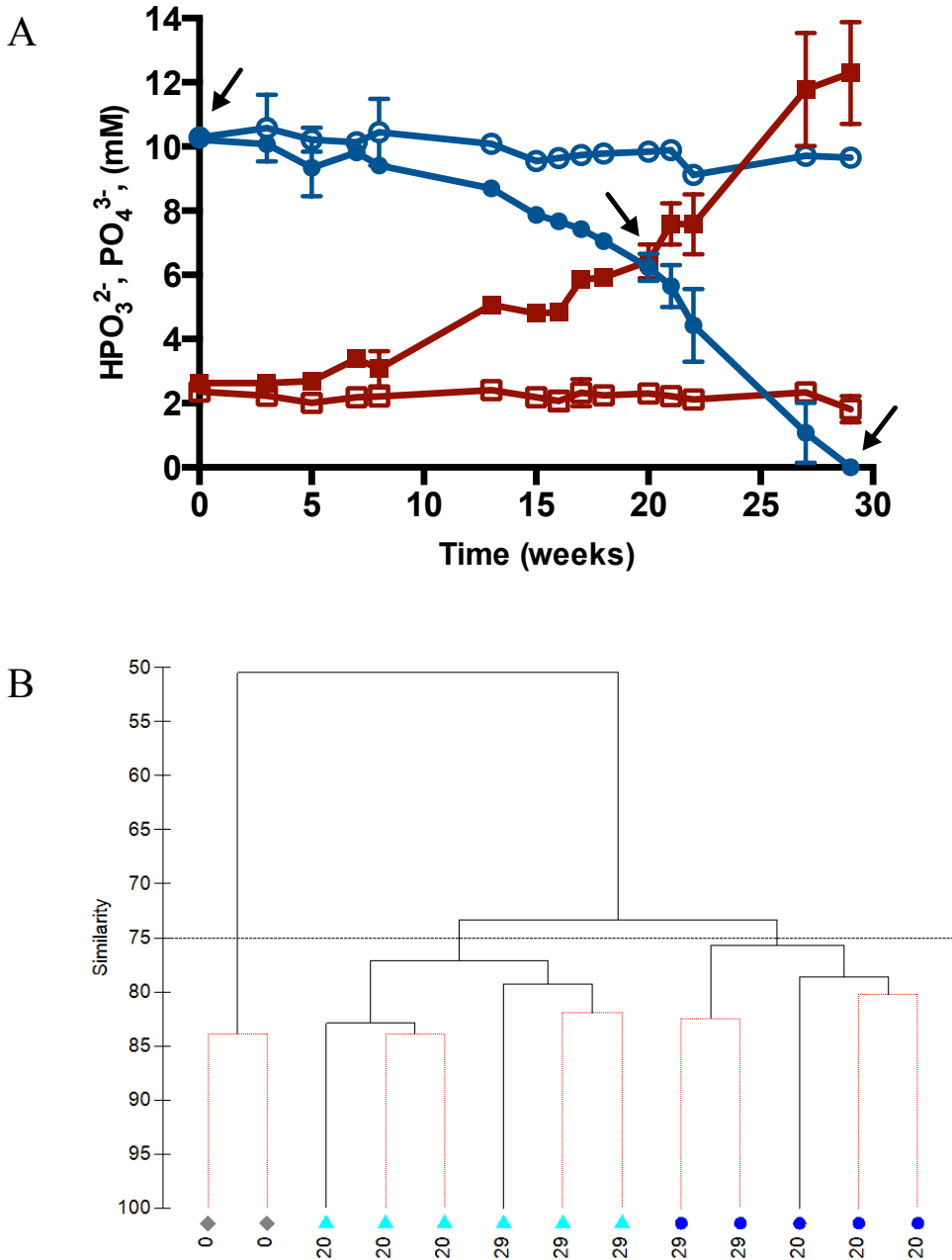


Figure 3.1. A. Phosphite oxidation by wastewater sludge enrichments. Phosphite concentrations in live cultures (closed blue circles) and killed controls (open blue circles). Phosphate concentrations in live cultures (closed red squares) and killed controls (open red squares). Data points represent the average of triplicate cultures, with error bars denoting one standard deviation. Arrows indicate time points at which DNA samples were obtained for community analysis. **B.** Hierarchical clustering of microbial communities depicted in panel A based on Bray Curtis similarity. Initial cultures (gray diamonds), phosphite-fed cultures (dark blue circles), and no donor controls (light blue triangles). Numbers under each symbol indicate the week the sample was collected. Solid black lines denote branches with significant differences, while dotted red lines denote branches with non-significant differences.

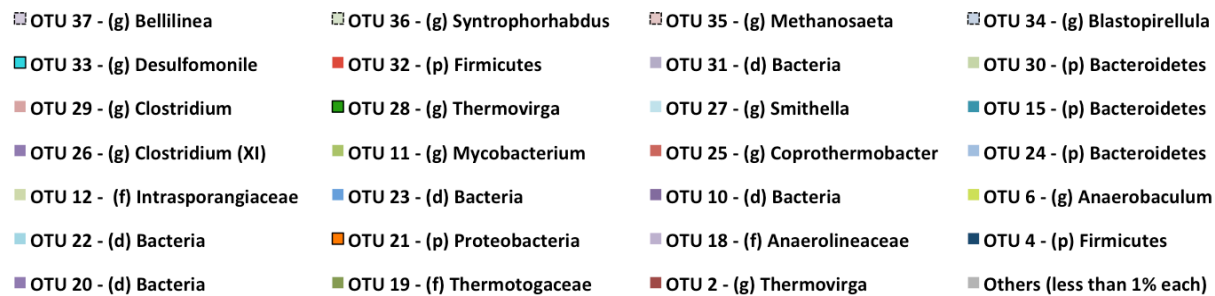
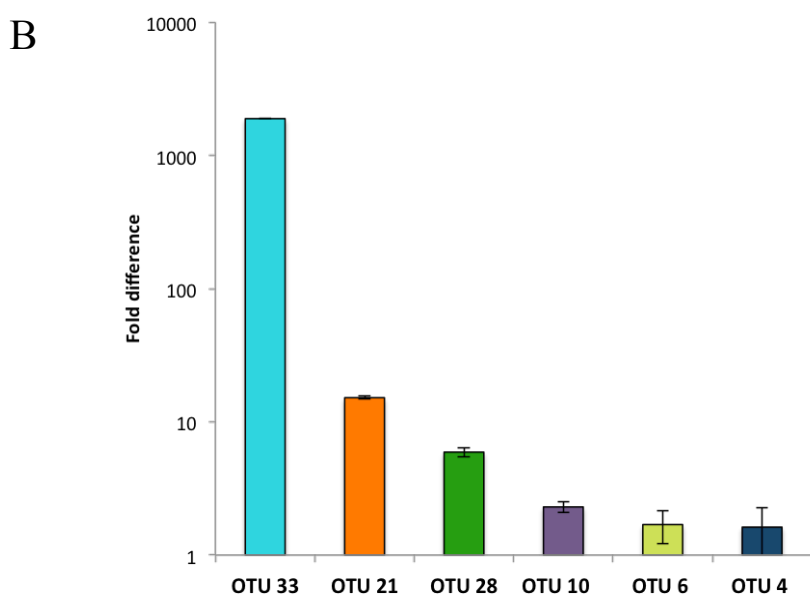
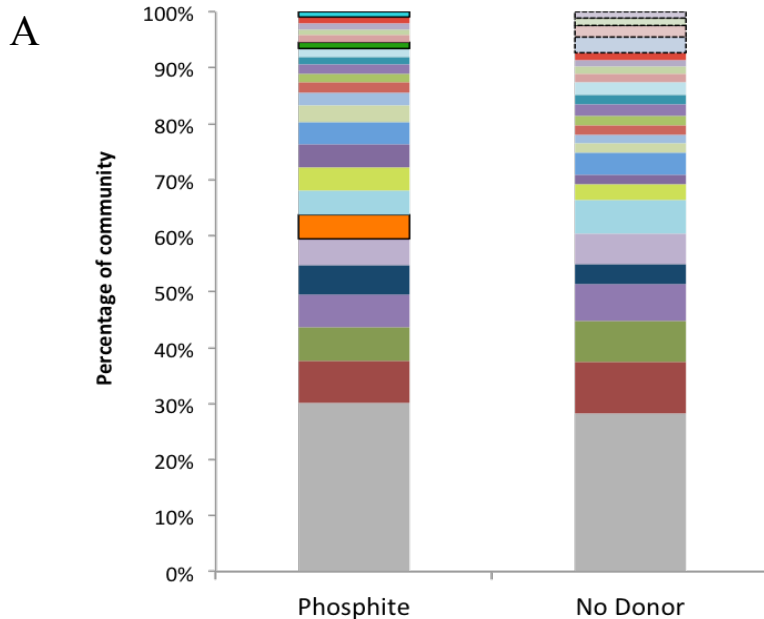


Figure 3.2. A. Taxonomic composition of microbial communities in phosphite-fed cultures and no donor controls. Each OTU with average normalized abundances $\geq 1\%$ of the community under either treatment (including samples at 20 and 29 weeks) is labeled according to the lowest taxonomic rank assigned to it by Mothur: d=domain, p=phylum, f=family, g=genus. Solid boxes denote OTUs with abundances $\geq 1\%$ only in phosphite-fed cultures, while dotted boxes denote OTUs with abundances $\geq 1\%$ only in no donor controls. **B.** Differences in abundance of the most highly enriched OTUs under phosphite-oxidizing conditions. Similarity percentage (SIMPER) analysis was used to identify the OTUs that contribute to the top 10% of disparity between each set of treatment samples. The fold difference of each of these OTUs was calculated by dividing its average normalized abundance in phosphite-fed cultures (n=5) by that in no donor controls (n=6), with error bars denoting one standard deviation.

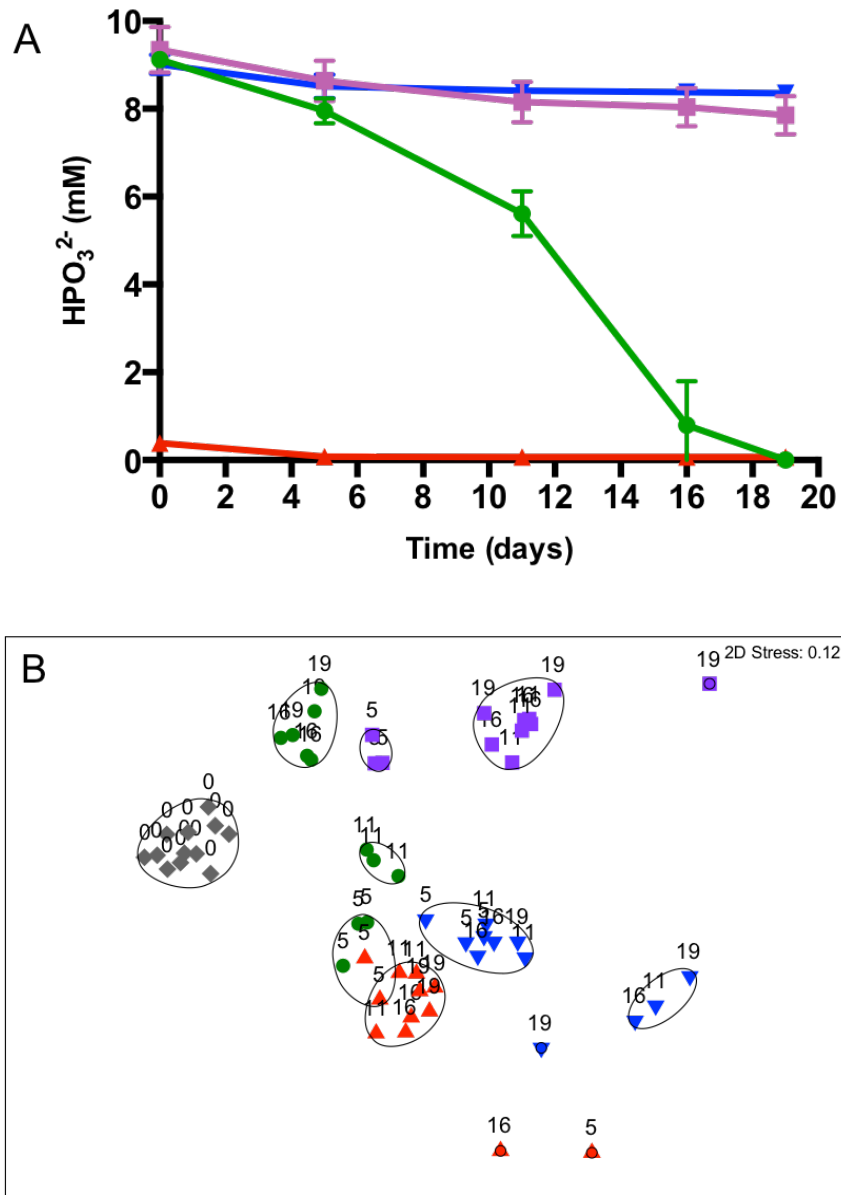


Figure 3.3. A. Phosphite oxidation by cultures derived from enrichments amended with rumen fluid. Phosphite concentrations in cultures containing 9 mM phosphite and 5% rumen fluid (green circles); 9 mM phosphite only (purple squares); 9 mM phosphite, 5% rumen fluid, and 5 mM molybdate (blue inverted triangles); and 5% rumen fluid only (red triangles). Data points represent the average of triplicate cultures, with error bars denoting one standard deviation. DNA samples for community analysis were obtained for all data points. **B.** Nonmetric multidimensional scaling (NMDS) plot of microbial communities depicted in panel A based on Bray-Curtis similarity. All symbols are as described above except for those depicting initial samples (gray diamonds). Numbers next to each symbol indicate the day the sample was collected. Circles denote samples that group together at an 87% similarity threshold.

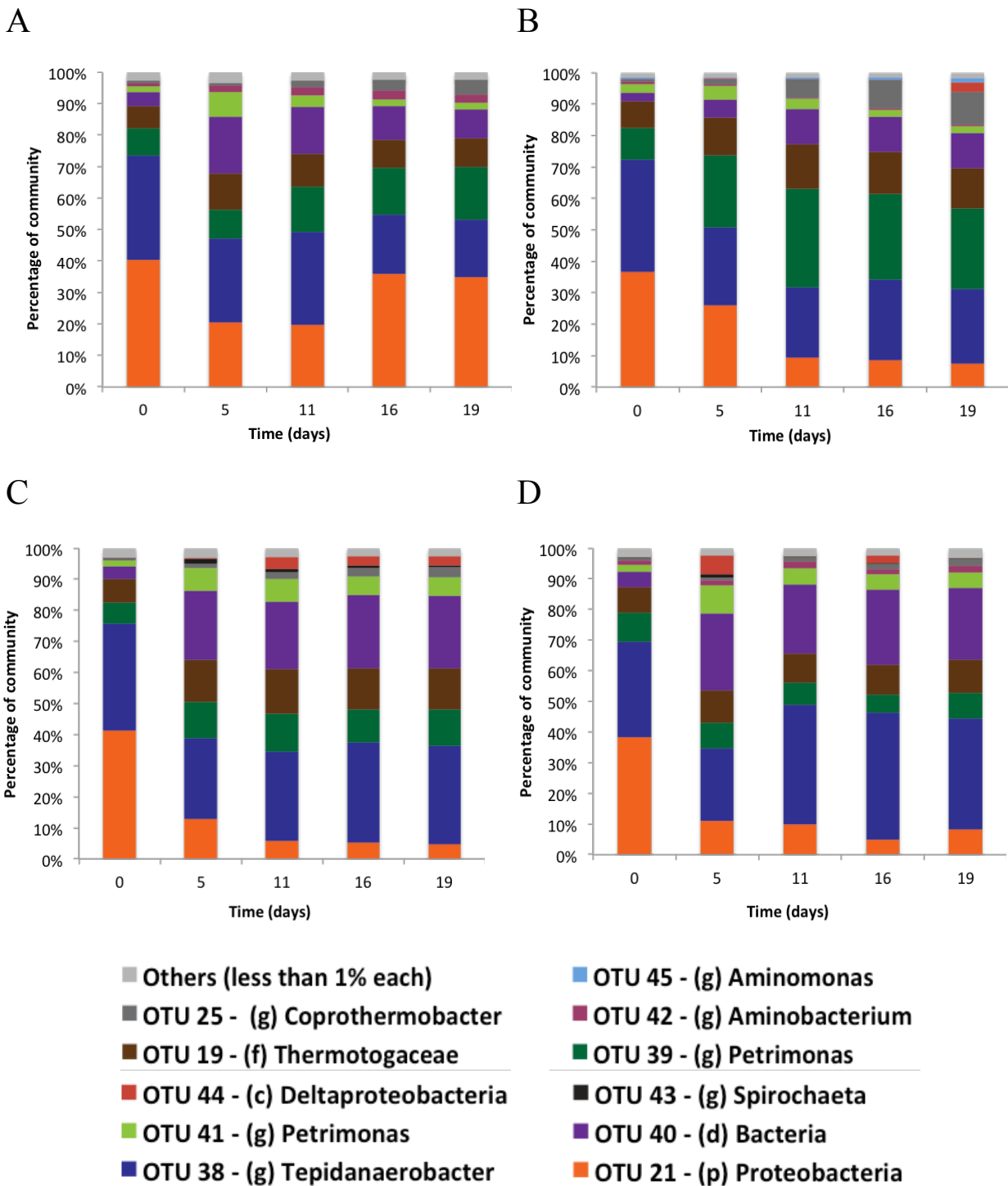


Figure 3.4. Taxonomic composition of microbial communities in cultures containing 9 mM phosphite and 5% rumen fluid (A); 9 mM phosphite only (B); 9 mM phosphite, 5% rumen fluid, and 5 mM molybdate (C); and 5% rumen fluid only (D). Each OTU with an average normalized abundance $\geq 1\%$ of the community under any treatment is labeled according to the lowest taxonomic rank assigned to it by Mothur: d=domain, p=phylum, c=class, f=family, g=genus.

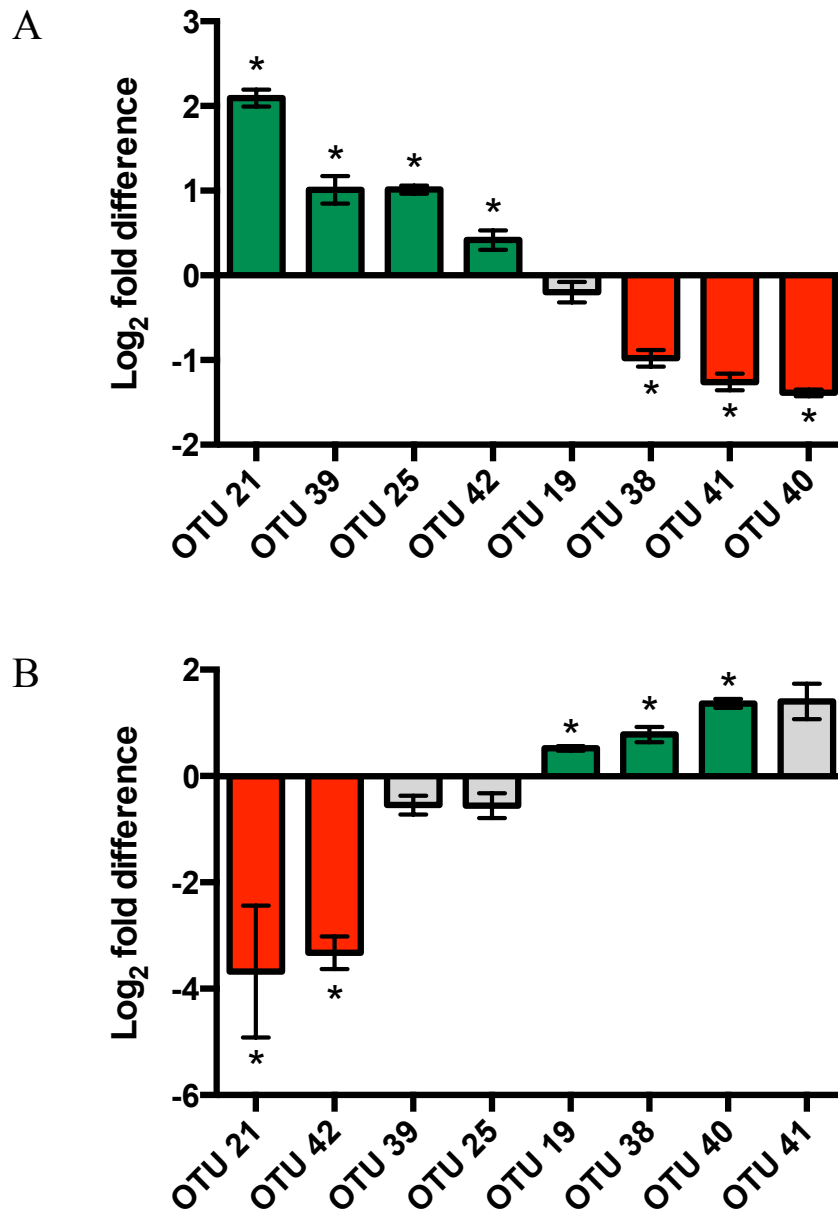


Figure 3.5. Differences in abundance of OTUs in response to phosphite (A) and molybdate (B). The normalized abundances at 19 days of each of the top ($\geq 1\%$) OTUs present in all treatments were log₂ transformed and averaged (n=3 for all treatments). Fold difference values depicted in panel A were calculated by dividing the abundances in phosphite + rumen fluid cultures by those in rumen fluid only cultures. Fold difference values depicted in panel B were calculated by dividing the abundances in phosphite + rumen fluid + molybdate cultures by those in phosphite + rumen fluid cultures. Error bars denote the standard error of the mean. Asterisks denote OTUs with significant ($p < 0.05$) differences between the two comparison treatments as determined by a pairwise t-test (green = positive fold difference, red = negative fold difference).

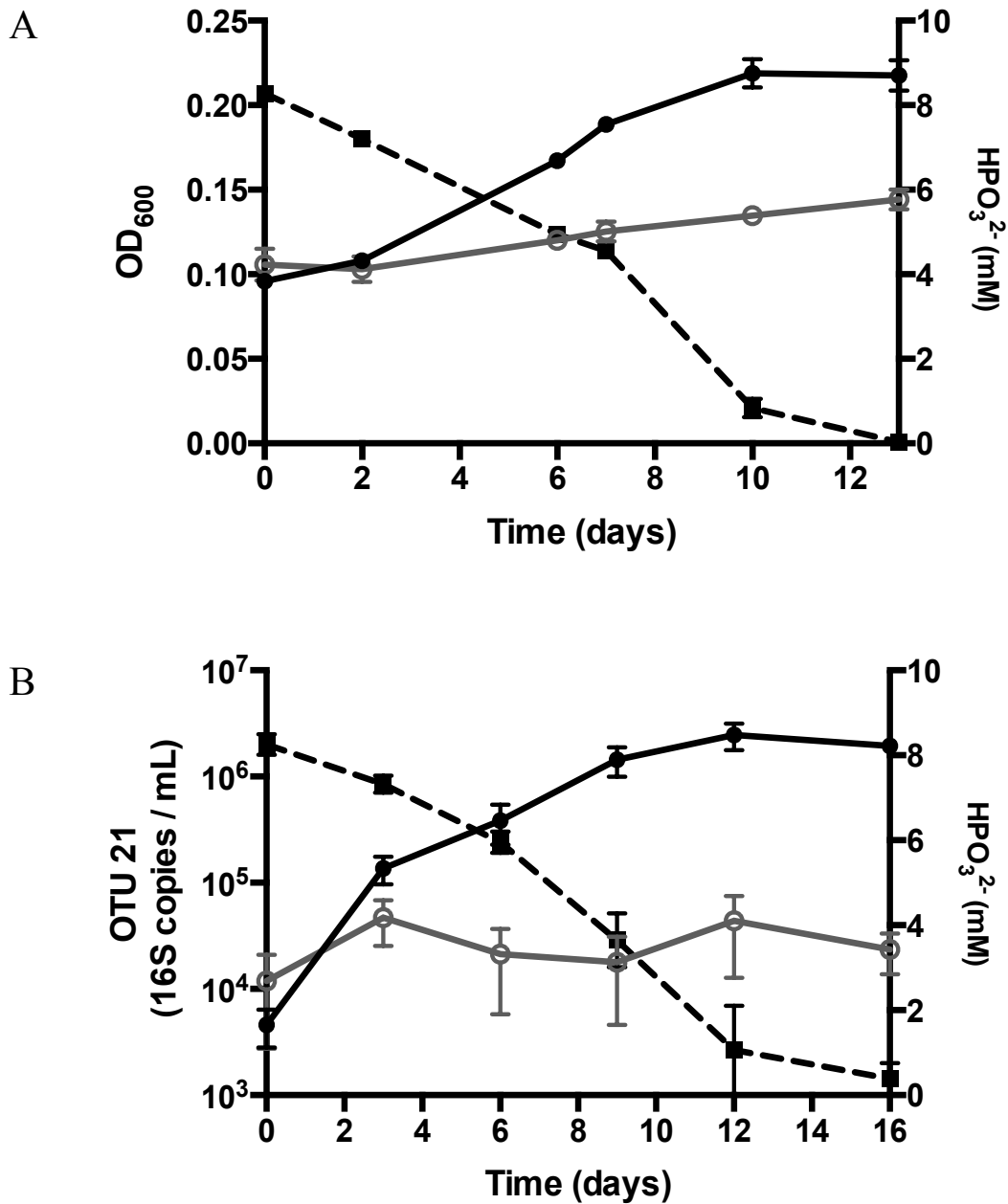


Figure 3.6. Optical density at 600 nm (A) and OTU 21 16S rDNA copy number (B) in enrichment cultures containing either 8 mM phosphite and 5% rumen fluid (closed black circles) or 5% rumen fluid only (open gray circles). Black squares with dotted lines indicate phosphite concentrations in phosphite-containing cultures. OTU 21 16S copy numbers were determined by qPCR using taxon-specific primers (see materials and methods) and normalized by the total volume of culture sampled for DNA extraction. All data points represent the average of triplicate cultures, with error bars denoting the standard error of the mean.

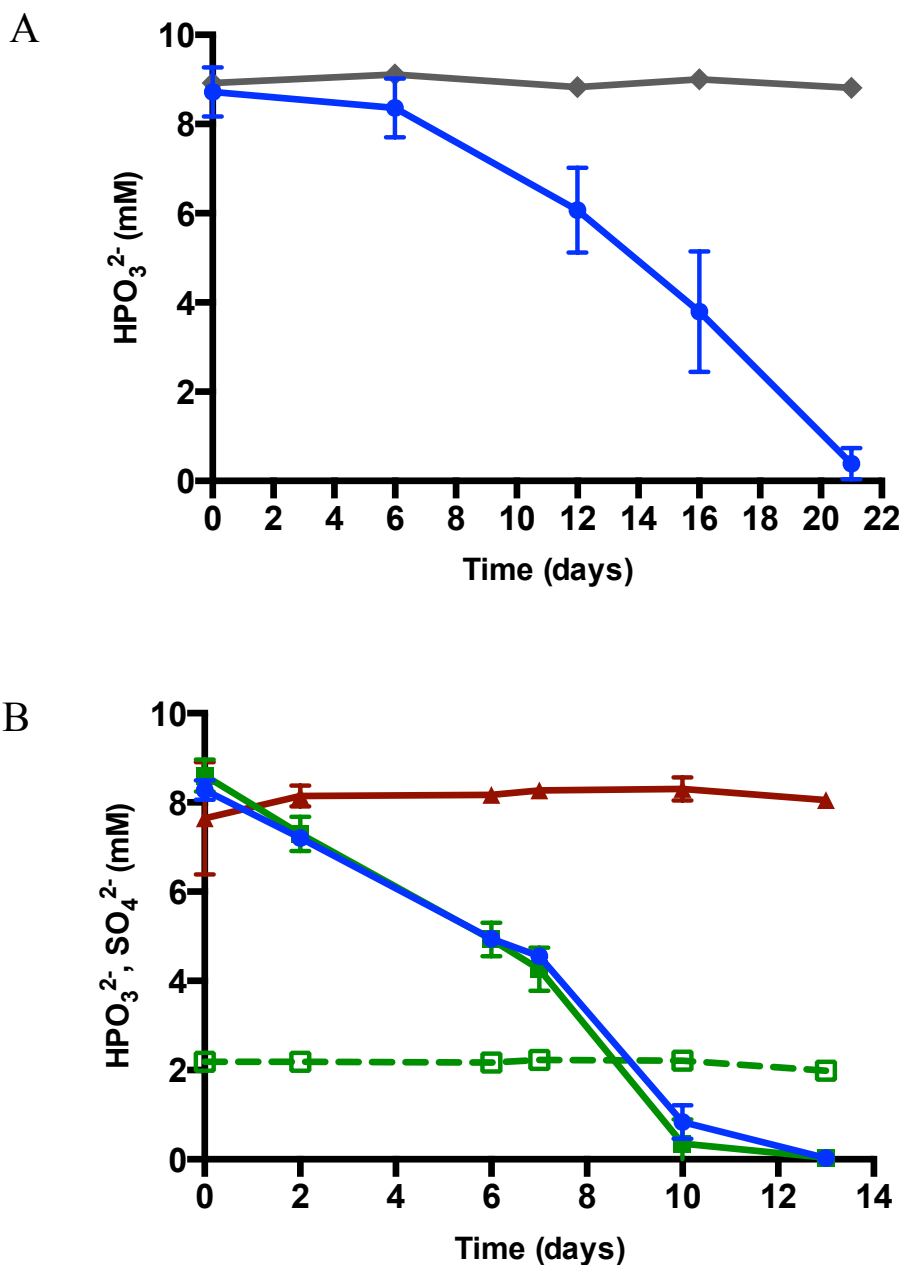


Figure 3.7. Effect of carbon dioxide (A) and sulfur oxyanions (B) on phosphite oxidation by enrichment cultures. All cultures contained 8 mM phosphite and 5% rumen fluid. Cultures depicted in panel A were grown in bicarbonate-free media with either 20% carbon dioxide (blue circles) or no carbon dioxide (gray diamonds) added to the headspace. Cultures depicted in panel B were grown in bicarbonate-containing media with 2 mM sulfate (green squares), 2 mM sulfite (red triangles), or no sulfur oxyanions (blue circles). Open green squares with a dotted line indicate sulfate concentrations in sulfate-containing cultures. All data points represent the average of triplicate cultures, with error bars denoting one standard deviation.

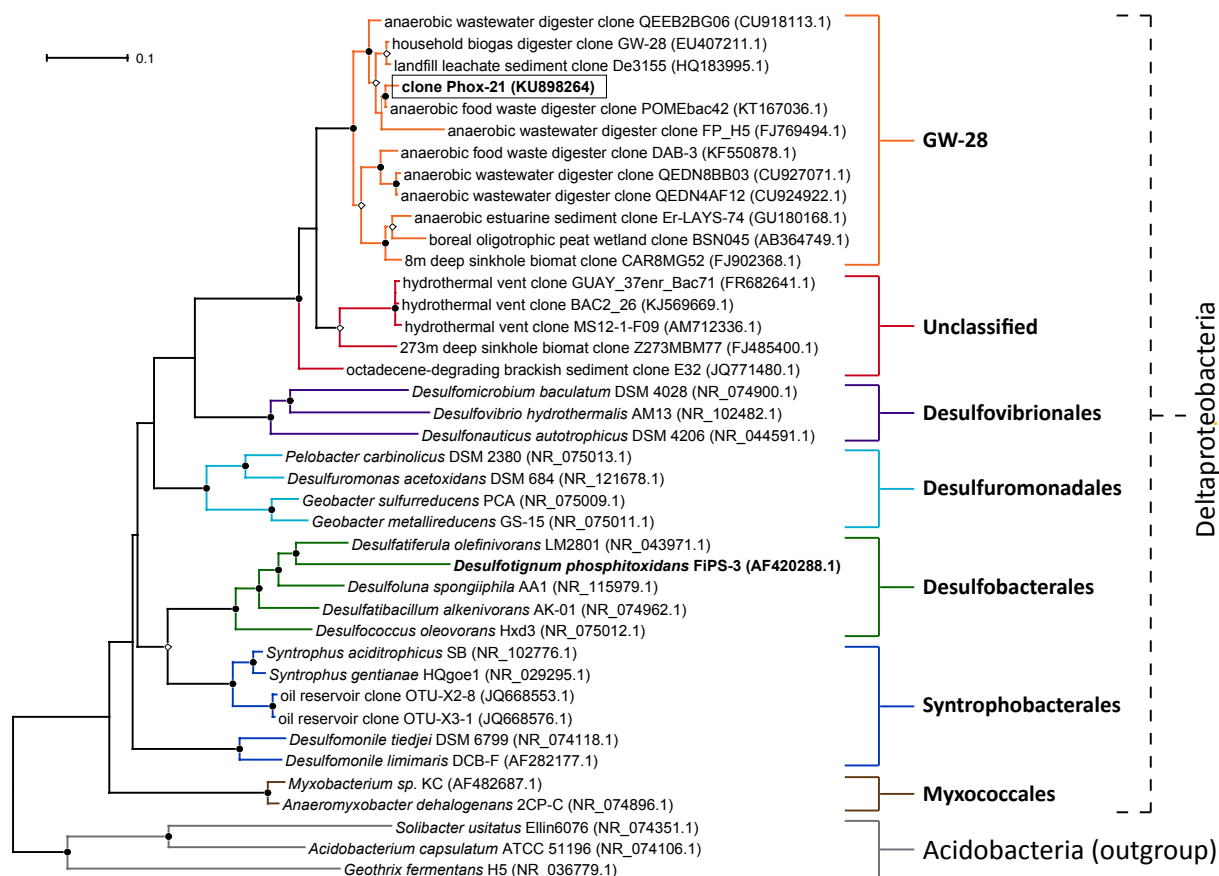


Figure 3.8. Phylogenetic tree showing the placement of clone Phox-21 within the *Deltaproteobacteria*. Selected 16S rRNA gene sequences (Appendix 3.2) were aligned using the Silva aligner and a maximum likelihood phylogenetic tree was constructed with 1,000 bootstrap resamplings using RAxML-HPC. Members of the *Acidobacteria* were included as an outgroup. Taxa represented in the Silva reference database were assigned to known orders within the *Deltaproteobacteria* based on their Greengenes taxonomic assignments. GenBank accession numbers are provided in parentheses. Taxa for which there is experimental evidence of DPO activity are indicated in bold. Internal nodes with bootstrap support >70% are indicated by closed circles and those with support >50% by open diamonds. The scale bar represents 0.1 change per nucleotide.

CHAPTER 4

Metagenomic profiling of dissimilatory phosphite-oxidizing wastewater microbial communities reveals presence of a *ptx-ptd* gene cluster in the uncultured bacterium Phox-21

(Unpublished data)

INTRODUCTION

The work presented in Chapter 3 revealed the presence in my wastewater enrichments of a novel bacterium from an uncultured clade within the *Deltaproteobacteria* whose abundance was strongly correlated with DPO activity. Based on this evidence, I hypothesized that this bacterium, designated as strain Phox-21, was the organism responsible for phosphite oxidation in my cultures. However, as my attempts to isolate Phox-21 were unsuccessful, I was unable to confirm that it was capable of carrying out this metabolism in pure culture. Therefore, I decided to perform a metagenomic analysis of some of the DNA samples I had previously collected for 16S rRNA gene analysis in order to look for possible functional markers of DPO, such as the *ptx-ptd* genes, in the genome of Phox-21. In addition to establishing a more conclusive link between Phox-21 and DPO, I also hoped that genomic profiling of this organism would reveal its broader metabolic characteristics and provide insights that could aid in its isolation and culturing. Furthermore, I expected the metagenomic dataset to shed light on the metabolic capabilities of other enrichment community members, thus providing a wider ecological context for the role of DPO in this system.

MATERIALS & METHODS

Metagenomic assembly, binning, and annotation

DNA samples chosen for metagenomic analysis were sent to the QB3 Vincent J. Coates Genomics Sequencing Laboratory at UC Berkeley for sequencing on an Illumina HiSeq 2000 (100 bp paired-end reads). Illumina sequencing reads were trimmed for quality and filtered using Sickle v1.33 with a quality threshold (-q) value of 28 and good-quality paired-end reads were then merged using IDBA-UD v1.0 (Joshi & Fass 2011; Peng et al. 2012). Merged reads from all samples were combined and assembled using MEGAHIT v1.0.2 with default parameters (D. Li et al. 2015; D. Li et al. 2016). MEGAHIT is an assembler developed specifically for metagenomic reads that uses succinct *de Bruijn* graphs and an iterative multiple k-mer size strategy. Merged reads from each sample were then mapped back to the combined assembly using BWA-MEM v0.7.10 with default parameters in order to assess sequencing coverage (H. Li & Durbin 2009). Contigs from the combined assembly were binned into individual genomes using the Anvi'o v1.1.0 platform (Eren et al. 2015). Anvi'o generates hierarchical clusters of related contigs using both tetranucleotide frequency and coverage across samples as the clustering parameters. The platform also provides a visualization interface that allows the user to further refine the contig clusters into genome bins based on coverage, GC content, and phylogenetic marker genes. Furthermore, Anvi'o assigns taxonomic lineages to the genome bins based on the presence of phylogenetic marker genes. Genome bins generated with Anvi'o were subsequently assessed for completeness and contamination based on the presence of lineage-specific, conserved, single-copy marker genes using the automated bin evaluation tool CheckM v1.0.1 (Parks et al. 2015). CheckM calculates 'completeness' based on the number of expected marker genes that are present in a given bin and 'contamination' based on the number of marker genes that are present in multiple copies and have less than 90% amino acid identity to each other. High-quality genomes (>80% completeness and <5% contamination) were submitted to the Integrated Microbial Genomes (IMG) database for gene calling and annotation (Markowitz et al. 2012). IMG utilizes Prodigal v2.50 for identification of protein-coding genes, which are then functionally annotated using a custom, manually-curated pipeline based on BLAST and HMMER searches against multiple protein databases (COG, KEGG, MetaCyc, Pfam, and TIGRfam) (Hyatt et al. 2010; Huntemann et al. 2015).

Protein sequence alignments and phylogenetic tree construction

Selected protein sequences were aligned using Clustal Omega and alignments were visualized with ESPript v3.0 (Sievers & Higgins 2014; Robert & Gouet 2014). Maximum likelihood phylogenetic trees were constructed from protein alignments using RAxML-HPC with 1,000 bootstrap resamplings and trees were visualized using Dendroscope v3.5.7 (Stamatakis 2006; Huson & Scornavacca 2012).

Sequence availability

The full metagenomic assembly is available on IMG under accession number Ga0100964. Individual genomes recovered from the full assembly are available on IMG and GenBank (GB) under the following accession numbers - *Tepidanaerobacter* sp. EBM-38: Ga0115060 (IMG),

MPOT00000000 (GB); *Deltaproteobacterium* Phox-21: Ga0115057 (IMG), MPOS00000000 (GB); Unclassified bacterium EBM-40: Ga0115061 (IMG), MPOU00000000 (GB); *Proteiniphilum* sp. EBM-39: Ga0115062 (IMG), MPOV00000000 (GB); *Thermotogales* bacterium EBM-19: Ga0115064 (IMG), MPOW00000000 (GB); *Proteiniphilum* sp. EBM-41: Ga0115065 (IMG), MPOX00000000 (GB); *Methanoculleus* sp. EBM-46: Ga0115067 (IMG), MPOY00000000 (GB); *Coprothermobacter* sp. EBM-25: Ga0115069 (IMG), MPOZ00000000 (GB); *Methanococcoides* sp. EBM-47: Ga0115071 (IMG), MPPA00000000 (GB); *Spirochaeta* sp. EBM-43: Ga0115073 (IMG), MPPB00000000 (GB); *Aminobacterium* sp. EBM-42: Ga0115070 (IMG), MPPC00000000 (GB); *Thermotogales* bacterium EBM-38: Ga0115076 (IMG), MPPD00000000 (GB); *Tepidanaerobacter* sp. EBM-49: Ga0115075 (IMG), MPPE00000000 (GB).

RESULTS

Genome bin statistics, taxonomic assignments, and coverage across samples

I chose four samples from the second round of enrichments for metagenomic analysis. Two of the samples were from enrichment culture A1, which contained 10 mM phosphite and 5% rumen fluid and displayed a high rate of phosphite oxidation. Sample A1-T2 was taken at day 11 by which time 3.8 mM phosphite had been oxidized and sample A1-T4 was taken at day 19 by which time 8.9 mM phosphite had been oxidized (Figures 3.3 & 3.4). The other two samples were from enrichment culture C1, which contained 5 mM molybdate in addition to 10 mM phosphite and 5% rumen fluid and exhibited a very low rate of phosphite oxidation due to molybdate inhibition. Sample C2-T1 was taken at day 5 by which time only 0.5 mM phosphite had been oxidized and sample C2-T4 was taken at day 19 by which time only 0.6 mM phosphite had been oxidized (Figures 3.3 & 3.4). Combined assembly of sequencing reads from these four samples yielded 50.95 Mbp of sequence data in 20,733 contigs with an average contig size of 2,458 bp and an N50 of 16,833 bp (Table 4.1). We were able to map >98% of reads from each of the samples back to the assembled contigs (Table 4.1). Contigs $\leq 1,000$ bp long were removed from the dataset and only the remaining 5,997 contigs (43.85 Mbp) were included in the binning step. A total of 2,531 contigs (42.2% of the contigs analyzed) representing 76.8% (33.66 Mbp) of the total sequence data in the analysis were binned into 13 high-quality genomes (Table 4.2, Appendix 4.1).

Binned genomes were assigned taxonomic identities based on the presence of phylogenetic marker genes (Table 4.2). In general, these taxonomic assignments corresponded well to those previously assigned to abundant community members based on 16S rRNA gene amplicon sequencing. Out of the 10 abundant OTUs ($\geq 1\%$ of total community) previously identified in our samples based on 16S rRNA analysis, 9 were recovered as binned genomes, with only OTU 44 (*Deltaproteobacteria*) missing. Of these 9 genome bins, 4 have identical taxonomic assignments at the genus level based on both functional gene markers and 16S rRNA: Bin 1 (*Tepidanaerobacter* sp.), Bin 8 (*Coprothermobacter* sp.), Bin 10 (*Spirochaeta* sp.), and Bin 11 (*Aminobacterium* sp.). The 2 bins assigned to the *Proteiniphilum* genus (Bins 4 and 6) had been classified as belonging to the *Petrimonas* genus based on 16S rRNA, which is not a substantial disagreement given that the two genera are closely related. Bin 5 (*Thermotogales* bacterium) appears to correspond to OTU 19, although the 16S rRNA assignment was resolved down to the family level (*Thermotogaceae*). Bin 3 was identified as an unclassified bacterium by both methods. Bin 2 (*Deltaproteobacterium*) matches the taxonomic assignment of Phox-21 and this correspondence was confirmed by aligning a partial 16S rRNA gene recovered in Bin 2 to the full 16S rRNA gene from the Phox-21 clone, which yielded a 99% sequence identity (Appendix 3.1b). In addition to these 9 genomes, we also recovered 4 genomes that were not among the abundant OTUs previously identified based on 16S rRNA analysis. Bins 7 and 9 were identified as *Methanoculleus* sp. and *Methanococcoides* sp. respectively. Bin 13 (*Tepidanaerobacter* sp.) and Bin 12 (*Thermotogales* bacterium) have the same taxonomic assignments as Bins 1 and 5 respectively. Binned genomes other than Phox-21 were assigned strain names based on their sampling location (East Bay Municipal Utilities District) and their corresponding OTU numbers (Figure 4.1). The 4 genomes with no corresponding abundant OTUs were assigned new strain numbers.

Average genome coverage across all samples ranged from 6x for *Tepidanaerobacter sp.* EBM-49 to 357x for *Tepidanaerobacter sp.* EBM-38 (Figure 4.1). Although Phox-21 had only the second highest overall coverage (281x), it had the highest coverage of any bin in the phosphite-oxidizing sample at day 19 (581x) (Figure 4.1). On the other hand, its coverage in the control sample at day 19 was only 95x, indicating that it had a substantially higher abundance under phosphite-oxidizing conditions, which is in accordance with what we had previously seen based on 16S rRNA analysis. All other genomes, with the exception of *Proteiniphilum sp.* EBM-39 and *Aminobacterium sp.* EBM-42, had higher coverage values in the control sample than in the phosphite-oxidizing sample at day 19 (Figure 4.1).

Heterotrophic carbon metabolism

Eleven out of the thirteen genomes contain the full glycolytic pathway for conversion of glucose to pyruvate (Figure 4.2). Unclassified bacterium EBM-40 lacks both *pfkA* (6-phosphofructokinase) and *pyk* (pyruvate kinase), while *Thermotogales* bacterium EBM-48 lacks *pgk* (phosphoglycerate kinase). The *porA* gene encoding the pyruvate:ferredoxin oxidoreductase (PFOR), which reversibly decarboxylates pyruvate to acetyl-CoA is present in all genomes (Figure 4.2). A complete TCA cycle is present only in *Proteiniphilum sp.* EBM-41; all other organisms have partial TCA cycles, although which genes are absent varies between the different genomes (Figure 4.2). Phox-21 is missing genes for both succinyl-CoA synthase and succinyl-CoA:acetate CoA transferase, which are alternate enzymes for the reversible conversion of succinyl-CoA to succinate. The lactate dehydrogenase gene *ldhA*, which enables the oxidation of lactate to pyruvate, is present only in *Tepidanaerobacter sp.* EBM-49 and *Thermotogales* bacterium EBM-48 (Figure 4.2). On the other hand, only Phox-21 and *Spirochaeta sp.* EBM-43 exhibit the capacity for ethanol metabolism, having both the alcohol dehydrogenase gene *adh* for conversion of ethanol to acetaldehyde and the aldehyde dehydrogenase gene *ald* for conversion of acetaldehyde to acetate (Figure 4.2). All of the organisms except *Coprothermobacter sp.* EBM-25 are capable of acetate assimilation to acetyl-CoA via either the acetate kinase and phosphotransacetylase (*ackA/pta*) pathway or the acetate-CoA ligase (*acsM*) pathway. The ability to use methanol as a growth substrate appears to be present only in *Methanococcoides sp.* EBM-47, which can convert it to methyl-CoM by means of a methanol:coenzyme M methyltransferase (*mtaABC*) (Figure 4.2). Genes for formate oxidation were found only in Phox-21 and *Methanoculleus sp.* EBM-46 (Figure 4.2). Phox-21 has a quinone-dependent, molybdate-binding formate dehydrogenase (*fdoGHI*), which is a membrane-bound periplasmic complex typically involved in formate oxidation coupled to nitrate or nitrite reduction (Maia et al. 2015). EBM-46 has an F420-dependent formate dehydrogenase complex, which can couple formate oxidation to F420 reduction in methanogens (Maia et al. 2015).

Electron transport and ion motive force

No organism has a full canonical (NADH-dependent) Complex I, but *Methanococcoides sp.* EBM-47 has the *nuoBCDIHAJKLMN* genes encoding an Fpo-type, F420-dependent Complex I. The Fpo-type complex, which is present in some methanogens, lacks the NADH binding module encoded by *nuoEFG* and instead couples proton translocation to the oxidation of coenzyme F420 (Efremov & Sazanov 2012). Only the *Proteiniphilum* genomes (EBM 39 & 41) have genes encoding Complex II (*sdhCAB*). Whether this complex functions as a succinate dehydrogenase

or a fumarate reductase in these organisms cannot be determined based on the sequence alone, although it is likely to function in the oxidative direction in EBM 41, which has a complete TCA cycle, and in the reductive direction in EBM 39, which lacks the ability to convert succinyl-CoA to succinate (Cecchini et al. 2002). Six genomes contain genes for the sodium-translocating NADH:quinone oxidoreductase (NQR complex), although only EBM 39 & 41 have the full *nqrABCDEF* gene cluster, with the other four genomes lacking *nqrA*. None of the binned genomes have genes for Complex III (cytochrome bc1) or Complex IV (cytochrome c oxidase). All of the genomes except for those of *Methanoculleus sp.* EBM-46 and *Coprothermobacter sp.* EBM-25 contain the full *rnfABCDEFG* gene cluster encoding the RNF Complex which acts as sodium-translocating ferredoxin:NADH oxidoreductase. All of the genomes have *nfnAB* genes encoding the NAD-dependent reduced ferredoxin:NADP oxidoreductase, which is an electron-bifurcating complex that catalyzes the reduction of two NADP molecules coupled to the oxidation of reduced ferredoxin and NADH in a reversible manner (Buckel & Thauer 2013). All of the organisms also have genes encoding ATP synthase complexes of either the F or V types or both (Figure 4.2, Table 4.3). Both types are present in Phox-21, with the F-type ATPase likely functioning as a sodium-translocating complex and the V-type ATPase as a proton-translocating complex based on the identity of key residues in the c subunits of both complexes (Figure 4.3) (Mulkidjanian et al. 2008).

Inorganic electron donors and acceptors, nitrogen metabolism, and amino acid and cofactor biosynthesis

Methanoculleus sp. EBM-46 and *Aminobacterium sp.* EBM-42 are the only two organisms that have genes for Ni,Fe hydrogenases, which generally function in H₂ oxidation (Figure 4.2) (Peters et al. 2015). The EBM-46 hydrogenase, encoded by *FrhADGB*, is predicted to be F420-dependent, whereas that of EBM-42, encoded by *HoxHY*, is predicted to be NAD(P)-dependent. Six genomes contain the *HndABCD* genes for the NAD(P)-dependent Fe,Fe hydrogenase, which is thought to function exclusively as an H₂-evolving complex (Figure 4.2) (Peters et al. 2015; Vignais et al. 2001). Only *Proteiniphilum sp.* EBM-41 appears capable of oxygen respiration, having the *cydAB* genes for cytochrome bd ubiquinol oxidase. No genes for dissimilatory sulfate reduction, dissimilatory nitrate reduction, denitrifying nitrite reduction, or anaerobic ammonium oxidation were found in any of the bins. However, *Proteiniphilum sp.* EBM-41 and Phox-21 have *nrfAH* genes for the ammonifying periplasmic nitrite reductase (Figure 4.2). As expected, the *mcrBDCGA* genes for methyl-CoM reductase were found only in the methanogens EBM-46 and EBM-47 (Figure 4.2). The two methanogens are also the only organisms that have the nitrogenase genes *nifHDK* (Figure 4.2). Furthermore, *Proteiniphilum sp.* EBM-41, *Spirochaeta sp.* EBM-43, and Phox-21 contain *amtB* genes encoding ammonia transporters. None of the organisms seem to be capable of synthesizing all amino acids de novo, with Phox-21 in particular predicted to be an auxotroph for alanine, histidine, and threonine (Table 4.4). The dihydrofolate reductase gene *folA*, which is necessary for conversion of folate to tetrahydrofolate (THF), is present only in the *Proteiniphilum* genomes (EBM-39 and 41) and the *Thermotogales* genomes (EBM 19 and 48), while only the *Tepidanaerobacter* strains (EBM-38 and 49) and the methanogens (EBM 46 and 47) have genes for Vitamin B12 biosynthesis (Figure 4.2).

Autotrophic carbon metabolism

The *acsB* gene encoding acetyl-CoA synthase, a key gene in the autotrophic Wood-Ljungdahl Pathway (WLP), is present in Phox-21 as well as in the *Tepidanaerobacter* strains EBM-38 and EBM-48, and the methanogens EBM-46 and EBM-47 (Figure 4.2). Key genes for all other known carbon fixation pathways are absent from all bins. Both EBM-46 and EBM-47 are missing the *acsE* gene, which encodes the methyl-THF:CFeSP methyltransferase (Figure 4.4). However, methanogens are known to lack canonical AcsE enzymes due to their use of tetrahydromethanopterin (THMPT) instead of THF as a methyl carrier and it is thought that they use a different methyltransferase to catalyze this step (Figure 4.4) (Sousa & Martin 2014). Additionally, although both are missing the formate:THF ligase gene *fhs*, they are capable of carrying out the methyl branch of the WLP by means of the methanogen-specific C1 carriers methanofuran (MFR) and THMPT, which allows them to bypass the THF-dependent pathway used in bacteria (Figure 4.4). On the other hand, the *Tepidanaerobacter* strains EBM-38 and 48 lack the tungsten-containing formate dehydrogenase encoded by *fdhAB* (Figure 4.4). In the model homoacetogen *Moorella thermoacetica*, FdhAB is a cytoplasmic NADPH-dependent enzyme that catalyzes the reduction of CO₂ to formate, the first step in the methyl branch of the WLP in bacteria (Figure 4.4) (Ragsdale & Pierce 2008).

Phox-21 has genes for both the catalytic subunit (*fdhA*) and the NADP-binding subunit (*fdhB*) of the CO₂-reducing formate dehydrogenase (Figure 4.4). It should be noted that the *fdhB* gene (Ga0115057_14053) was annotated by IMG as an NADH-quinone oxidoreductase subunit F (*nuoF*), but subsequent phylogenetic analysis revealed that the product of this gene is in fact more closely related to known FdhB proteins, including that of *M. thermoacetica*, than to NuoF (Figure 4.5). Phox-21 also has genes for formate:THF ligase (*fhs*), methenyl-THF cyclohydrolase / methylene-THF dehydrogenase (*folD*), and methylene-THF reductase (*metF*), which together constitute the rest of the methyl branch of the WLP (Figure 4.4). Surprisingly, however, it is missing all of the genes in the carbonyl branch of the pathway except for the acetyl-CoA synthase gene *acsB* (Figure 4.4). It also lacks the *pta* (phosphotransacetylase) and *ackA* (acetate kinase) genes for acetate production, but does have an *acsM* gene encoding acetate-CoA ligase, an enzyme that catalyzes the reversible conversion of acetate and ATP to acetyl-CoA. Phox-21 lacks the acetate transporters ActP, MctP, and MctC, but contains the gene for FocA, which is a channel-like transporter known to passively export various monovalent organic acids including acetate and formate in *Salmonella typhimurium* (Lü et al. 2012). FocA has also been shown to be capable of actively importing formate into the cell by means of proton symport and could, therefore, potentially function as an acetate importer as well (Lü et al. 2012).

Reduced phosphorus metabolism

The phosphite dehydrogenase gene *ptxD* is present only in Phox-21 and no genes for hypophosphite oxidation or phosphonate degradation were found in any of the binned genomes (Figure 4.2). The *ptxD* gene of Phox-21 is part of a 6 gene *ptx-ptd* cluster similar to the one found in *D. phosphitoxidans* FiPS-3 (Figure 4.6). All of the genes found in the FiPS-3 cluster are also present in Phox-21 with the exception of *ptdG*. In contrast to the FiPS-3 *ptx-ptd* cluster, which is flanked by transposases, there is no genomic evidence that the *ptx-ptd* cluster from Phox-21 was horizontally acquired. Nonetheless, the closest homologs of the Phox-21 Ptx-

Ptd proteins in both the IMG and NCBI databases are the Ptx-Ptd proteins of FiPS-3, with amino acid identities of 56% for PtxE, 55% for PtxD, 66% for PtdF, 77% for PtdC, 67% for PtdH, and 47% for PtdI. The close homology of the phosphite dehydrogenases from Phox-21 and FiPS-3 is further supported by phylogenetic analysis showing that the PtxD proteins from these two organisms cluster together to form a separate clade from the PtxD proteins of APO-capable organisms (Figure 4.7).

DISCUSSION

The presence of a *ptx-ptd* gene cluster in the genome of Phox-21, as well as its higher abundance during phosphite-oxidizing conditions, clearly indicates that this is the organism responsible for DPO in our enrichments. In addition, the observed CO₂ dependence of DPO in our enrichments coupled with the fact that no other terminal electron acceptors were added to our media implies that Phox-21 is capable of growing by coupling phosphite oxidation to CO₂ reduction. The presence of a formate dehydrogenase complex FdhAB similar to that of *M. thermoacetica* in Phox-21 provides a putative means by which CO₂ reduction could occur. However, the absence of key WLP genes suggests that this organism is unable to generate acetyl-CoA from CO₂ alone and therefore is not a true autotroph. Furthermore, it lacks an electron transport chain and thus appears to be incapable of energy conservation through oxidative phosphorylation.

Instead, we propose that Phox-21 couples phosphite oxidation to CO₂ reduction to formate by means of FdhAB and uses the energy generated by this reaction to assimilate organic carbon sources such as acetate (Figure 4.8). Based on thermodynamic calculations and physiological evidence, Schink et al. (2002) have previously proposed that FiPS-3 is able to conserve energy during DPO by directly generating ATP as well as NADH from the oxidation of phosphite. This putative substrate-level phosphorylation step during DPO is likely mediated by PtdFHI and would allow for energy conservation in the absence of membrane-associated electron transport (Figure 4.8). ATP produced in this manner could be used by Phox-21 to incorporate acetate into biomass via AcsM and the partial TCA cycle as well as to run the proton and sodium translocating ATP synthases in reverse in order to establish an ion motive force across the cell membrane (Figure 4.8). The resulting sodium ion gradient could drive the RNF complex to reduce ferredoxin, which could then serve as an electron donor for pyruvate synthesis by the PFOR enzyme as well as for NADPH production by the NfnAB complex (Figure 4.8). The FocA transporter could serve both to import acetate for assimilation and to export formate from the cell as a metabolic waste product (Figure 4.8). However, in the presence of nitrite, formate could be re-oxidized to CO₂ by FdoGHI coupled to the reduction of nitrite by NrfAH (Figure 4.8). This reaction would contribute to the maintenance of a proton motive force and would also yield ammonia, which could be imported into the cell via the AmtB transporter to serve as a nitrogen source.

Our metabolic model predicts that Phox-21 should require an organic carbon substrate such as acetate for growth and should also excrete formate into the medium as a product of CO₂ reduction. A requirement for organic carbon may at least partly explain the stimulatory effect of rumen fluid on DPO, since rumen fluid has been shown to contain as much as 60 mM acetate in addition to various carbohydrates, organic acids, amino acids, and fatty acids (Saleem et al. 2013). Additionally, Phox-21 is predicted to be incapable of synthesizing alanine, histidine, threonine, or THF, all of which were absent from our original growth media but may be present in rumen fluid. However, attempts to grow our enrichments in media supplemented with acetate, THF, and amino acids but lacking rumen fluid have so far resulted in substantially lower phosphite oxidation rates, indicating that there may be other components in the rumen fluid that promote the growth of Phox-21.

Acetate present in rumen fluid amended cultures could also have served as a growth substrate for the *Tepidanaerobacter* strains and methanogens present in the communities. Both *Tepidanaerobacter* genomes (EBM 38 and 49) have all the genes for the carbonyl branch of the WLP but lack a formate dehydrogenase and an uptake hydrogenase, which is consistent with previous genomic analysis of *Tepidanaerobacter acetatoxydans* and indicates that these organisms are capable of syntrophic acetate oxidation but not of autotrophic growth (Muller et al. 2015). Likewise, both *Methanoculleus* sp. EBM-46 and *Methanococcoides* sp. EBM-47 appear to be capable of acetoclastic methanogenesis, although only EBM-46 has the genes necessary for growth on H₂/CO₂ and formate as well. The remaining enrichment community members had no WLP genes and mostly lacked genes involved in respiratory processes and were therefore likely involved in the fermentation of organic acids, amino acids, and carbohydrates present in the rumen fluid.

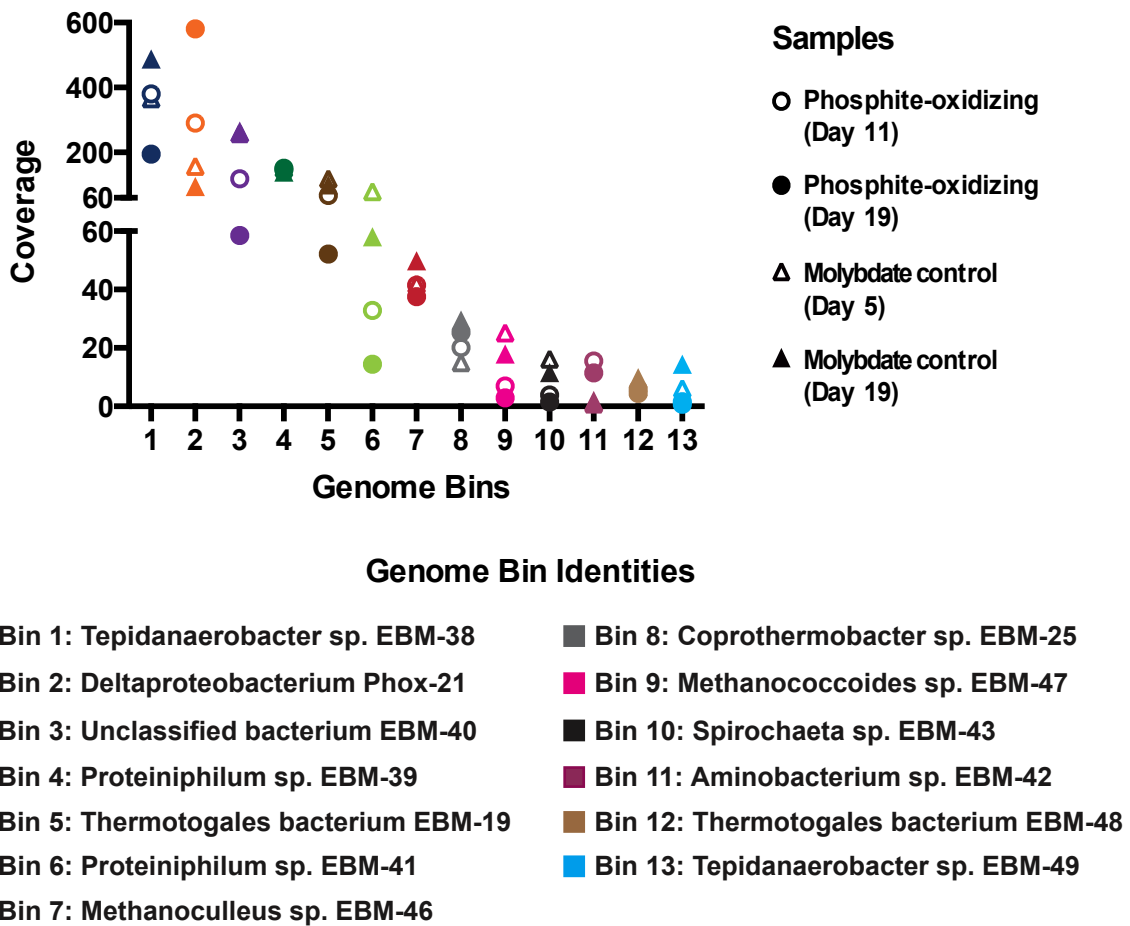


Figure 4.1. Genome bin taxonomic identities and sequence coverage by sample.

Heterotrophic Carbon Metabolism

Glucose \longrightarrow Pyruvate	
Pyruvate \longleftrightarrow Acetyl-CoA	
Citrate \longleftrightarrow 2-Oxoglutarate (TCA Cycle)	
2-Oxoglutarate \longleftrightarrow Succinyl-CoA (TCA Cycle)	
Succinyl-CoA \longleftrightarrow Succinate (TCA Cycle)	
Malate \longleftrightarrow Oxaloacetate (TCA Cycle)	
Lactate \longleftrightarrow Pyruvate	
Ethanol \longleftrightarrow Acetate	
Acetate \longleftrightarrow Acetyl-CoA	
Methanol Metabolism	
Formate \longrightarrow CO ₂	

Electron Transport & Ion Motive Force

Complex I (NADH / F420 DH)	
Complex II (Succinate DH / Fumarate Reductase)	
Rnf Complex	
Nfn Complex	
ATP Synthase	

Inorganic Electron Donors & Acceptors

Hydrogenotrophy	
Hydrogen Production	
Oxygen Respiration	
Methanogenesis	

Nitrogen Metabolism

Nitrite Reduction (Ammonifying)	
Nitrogen Fixation	

Cofactor Biosynthesis

Tetrahydrofolate Biosynthesis	
Vitamin B12 Biosynthesis	

Autotrophic Carbon Metabolism

Wood-Ljungdahl Pathway (Methyl Branch)	
Wood-Ljungdahl Pathway (Carbonyl Branch)	

Reduced Phosphorus Metabolism

Phosphite Oxidation	
---------------------	--

Genome Bins

- | | |
|---|--|
| ■ Bin 1: Tepidanaerobacter sp. EBM-38 | ■ Bin 8: Coprothermobacter sp. EBM-25 |
| ■ Bin 2: Deltaproteobacterium Phox-21 | ■ Bin 9: Methanococcoides sp. EBM-47 |
| ■ Bin 3: Unclassified bacterium EBM-40 | ■ Bin 10: Spirochaeta sp. EBM-43 |
| ■ Bin 4: Proteiniphilum sp. EBM-39 | ■ Bin 11: Aminobacterium sp. EBM-42 |
| ■ Bin 5: Thermotogales bacterium EBM-19 | ■ Bin 12: Thermotogales bacterium EBM-48 |
| ■ Bin 6: Proteiniphilum sp. EBM-41 | ■ Bin 13: Tepidanaerobacter sp. EBM-49 |
| ■ Bin 7: Methanoculleus sp. EBM-46 | |

Figure 4.2. Overview of key metabolic pathways present in binned genomes. Filled boxes (color coded by genome) indicate presence of the full pathway in the corresponding genome, while empty boxes indicate absence of the pathway. See text for a detailed discussion of which genes were used to determine the presence or absence of the different pathways.

	20	30	40	50	60	70
<i>I. tartaricus</i> F-type (Na ⁺)	TAMIAGIGPGVG	QGYAAGKAVESVARQPEAKGDI	IISTMVLGQAV	AE	STGI	YSLVIALI
<i>A. woodii</i> F-type (Na ⁺)	IAMIAGIGPGTG	QGYAAGKGAEAVGIRPEMKSAILRVMLLGQAV	AE	TTGI	YALIVALI	
<i>T. maritima</i> F-type (Na ⁺)	CMGIGAIGPGIG	ENIGAHAMDAMARQPEMVGTITTRMLLADAV	AE	TTGI	YSLLIAFM	
<i>C. paradoxum</i> F-type (Na ⁺)	LAMIAGIGPGIG	QGYAAGKGAEAVGKQPEAQGDILRTMLLGAAV	AE	STGI	YALVVALI	
Phox-21 F-type	TISIGSIGCALG	EGKAVASSLTAIAQQPDES	GISRTLFVGLA	MIE	STAI	YCLVVAMI
Phox-21 V-type	MAASAELFSAIY	QGSVCA . . . SGIALLPKTRGQILTSSMMLAV	FVE	LIGV	LGLVFTIM	
<i>S. acidocaldarius</i> V-type (H ⁺)	AVGLAAIGAGVA	VGTAAAAGIGVLTEKREMF	GTVLI . . . FVA	I	GE	GI
<i>E. coli</i> F-type (H ⁺)	MMGLAAIGAAIG	I	GILGGKFLEGAARQPD	LIP	LLRTQFFIVMGL	VDAIPM
<i>B. pseudofirmus</i> F-type (H ⁺)	AAGLAAVAGAI	AVAIIVKATIEGTT	RQPELRGTLQ	TL	LMFIGVPL	LA
<i>R. rubrum</i> F-type (H ⁺)	LAAIGMIGSGIG	VGNIWANLIATVGRNPAAK	STVELY	GWIGFA	VTE	AIAL
<i>S. lividans</i> F-type (H ⁺)	GYGLAAIGPGVG	VGIIFGNGTQAMARQPEAA	GLIRANQILGFA	FC	EALAL	I

Figure 4.3. Partial protein sequence alignment of ATP synthase c subunits present in Phox-21 showing key residues that determine ion-binding specificity. Protein sequences from Phox-21 as well as proteins from known sodium-translocating or proton-translocating ATP synthases were aligned using Clustal Omega. Amino acid residues are numbered based on the *Ilyobacter tartaricus* sequence, with key ion-binding residues as determined by Mulkidjanian et al. (2008) indicated by boxes. Key conserved residues found in proteins from sodium-translocating complexes (Gln/Glu32, Val/Leu/Met63, Ser/Thr66, and Tyr70) are highlighted in red, whereas non-conserved residues are highlighted in blue. Only proteins having all of the key conserved residues are predicted to be from sodium-translocating complexes.

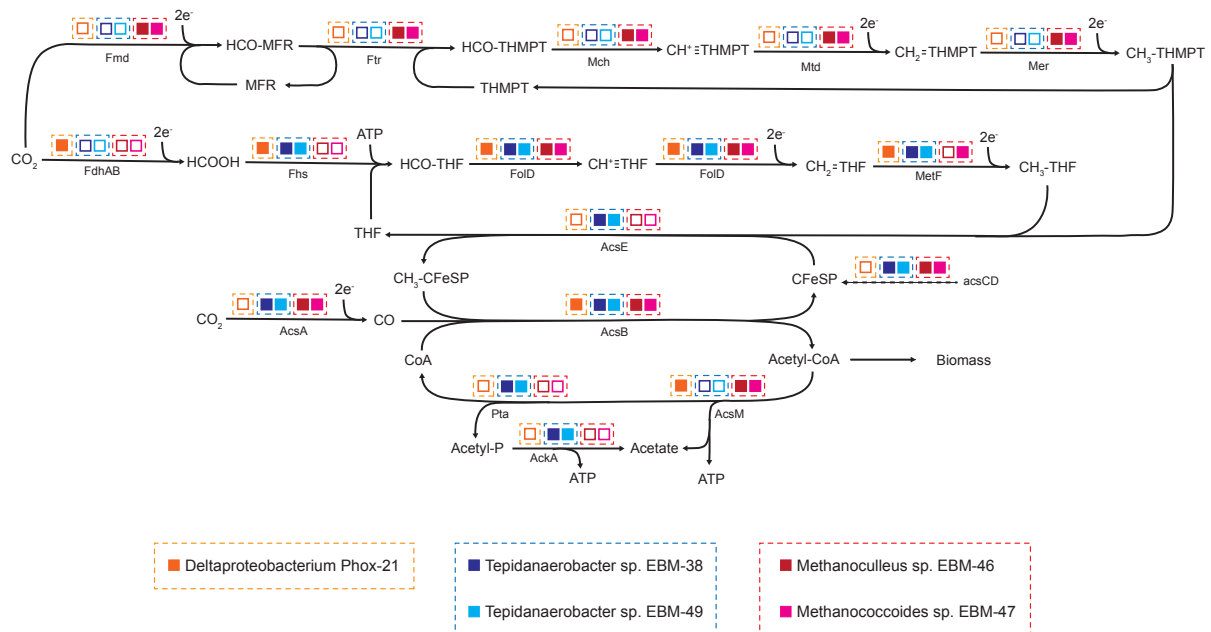


Figure 4.4. Presence or absence of Wood-Ljungdahl Pathway (WLP) genes in binned genomes containing the WLP marker gene *acsB*. Filled boxes (color coded by genome) indicate presence of the gene in corresponding genome, while empty boxes indicate absence of the gene. Methyl branch (bacteria) proteins: FdhAB = NADP-dependent formate dehydrogenase, Fhs = formate:THF ligase, FolsD = methenyl-THF cyclohydrolase / methylene-THF dehydrogenase, MetF = methylene-THF reductase. Methyl branch (archaea) proteins: Fmd = formylmethanofuran dehydrogenase, Ftr = formylmethanofuran:tetrahydromethanopterin N-formyltransferase, Mch = methenyltetrahydromethanopterin cyclohydrolase, Mtd = methylenetetrahydromethanopterin dehydrogenase, Mer = methylenetetrahydromethanopterin reductase. Carbonyl branch proteins: AcsA = carbon monoxide dehydrogenase, AcsB = acetyl-CoA synthase, CFeSP = corrinoid iron-sulfur protein, AcsE = methyl-THF:CFeSP methyltransferase. Acetate metabolism proteins: Pta = phosphotransacetylase, AckA = acetate kinase, AcsM = acetate-CoA ligase. Cofactors: THF = tetrahydrofolate, MFR = methanofuran, THMPT = tetrahydromethanopterin, CoA = coenzyme A.

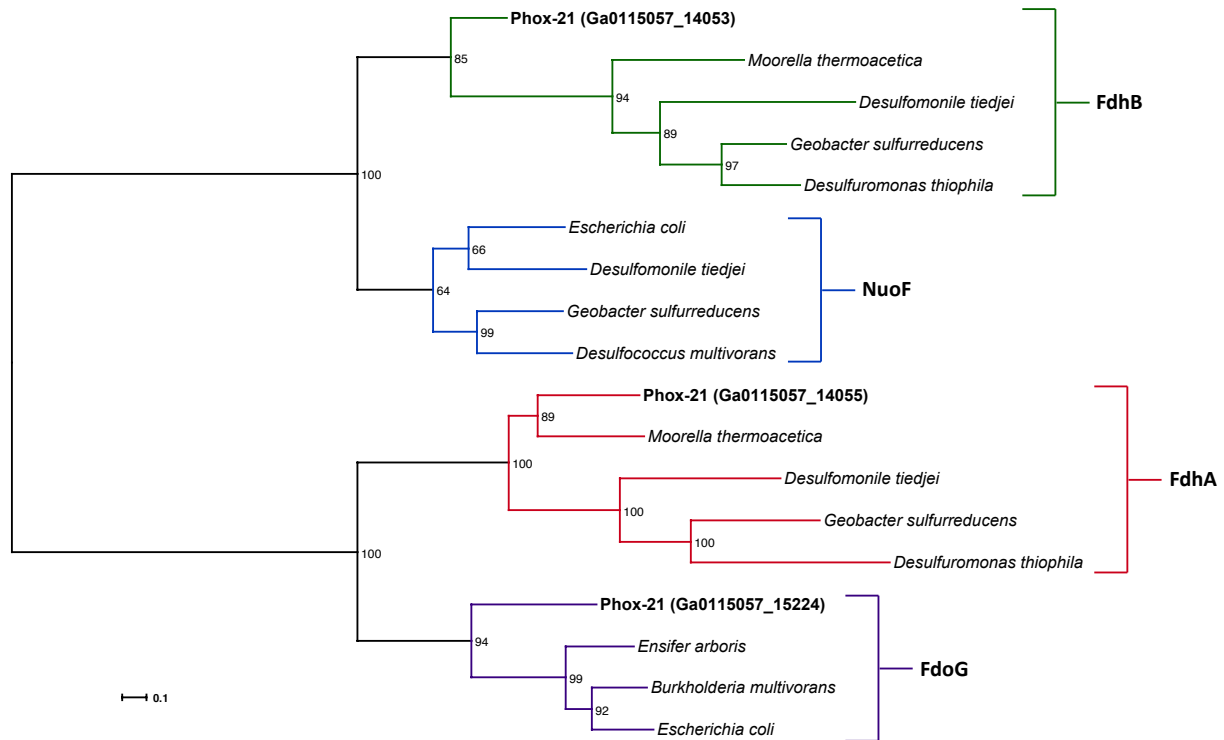


Figure 4.5. Phylogenetic tree of formate dehydrogenase subunits present in Phox-21. Protein sequences were aligned using Clustal Omega and a maximum likelihood tree was constructed with 1,000 bootstrap resamplings using RAxML-HPC. Proteins present in Phox-21 are indicated in bold with their IMG locus tags in parentheses. Bootstrap support values are indicated at internal nodes. The scale bar represents 0.1 change per amino acid residue. FdhA = NADP-dependent formate dehydrogenase catalytic subunit; FdhB = NADP-dependent formate dehydrogenase NADP-binding subunit; FdoG = quinone-dependent formate dehydrogenase catalytic subunit; NuoF = NADH:quinone oxidoreductase NADH-binding subunit.

Deltaproteobacterium Phox-21



D. phosphitoxidans FiPS-3



Gene Annotation

- Transcriptional regulator
- Phosphite dehydrogenase
- Nucleoside-diphosphate-sugar epimerase
- Major facilitator superfamily transporter
- Nucleotide-binding universal stress protein
- Radical SAM superfamily enzyme
- Hypothetical protein

Function in FiPS-3

- Unknown
- Phosphite oxidation
- Unknown
- Phosphite uptake
- Unknown
- Unknown
- Unknown

Figure 4.6. *Ptx-ptd* gene clusters of *Deltaproteobacterium* Phox-21 and the DPO-capable bacterium *Desulfotignum phosphitoxidans* FiPS-3.

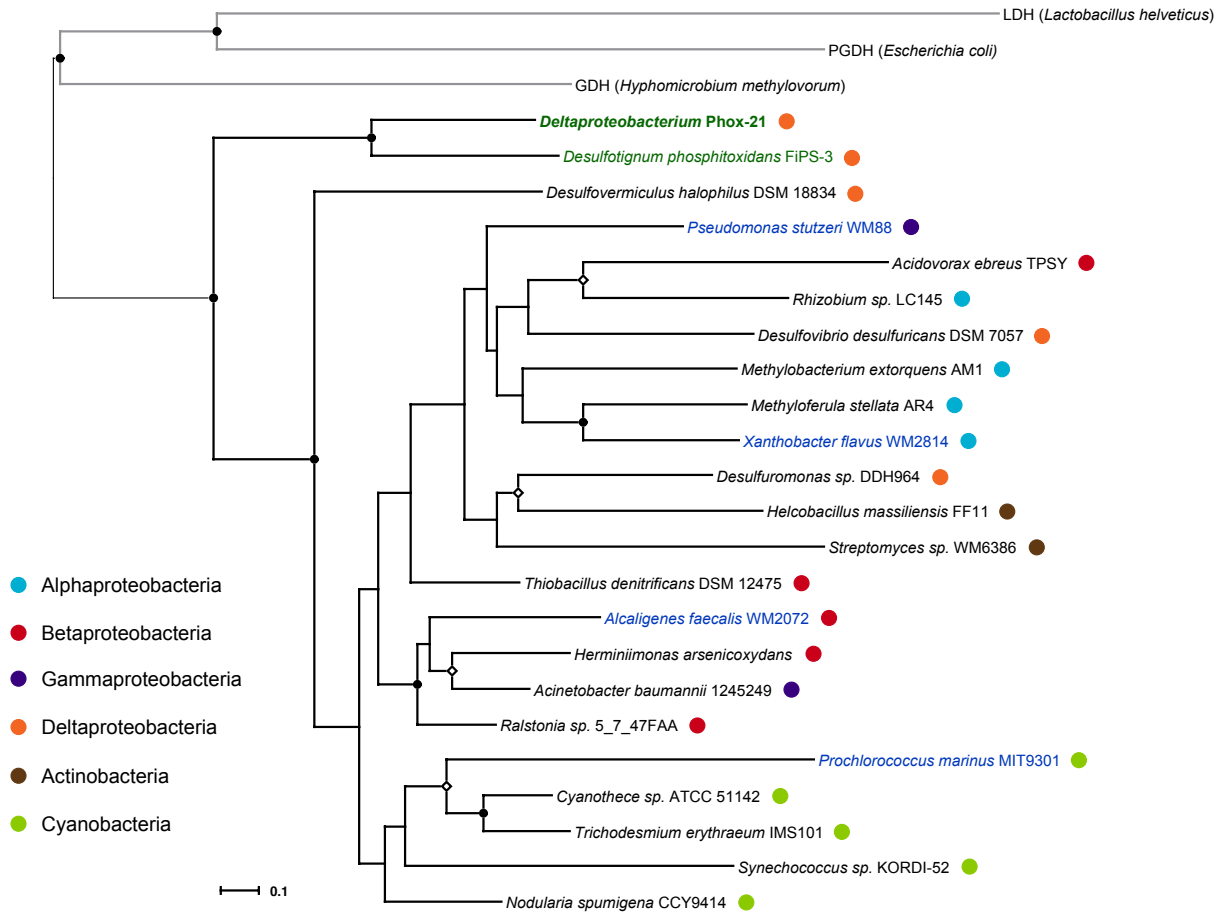


Figure 4.7. Phylogenetic tree of the phosphite dehydrogenase PtxD. Protein sequences from selected organisms were aligned using Clustal Omega and a maximum likelihood tree was constructed with 1,000 bootstrap resamplings using RAxML-HPC. Black branches indicate PtxD sequences, while gray branches indicate related outgroup sequences belonging to the D-hydroxyacid dehydrogenase protein family (LDH = lactate dehydrogenase, PGDH = 3-phosphoglycerate dehydrogenase, GDH = glycerate dehydrogenase). The PtxD from Phox-21 is indicated in bold. Organisms for which there is experimental evidence of DPO are highlighted in green, while those for which there is experimental evidence of APO are highlighted in blue. Colored circles indicate the taxonomic affiliations of the organisms harboring each PtxD sequence. Internal nodes with bootstrap support >70% are indicated by closed circles and those with support >50% by open diamonds. The scale bar represents 0.1 change per amino acid residue.

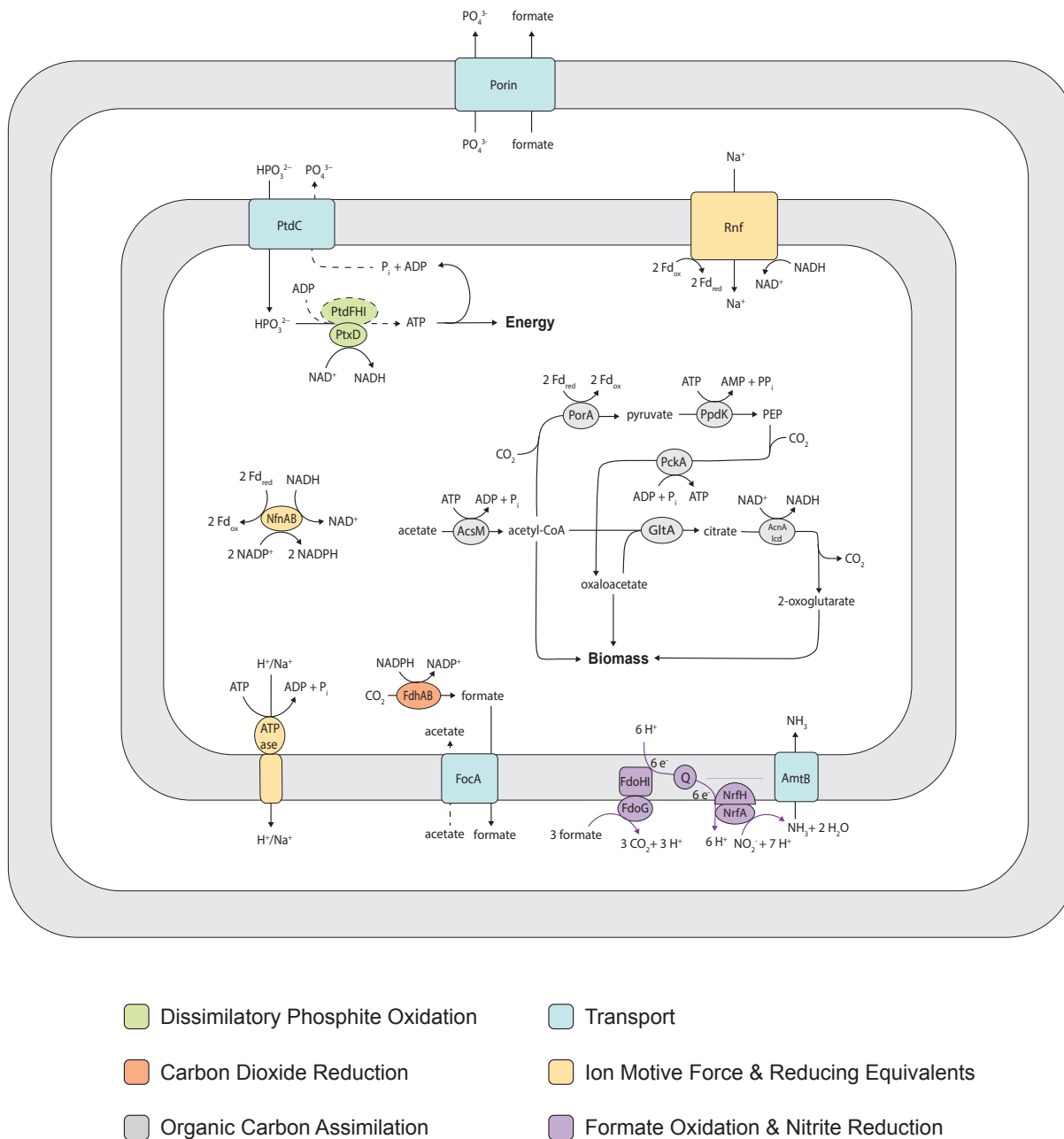


Figure 4.8. Genomics-based metabolic model of Phox-21 (not drawn to scale). Dotted lines denote putative mechanisms based on physiological and genomic observations that have yet to be confirmed by biochemical evidence. Dissimilatory phosphite oxidation proteins: PtdD = phosphite dehydrogenase, PtdF = nucleoside-diphosphate-sugar epimerase, PtdH = radical SAM superfamily enzyme, PtdI = hypothetical protein. Transport proteins: PtdC = phosphite transporter, FocA = formate channel, AmtB = ammonium transporter. Carbon dioxide reduction proteins: FdhAB = NADP-dependent formate dehydrogenase. Ion motive force and reducing equivalents related proteins: ATPase = ATP synthase, Rnf = sodium-translocating

ferredoxin:NAD oxidoreductase, NfnAB = NAD-dependent ferredoxin:NADP oxidoreductase. Organic carbon assimilation proteins: AcsM = acetate-CoA ligase, PorA = pyruvate:ferredoxin oxidoreductase, PpdK = pyruvate:orthophosphate dikinase, PckA = phosphoenolpyruvate carboxykinase, GltA = citrate synthase, AcnA/Icd = aconitate hydratase / isocitrate dehydrogenase. Formate oxidation and nitrite reduction proteins: FdoGHI = quinone-dependent formate dehydrogenase, NrfAH = periplasmic nitrite reductase. Fd = ferredoxin, PEP = phosphoenolpyruvate, Q = quinone.

Table 4.1. Metagenomic assembly and read mapping statistics.

Total Contigs Assembled	20,733
Total Assembly Length (bp)	50,954,199
Minimum Contig Length (bp)	200
Maximum Contig Length (bp)	442,933
Average Contig Length (bp)	2,458
N50 (bp)	16,833
A1T2 Reads Mapped (%)	99.11
A1T4 Reads Mapped (%)	99.33
C2T1 Reads Mapped (%)	98.45
C2T4 Reads Mapped (%)	99.07

Table 4.2. Genome binning statistics. Mbp = megabase pair, Kbp = kilobase pair.

Bin	Lineage	Completeness (%)	Contamination (%)	Genome size (Mbp)	Contigs	Mean contig length (Kbp)	N50 (Kbp)
1	Tepidanaerobacter	97.12	0.96	2.39	103	23.16	52.12
2	Deltaproteobacteria	98.49	1.94	3.31	62	53.36	123.28
3	Unclassified Bacteria	98.85	0	2.88	38	75.82	259.58
4	Proteiniphilum	100	0.55	2.09	170	12.29	25.67
5	Thermotogales	96.39	1.68	2.81	577	4.86	9.72
6	Proteiniphilum	100	0.55	2.85	43	66.38	151.63
7	Methanoculleus	88.67	2.61	2.80	664	4.22	6.57
8	Coprothermobacter	92.86	1.79	1.38	181	7.60	24.11
9	Methanococcoides	99.18	0	2.12	37	57.18	215.26
10	Spirochaeta	97.73	0	3.29	169	19.46	44.42
11	Aminobacterium	100	0	1.94	26	74.48	151.97
12	Thermotogales	99.84	0	3.48	395	8.81	19.86
13	Tepidanaerobacter	95.19	0	2.33	66	35.37	59.59

Table 4.3. ATP synthase types present in genome bins. Gray shading indicates presence and no shading indicates absence.

	F-Type ATPase	V-Type ATPase
Bin 1		
Bin 2		
Bin 3		
Bin 4		
Bin 5		
Bin 6		
Bin 7		
Bin 8		
Bin 9		
Bin 10		
Bin 11		
Bin 12		
Bin 13		

Table 4.4. Amino acid biosynthesis pathways present in genome bins. Gray shading indicates presence of full pathway and no shading indicates an absent or incomplete pathway.

	Bin 1	Bin 2	Bin 3	Bin 4	Bin 5	Bin 6	Bin 7	Bin 8	Bin 9	Bin 10	Bin 11	Bin 12	Bin 13
Alanine	Gray	White	Gray	Gray	Gray	Gray	Gray	White	White	Gray	Gray	Gray	Gray
Arginine	White	Gray	Gray	Gray	White	Gray	Gray	White	Gray	Gray	Gray	White	Gray
Asparagine	White	Gray	Gray	Gray	Gray	Gray	Gray	White	Gray	Gray	White	Gray	White
Aspartate	Gray	Gray	Gray	Gray	Gray	Gray	Gray	White	Gray	Gray	Gray	Gray	Gray
Cysteine	Gray	Gray	Gray	Gray	White	Gray	White	Gray	White	Gray	Gray	Gray	Gray
Glutamate	Gray	Gray	Gray	Gray	Gray	Gray	Gray	White	Gray	Gray	Gray	Gray	Gray
Glutamine	Gray	Gray	Gray	Gray	Gray	Gray	Gray	Gray	Gray	Gray	Gray	Gray	Gray
Glycine	Gray	Gray	Gray	Gray	Gray	Gray	White	Gray	White	Gray	Gray	Gray	Gray
Histidine	Gray	White	White	Gray	White	Gray	White	White	Gray	White	White	White	Gray
Isoleucine	Gray	Gray	Gray	Gray	White	Gray	Gray	White	Gray	Gray	White	White	Gray
Leucine	Gray	Gray	Gray	Gray	White	Gray	Gray	White	Gray	Gray	White	White	Gray
Lysine	Gray	Gray	Gray	Gray	Gray	Gray	Gray	White	White	White	White	Gray	Gray
Methionine	White	Gray	White	White	White	White	White	White	Gray	White	White	Gray	White
Phenylalanine	Gray	Gray	Gray	Gray	Gray	Gray	White	White	Gray	White	White	White	Gray
Proline	Gray	Gray	Gray	Gray	Gray	Gray	White	White	Gray	Gray	Gray	Gray	Gray
Serine	Gray	Gray	Gray	Gray	Gray	Gray	White	Gray	White	Gray	Gray	Gray	Gray
Threonine	Gray	White	Gray	Gray	Gray	Gray	White	Gray	White	Gray	Gray	Gray	Gray
Tryptophan	White	Gray	White	Gray	White	Gray	White	White	Gray	Gray	White	White	Gray
Tyrosine	White	Gray	White	White	Gray	Gray	White	White	Gray	White	White	Gray	Gray
Valine	Gray	Gray	Gray	Gray	White	Gray	Gray	White	Gray	Gray	White	White	Gray

CHAPTER 5

Conclusions and future directions

DPO was discovered over a decade ago in the marine sediment isolate *D. phosphitoxidans* FiPS-3, but there had so far been no additional reports of this metabolism in other environments. This study, therefore, represents only the second ever observation of DPO and the first ever description of a community structure and metagenome related to this metabolism. Furthermore, the organism responsible for phosphite oxidation in our system, Phox-21, is a novel bacterium belonging to a candidate order within the *Deltaproteobacteria* that currently has no cultured representatives. Although my attempts to isolate Phox-21 were unsuccessful, metagenomic analysis revealed the presence of a *ptx-ptd* cluster in its genome, similar to the one found in FiPS-3. Previous work has shown that *ptxD* and *ptdC* are necessary for phosphite oxidation in FiPS-3 (Simeonova et al. 2010). Additionally, as part of this study, I found that *ptdFGHI* are significantly upregulated in FiPS-3 in the presence of phosphite.

That *ptdCFHI* are also found in Phox-21, but not in any other genome currently available in the IMG database, is further evidence that these genes play an important role in DPO. Interestingly, *ptdG* is present in FiPS-3 but not in Phox-21, which suggests that this gene may not be essential for DPO in every organism, although it may still be required by FiPS-3. However, much work is still needed in order to elucidate how energy for growth is conserved during DPO. The involvement of PtdFHI in this process has yet to be experimentally confirmed and the mechanism of action of these enzymes has not been determined. Whether ATP is indeed produced from substrate-level phosphorylation during DPO is another outstanding question that requires additional experiments, both *in vivo* and *in vitro*, in order to conclusively address. The actual mechanism of phosphite transport by PtdC also remains currently undetermined. It is assumed to function as a phosphite/phosphate antiporter based on its homology to known antiporters, but this assertion still needs to be tested.

The presence of an incomplete Wood-Ljungdahl Pathway (WLP) in Phox-21 was unexpected, since we had previously assumed that it was capable of growing autotrophically. Nonetheless, this predicted requirement for organic carbon could at least partially explain why the growth of Phox-21 improved so markedly when rumen fluid was added to the enrichments. Although there have been previous reports of organisms with incomplete WLPs (Zhuang et al. 2014; Muller et al. 2015), to our knowledge, this study provides the first genomic evidence of an organism capable of using CO₂ as a terminal electron acceptor but not as a carbon source. Due to its extremely low redox potential, phosphite is the only known biological electron donor that could drive the reduction of CO₂ to formate while generating enough energy to produce ATP for the incorporation of acetate into biomass. As such, this unprecedented metabolism may be unique to DPO-capable organisms. However, as discussed above, the feasibility of this proposed metabolism hinges on whether or not DPO can generate ATP through substrate-level phosphorylation, which is still an open question. Still, the apparent lack of any electron transport chain components in Phox-21 (other than the nitrite reductase associated quinone loop) suggests that under phosphite-oxidizing, CO₂-reducing conditions, energy conservation in this organism would have to proceed exclusively by means of substrate-level phosphorylation. Ultimately, though, this metabolic model still needs to be experimentally confirmed. I have so far been unable to detect significant formate production or acetate consumption under DPO conditions in my enrichments. However, it may not be possible to detect these processes in enrichment cultures due to the presence of other community members capable of using formate and

producing acetate. Obtaining a pure culture of Phox-21 would therefore greatly facilitate any future investigations of its physiology.

The environmental prevalence and phylogenetic diversity of DPO-capable organisms remains unclear. Like FiPS-3, Phox-21 belongs to the *Deltaproteobacteria*, but the sample size of known DPO-capable organisms is still far too small to allow us to determine whether this metabolism is restricted to a specific phylogenetic group. There is evidence that the *ptx-ptd* genes in FiPS-3 were acquired by lateral gene transfer, but we do not know how common it is for these genes to be horizontally propagated in the environment or what the phylogenetic range of these events might be. Since growth by DPO requires relatively high concentrations of phosphite it is probably less prevalent than APO on a global scale. Nevertheless, it may have a greater impact on P cycling in areas of phosphite enrichment, due to the substantially higher rates of phosphate production during DPO compared to APO.

Marine or estuarine sediments, such as the one from which FiPS-3 was isolated, are likely sites of phosphite accumulation due to the presence of biogenic phosphonates as well as the sulfidogenic nature of most marine sediments, which would help protect phosphite from abiotic oxidation. Furthermore, many coastal sediments are impacted by industrial wastewater and agricultural runoff, which might serve as additional sources of reduced phosphorus. Since abiotic phosphite oxidation is a slow process even under aerobic conditions, microbial oxidation is likely the principal mechanism by which phosphite is converted to phosphate at biologically relevant timescales. Given that phosphorus tends to be the limiting nutrient for marine life due to the low solubility of phosphate in the oceans (Redfield 1958), phosphite oxidizers could play a key role in stimulating eutrophication in coastal waters as well as in promoting the growth of primary producers in the oligotrophic open ocean.

Anaerobic waste digesters, like the one where Phox-21 was found, may also be good places to look for DPO-capable organisms due to the high input of anthropogenic wastes, the lack of strong oxidants, and the diversity of microorganisms typically present in such systems. Phox-21's closest relatives are uncultured clones belonging to the GW-28 candidate order of the *Deltaproteobacteria*, most of which have been found in a variety of anaerobic waste treatment systems throughout the world. Whether the capacity for DPO is idiosyncratic to Phox-21 or a common feature of the GW-28 clade remains to be determined. Nonetheless, the lack of genomic evidence for lateral acquisition of the *ptx-ptd* genes in Phox-21 raises the possibility that this metabolism may indeed be a shared characteristic of this phylogenetic group. One close relative of Phox-21 was identified in anaerobic estuarine sediments, an environment similar to the one where FiPS-3 was found and which would be a likely site of phosphite accumulation as discussed above. Additionally, several uncultured clones related to Phox-21 were found in deep-ocean hydrothermal vent systems, which are environments that may potentially be exposed to phosphite derived from geothermal phosphate reduction occurring in the subsurface.

DPO could serve as a key electron donating process in deep aphotic zones. Phosphite oxidation can be coupled to sulfate, nitrate, and carbon dioxide reduction in FiPS-3 and, given its extremely low redox potential, could theoretically be coupled to the reduction of any other known electron acceptor while yielding more energy per electron than any other known electron donor. This property would make phosphite especially attractive as a donor in aphotic

environments such as the deep ocean and the seafloor basaltic crust, where phosphite might be geochemically produced at biologically relevant timescales. Since no light and very little organic matter reaches the deep ocean, energy and organic carbon availability are thought to be the main factors limiting growth in these regions (Edwards et al. 2005; Lever 2011). At hydrothermal vents and in the upper layers of seafloor basalts, chemoautotrophic growth may be driven by the oxidation of geothermally derived reduced species such as H_2 , CH_4 , H_2S , $Fe(II)$, and $Mn(II)$ coupled to the reduction of O_2 or NO_3^- present in seawater (Edwards et al. 2005; D'Hondt et al. 2004). However, organisms living below this redox transition zone do not have access to strong oxidants and have to depend on less energetically favorable metabolisms such as sulfate reduction, methanogenesis, and acetogenesis (Edwards et al. 2005; Lever 2011).

Deep seafloor microbes are thus thought to exist in a near constant state of starvation, so autotrophic growth poses a huge challenge even for organisms that utilize the Wood-Ljungdahl pathway, which is the most energy efficient of the known carbon fixation pathways (Lever 2011). However, the use of phosphite as an electron donor could help overcome this energetic obstacle, as evidenced by the 10-fold higher cell yields seen during growth of FiPS-3 on phosphite and CO_2 compared to those typically observed for homoacetogenic autotrophs. If phosphite were, in fact, prevalent in seafloor basalts, it would provide a substantial competitive advantage to DPO-capable autotrophs and could serve as a key driver of primary production in the deep biosphere. Porous oceanic basaltic crust covers approximately 60% of the Earth's surface and extends down to 500 m deep, making it the largest aquifer in the world (Edwards et al. 2005; Nielsen & Fisk 2010). By some estimates this seafloor biosphere may contain up to a third of the Earth's total living biomass (D'Hondt et al. 2004; Whitman et al. 1998). Subsurface carbon fixation driven by phosphite oxidation could therefore play an important and currently unrecognized role in the global carbon cycle.

The paucity of DPO-capable organisms discovered so far compared to those capable of APO is somewhat puzzling, but may simply be due to the fact that most efforts to identify phosphite-oxidizing organisms have so far been carried out in aerobic freshwater and soil environments in which phosphite concentrations tend to be relatively low. Given the widespread presence of phosphite in the environment and its suitability as an electron donor, DPO-capable microbes are likely to be more prevalent than current sampling would indicate. The work presented here suggests that microbes capable of this metabolism are more likely to be found in anoxic marine environments or anaerobic wastewater digesters in which phosphite from anthropogenic and/or natural sources might accumulate to high enough levels to support growth by DPO. Additionally, the prospect of finding novel DPO-capable organisms among the microbial 'dark matter' of the subsurface is particularly exciting and I hope that future work in this area will be undertaken. This study brings us one step closer to addressing some of the many unanswered questions regarding dissimilatory phosphite oxidation and hopefully will serve to raise awareness of the existence and potential significance of phosphorus redox cycling among geochemists and biologists alike and spur the further development of this promising area of research.

REFERENCES

- Adams, F. & Conrad, J.P., 1953. Transition of Phosphite to Phosphate in Soils. *Soil Science*, 75(5), pp.361–371.
- Anders, S. & Huber, W., 2010. Differential expression analysis for sequence count data. *Genome biology*, 11:R106.
- Anderson, M.J., 2001. Permutation tests for univariate or multivariate analysis of variance and regression. *Canadian Journal of Fisheries and Aquatic Sciences*, 58(3), pp.626–639.
- Badziong, W. & Thauer, R.K., 1978. Growth yields and growth rates of *Desulfovibrio vulgaris* (Marburg) growing on hydrogen plus sulfate and hydrogen plus thiosulfate as the sole energy sources. *Archives of Microbiology*, 117(2), pp.209–214.
- Balch, W.E. et al., 1979. Methanogens: reevaluation of a unique biological group. *Microbiological Reviews*, 43(2), pp.260–296.
- Barton, L.L. & Fauque, G.D., 2009. Biochemistry, Physiology and Biotechnology of Sulfate-Reducing Bacteria. *Advances in Applied Microbiology*. Elsevier, pp. 41–98.
- Bauer, A.J. et al., 1992. The molecular structure of UDP-galactose 4-epimerase from *Escherichia coli* determined at 2.5 Å resolution. *Proteins*, 12(4), pp.372–381.
- Blankenship, R.E. & Prince, R.C., 1985. Excited-state redox potentials and the Z scheme of photosynthesis. *Trends in Biochemical Sciences*, 10(10), pp.382–383.
- Britvin, S.N. et al., 2015. Earth's Phosphides in Levant and insights into the source of Archean prebiotic phosphorus. *Scientific Reports*, 5(8355), pp.1-5.
- Broderick, J.B. et al., 2014. Radical S-Adenosylmethionine Enzymes. *Chemical Reviews*, 114(8), pp.4229–4317.
- Bryant, D.E. & Kee, T.P., 2006. Direct evidence for the availability of reactive, water soluble phosphorus on the early Earth. H-Phosphinic acid from the Nantan meteorite. *Chemical Communications*, (22), pp.2344–2346.
- Buckel, W., 2013. Bacterial methanogenesis proceeds by a radical mechanism. *Angewandte Chemie International Edition*, 52(33), pp.8507–8509.
- Buckel, W. & Thauer, R.K., 2013. Energy conservation via electron bifurcating ferredoxin reduction and proton/Na(+) translocating ferredoxin oxidation. *Biochimica et biophysica acta*, 1827(2), pp.94–113.
- Carlson, H.K. et al., 2015. Monofluorophosphate Is a Selective Inhibitor of Respiratory Sulfate-Reducing Microorganisms. *Environmental science & technology*, 49(6), pp.3727–3736.

- Carlström, C. et al., 2016. Characterization of an anaerobic marine microbial community exposed to combined fluxes of perchlorate and salinity. *Applied Microbiology and Biotechnology*, 100(22), pp.1–36.
- Casida, L.E., Jr, 1960. Microbial Oxidation and Utilization of Orthophosphite During Growth. 80(2), pp.237–241.
- Cecchini, G. et al., 2002. Succinate dehydrogenase and fumarate reductase from *Escherichia coli*. *Biochimica et biophysica acta*, 1553(1-2), pp.140–157.
- Clarke, F.W. & Washington, H.S., 1924. The Composition of the Earth's Crust. *United States Geological Survey Report*.
- Clarke, K.R., 1993. Non-parametric multivariate analyses of changes in community structure. *Australian Journal of Ecology*, 18, pp.117-143.
- Clarke, K.R., Somerfield, P.J. & Gorley, R.N., 2008. Testing of null hypotheses in exploratory community analyses: similarity profiles and biota-environment linkage. *Journal of Experimental Marine Biology and Ecology*, 366(1-2), pp.56–69.
- Clark, L.L., Ingall, E.D. & Benner, R., 1999. Marine organic phosphorus cycling: novel insights from nuclear magnetic resonance. *American Journal of Science*, 299, pp.724-737.
- Costas, A., White, A. & Metcalf, W., 2001. Purification and characterization of a novel phosphorus-oxidizing enzyme from *Pseudomonas stutzeri* WM88. *Journal of Biological Chemistry*, 276(20), pp.17429–17436.
- Crofts, T.S. et al., 2014. A bioassay for the detection of benzimidazoles reveals their presence in a range of environmental samples. *Frontiers in Microbiology*, 5:592.
- D'Hondt, S. et al., 2004. Distributions of Microbial Activities in Deep Subseafloor Sediments. *Science*, 306(5705), pp.2216–2221.
- Deweerd, K.A. et al., 1990. Desulfomonile-Tiedjei Gen-Nov and Sp-Nov, a Novel Anaerobic, Dehalogenating, Sulfate-Reducing Bacterium. *Archives of Microbiology*, 154(1), pp.23–30.
- Dévai, I. & Delaune, R.D., 1995. Evidence for phosphine production and emission from Louisiana and Florida marsh soils. *Organic Geochemistry*, 23(3), pp.277–279.
- Dévai, I. et al., 1988. Detection of phosphine: new aspects of the phosphorus cycle in the hydrosphere. *Nature*, 333(6171), pp.343–345.
- Dilling, W. & Cypionka, H., 1990. Aerobic respiration in sulfate-reducing bacteria. *FEMS Microbiology Letters*, 71(1-2), pp.123–127.
- Edwards, K.J., Bach, W. & McCollom, T.M., 2005. Geomicrobiology in oceanography: microbe-mineral interactions at and below the seafloor. *Trends in microbiology*, 13(9), pp.449–456.

- Efremov, R.G. & Sazanov, L.A., 2012. The coupling mechanism of respiratory complex I — A structural and evolutionary perspective. *Biochimica et Biophysica Acta (BBA)-Bioenergetics*, 1817(10), pp.1785–1795.
- Eren, A.M. et al., 2015. Anvi'o: an advanced analysis and visualization platform for 'omics data. *PeerJ*, 3:1319.
- Fagerbakke, K.M., Heldal, M. & Norland, S., 1996. Content of carbon, nitrogen, oxygen, sulfur and phosphorus in native aquatic and cultured bacteria. *Aquatic Microbial Ecology*, 10, pp.15-27.
- Figueroa, I.A. & Coates, J.D., 2016. Microbial Phosphite Oxidation and Its Potential Role in the Global Phosphorus and Carbon Cycles. *Advances in Applied Microbiology* (in press).
- Foster, T.L., Winans, L. & Helms, S., 1978. Anaerobic Utilization of Phosphite and Hypophosphite by *Bacillus*-sp. *Applied and Environmental Microbiology*, 35(5), pp.937–944.
- Freeman, S., Irwin, W.J. & Schwalbe, C.H., 1991. Synthesis and hydrolysis studies of phosphonopyruvate. *Journal of the Chemical Society, Perkin Transactions 2*, (2), pp.263–267.
- Frost, J.W. et al., 2002. Radical-based dephosphorylation and organophosphonate biodegradation. *Journal of the American Chemical Society*, 109(7), pp.2166–2171.
- Glindemann, D. et al., 1998. Phosphine by bio-corrosion of phosphide-rich iron. *Environmental Science and Pollution Research*, 5(2), pp.71–74.
- Glindemann, D., De Graaf, R.M. & Schwartz, A.W., 1999. Chemical reduction of phosphate on the primitive earth. *Origins of life and evolution of the biosphere : the journal of the International Society for the Study of the Origin of Life*, 29(6), pp.555–561.
- Gould, G.W. & Russell, N.J., 2003. Sulfite. In *Food Preservatives*. Boston, MA: Springer US, pp. 85–101.
- Gulick, A., 1955. Phosphorus as a factor in the origin of life. *American Scientist*, 43(3), pp.479-489.
- Han, C. et al., 2013. Phosphite in Sedimentary Interstitial Water of Lake Taihu, a Large Eutrophic Shallow Lake in China. *Environmental science & technology*, 47(11), pp.5679–5685.
- Huang, Y.T. et al., 2014. PRISE2: Software for designing sequence-selective PCR primers and probes. *BMC Bioinformatics*, 15:317.
- Huntemann, M. et al., 2015. The standard operating procedure of the DOE-JGI Microbial Genome Annotation Pipeline (MGAP v.4). *Standards in Genomic Sciences*, 10:86.

- Huson, D.H. & Scornavacca, C., 2012. Dendroscope 3: An Interactive Tool for Rooted Phylogenetic Trees and Networks. *Systematic Biology*, 61(6), pp.1061–1067.
- Hyatt, D. et al., 2010. Prodigal: prokaryotic gene recognition and translation initiation site identification. *BMC Bioinformatics*, 11:119.
- Joshi N.A. & Fass J.N. (2011). Sickle: A sliding-window, adaptive, quality-based trimming tool for FastQ files (Version 1.33) [Software]. Available at <https://github.com/najoshi/sickle>.
- Kamat, S.S. et al., 2013. The catalytic mechanism for aerobic formation of methane by bacteria. *Nature*, 497(7447), pp.132–136.
- Karl, D.M. et al., 2008. Aerobic production of methane in the sea. *Nature Geoscience*, 1(7), pp.473–478.
- Kelley, D.S., Baross, J.A. & Delaney, J.R., 2003. Volcanoes, Fluids, and Life at Mid-Ocean Ridge Spreading Centers. *Annual Review of Earth and Planetary Sciences*, 30(1), pp.385–491.
- Klindworth, A. et al., 2012. Evaluation of general 16S ribosomal RNA gene PCR primers for classical and next-generation sequencing-based diversity studies. *Nucleic Acids Research*, 41(1), pp.1–11.
- Kolowith, L.C., Ingall, E.D. & Benner, R., 2001. Composition and Cycling of Marine Organic Phosphorus. *Limnology and Oceanography*, 46(2), pp.309–320.
- Kvint, K. et al., 2003. The bacterial universal stress protein: function and regulation. *Current opinion in microbiology*, 6(2), pp.140–145.
- Lemieux, M.J., Huang, Y. & Wang, D.N., 2005. Crystal structure and mechanism of GlpT, the glycerol-3-phosphate transporter from *E. coli*. *Journal of electron microscopy*, 54 (Suppl. 1), pp.i43–i46.
- Lever, M.A., 2011. Acetogenesis in the energy-starved deep biosphere - a paradox? *Frontiers in microbiology*, 2, p.284.
- Li, D. et al., 2016. MEGAHIT v1.0: A fast and scalable metagenome assembler driven by advanced methodologies and community practices. *Methods*, 102, pp.3–11.
- Li, D. et al., 2015. MEGAHIT: an ultra-fast single-node solution for large and complex metagenomics assembly via succinct de Bruijn graph. *Bioinformatics (Oxford, England)*, 31(10), pp.1674–1676.
- Li, H. & Durbin, R., 2009. Fast and accurate short read alignment with Burrows-Wheeler transform. *Bioinformatics (Oxford, England)*, 25(14), pp.1754–1760.
- Liu, J. et al., 2011. Prokaryotic diversity, composition structure, and phylogenetic analysis of

- microbial communities in leachate sediment ecosystems. *Applied Microbiology and Biotechnology*, 91(6), pp.1659–1675.
- Lü, W. et al., 2012. The formate channel FocA exports the products of mixed-acid fermentation. *Proceedings of the National Academy of Sciences of the United States of America*, 109(33), pp.13254–13259.
- Maia, L.B., Moura, J.J.G. & Moura, I., 2015. Molybdenum and tungsten-dependent formate dehydrogenases. *Journal of Biological Inorganic Chemistry*, 20(2), pp.287–309.
- Malacinski, G. & Konetzka, W.A., 1966. Bacterial Oxidation of Orthophosphite. *Journal of Bacteriology*, 91(2), pp.578–582.
- Markowitz, V.M. et al., 2012. IMG: the Integrated Microbial Genomes database and comparative analysis system. *Nucleic Acids Research*, 40(Database issue), pp.D115–22.
- Martinez, A. et al., 2011. Phosphite utilization by the marine picocyanobacterium *Prochlorococcus* MIT9301. *Environmental Microbiology*, 14(6), pp.1363–1377.
- McDonald, D. et al., 2012. An improved Greengenes taxonomy with explicit ranks for ecological and evolutionary analyses of bacteria and archaea. *The ISME journal*, 6(3), pp.610–618.
- Metcalf, W.W. & Wanner, B.L., 1991. Involvement of the *Escherichia coli* phn (psiD) gene cluster in assimilation of phosphorus in the form of phosphonates, phosphite, Pi esters, and Pi. *Journal of Bacteriology*, 173(2), pp.587–600.
- Metcalf, W.W. & Wolfe, R.S., 1998. Molecular genetic analysis of phosphite and hypophosphite oxidation by *Pseudomonas stutzeri* WM88. *Journal of Bacteriology*, 180(21), pp.5547–5558.
- Morton, S.C. et al., 2005. Analysis of Reduced Phosphorus in Samples of Environmental Interest. *Environmental Science & Technology*, 39(12), pp.4369-4376.
- Mulkidjanian, A.Y. et al., 2008. Evolutionary primacy of sodium bioenergetics. *Biology Direct*, 3:13.
- Muller, B. et al., 2015. Genome-Guided Analysis of Physiological Capacities of *Tepidanaerobacter acetatoydans* Provides Insights into Environmental Adaptations and Syntrophic Acetate Oxidation. *Plos One*, 10(3):e0121237.
- Nagaosa, Y. & Aoyama, E., 2001. Catalytic oxidation of phosphite and hypophosphite to phosphate on Pd/activated carbon powder. *Carbon*, 39, pp.2077-2088.
- Nielsen, M.E. & Fisk, M.R., 2010. Surface area measurements of marine basalts: Implications for the seafloor microbial biomass. *Geophysical Research Letters*, 37(15), pp.1-5.
- Nowack, B., 2003. Environmental chemistry of phosphonates. *Water Research*, 37(11), pp.2533–2546.

- Parks, D.H. et al., 2015. CheckM: assessing the quality of microbial genomes recovered from isolates, single cells, and metagenomes. *Genome research*, 25(7), pp.1043–1055.
- Pasek, M. & Block, K., 2009. Lightning-induced reduction of phosphorus oxidation state. *Nature Geoscience*, 2(8), pp.553–556.
- Pasek, M. & Lauretta, D., 2008. Extraterrestrial flux of potentially prebiotic C, N, and P to the early Earth. *The journal of the International Society for the Study of the Origin of Life*, 38(1), pp.5–21.
- Pasek, M.A., 2008. Rethinking early Earth phosphorus geochemistry. *Proceedings of the National Academy of Sciences of the United States of America*, 105(3), pp.853–858.
- Pasek, M.A. & Kee, T.P., 2011. On the Origin of Phosphorylated Biomolecules. In R. Egel, D. H. Lankenau, & A. Y. Mulkidjanian, eds. *Origins of Life: The Primal Self-Organization*. Berlin, Heidelberg: Springer Berlin Heidelberg, pp.57–84.
- Pasek, M.A. & Lauretta, D.S., 2005. Aqueous corrosion of phosphide minerals from iron meteorites: a highly reactive source of prebiotic phosphorus on the surface of the early Earth. *Astrobiology*, 5(4), pp.515–535.
- Pasek, M.A. et al., 2013. Evidence for reactive reduced phosphorus species in the early Archean ocean. *Proceedings of the National Academy of Sciences of the United States of America*, 110(25), pp.10089–10094.
- Pasek, M.A., Dworkin, J.P. & Lauretta, D.S., 2007. A radical pathway for organic phosphorylation during schreibersite corrosion with implications for the origin of life. *Geochimica Et Cosmochimica Acta*, 71(7), pp.1721–1736.
- Pasek, M.A., Sampson, J.M. & Atlas, Z., 2014. Redox chemistry in the phosphorus biogeochemical cycle. *Proceedings of the National Academy of Sciences of the United States of America*, 111(43), pp.15468–15473.
- Patzlaff, J.S., van der Heide, T. & Poolman, B., 2003. The ATP/substrate stoichiometry of the ATP-binding cassette (ABC) transporter OpuA. *Journal of Biological Chemistry*, 278(32), pp.29546–29551.
- Pauly, H., 1969. White cast iron with cohenite, schreibersite, and sulphides from Tertiary basalts on Disko, Greenland. *Medd Dansk Geol Foren*, 19, pp.8-30.
- Pech, H. et al., 2009. Detection of Geothermal Phosphite Using High-Performance Liquid Chromatography. *Environmental science & technology*, 43(20), pp.7671–7675.
- Peck, H.D., 1959. The ATP-Dependent Reduction of Sulfate with Hydrogen in Extracts of *Desulfovibrio Desulfuricans*. *Proceedings of the National Academy of Sciences of the United States of America*, 45(5), pp.701–708.
- Pedersen, A.K., 1981. Armalcolite-bearing Fe-Ti oxide assemblages in graphite-equilibrated

- salic volcanic rocks with native iron from Disko, central West Greenland. *Contributions to Mineralogy and Petrology*, 77(4), pp.307–324.
- Peng, Y. et al., 2012. IDBA-UD: a de novo assembler for single-cell and metagenomic sequencing data with highly uneven depth. *Bioinformatics (Oxford, England)*, 28(11), pp.1420–1428.
- Peters, J.W. et al., 2015. [FeFe]- and [NiFe]-hydrogenase diversity, mechanism, and maturation. *Biochimica et Biophysica Acta (BBA) - Molecular Cell Research*, 1853(6), pp.1350–1369.
- Poehlein, A., Daniel, R., Schink, B., et al., 2013. Life based on phosphite: a genome-guided analysis of *Desulfotignum phosphitoxidans*. *BMC genomics*, 14(753), pp.1-14.
- Prins, R. & Bussell, M.E., 2012. Metal Phosphides: Preparation, Characterization and Catalytic Reactivity. *Catalysis letters*, 142(12), pp.1413–1436.
- Pruesse, E. et al., 2007. SILVA: a comprehensive online resource for quality checked and aligned ribosomal RNA sequence data compatible with ARB. *Nucleic Acids Research*, 35(21), pp.7188–7196.
- Ragsdale, S.W. & Pierce, E., 2008. Acetogenesis and the Wood-Ljungdahl pathway of CO₂ fixation. *Biochimica et biophysica acta*, 1784(12), pp.1873–1898.
- Redfield, A.C., 1958. The biological control of chemical factors in the environment. *American scientist*, 46(3), pp.205-221.
- Relyea, H.A. & van der Donk, W.A., 2005. Mechanism and applications of phosphite dehydrogenase. *Bioorganic Chemistry*, 33(3), pp.171–189.
- Rich, P.R., 2003. The molecular machinery of Keilin's respiratory chain. *Biochemical Society transactions*, 31(6), pp.1095–1105.
- Rivière, D. et al., 2009. Towards the definition of a core of microorganisms involved in anaerobic digestion of sludge. *The ISME journal*, 3(6), pp.700–714.
- Robert, X. & Gouet, P., 2014. Deciphering key features in protein structures with the new ENDscript server. *Nucleic Acids Research*, 42(Web Server issue), pp.W320–4.
- Roels, J. & Verstraete, W., 2001. Biological formation of volatile phosphorus compounds. *Bioresource Technology*, 79(3), pp.243–250.
- Roels, J. & Verstraete, W., 2004. Occurrence and origin of phosphine in landfill gas. *Science of the Total Environment*, 327(1-3), pp.185–196.
- Saleem, F. et al., 2013. The Bovine Ruminant Fluid Metabolome. *Metabolomics*, 9(2), pp.360–378.
- Schink, B. & Friedrich, M., 2000. Bacterial metabolism - phosphite oxidation by sulphate

- reduction. *Nature*, 406(6791), p.37.
- Schink, B. et al., 2002. Desulfotignum phosphitoxidans sp. nov., a new marine sulfate reducer that oxidizes phosphite to phosphate. *Archives of Microbiology*, 177(5), pp.381–391.
- Schloss, P.D. et al., 2009. Introducing mothur: open-source, platform-independent, community-supported software for describing and comparing microbial communities. *Applied and Environmental Microbiology*, 75(23), pp.7537–7541.
- Seifan, M., Samani, A.K. & Berenjian, A., 2016. Bioconcrete: next generation of self-healing concrete. *Applied Microbiology and Biotechnology*, 100(6), pp.2591–2602.
- Shelton, D.R. & Tiedje, J.M., 1984. Isolation and Partial Characterization of Bacteria in an Anaerobic Consortium That Mineralizes 3-Chlorobenzoic Acid. *Applied and Environmental Microbiology*, 48(4), pp.840–848.
- Sievers, F. & Higgins, D.G., 2014. Clustal omega. *Current protocols in bioinformatics*, 48, pp.3.13.1–16.
- Sigalevich, P. & Cohen, Y., 2000. Oxygen-Dependent Growth of the Sulfate-Reducing Bacterium Desulfovibrio oxyclineae in Coculture with Marinobacter sp. Strain MB in an Aerated Sulfate-Depleted Chemostat. *Applied and Environmental Microbiology*, 66(11), pp.5019-5023.
- Simeonova, D.D. et al., 2009. “Unknown genome” proteomics: a new NADP-dependent epimerase/dehydratase revealed by N-terminal sequencing, inverted PCR, and high resolution mass spectrometry. *Molecular & Cellular Proteomics*, 8(1), pp.122–131.
- Simeonova, D.D. et al., 2010. Identification and Heterologous Expression of Genes Involved in Anaerobic Dissimilatory Phosphite Oxidation by Desulfotignum phosphitoxidans. *Journal of Bacteriology*, 192(19), pp.5237–5244.
- Sousa, F.L. & Martin, W.F., 2014. Biochemical fossils of the ancient transition from geoenergetics to bioenergetics in prokaryotic one carbon compound metabolism. *Biochimica et biophysica acta*, 1837(7), pp.964–981.
- Stamatakis, A., 2006. RAxML-VI-HPC: maximum likelihood-based phylogenetic analyses with thousands of taxa and mixed models. *Bioinformatics (Oxford, England)*, 22(21), pp.2688–2690.
- Stone, B.L. & White, A.K., 2012. Most probable number quantification of hypophosphite and phosphite oxidizing bacteria in natural aquatic and terrestrial environments. *Archives of Microbiology*, 194(3), pp.223–228.
- Taylor, B.F. & Oremland, R.S., 1979. Depletion of adenosine triphosphate in Desulfovibrio by oxyanions of group VI elements. *Current Microbiology*, 3(2), pp.101–103.
- Ternan, N.G. et al., 1998. Review: Organophosphonates: occurrence, synthesis and

- biodegradation by microorganisms. *World Journal of Microbiology and Biotechnology*, 14(5), pp.635–647.
- Thauer, R.K., Jungermann, K. & Decker, K., 1977. Energy conservation in chemotrophic anaerobic bacteria. *Bacteriological reviews*, 41(3), pp.809–180.
- Thi Bich Thao, H., Yamakawa, T. & Shibata, K., 2009. Effect of phosphite–phosphate interaction on growth and quality of hydroponic lettuce (*Lactuca sativa*). *Journal of Plant Nutrition and Soil Science*, 172(3), pp.378–384.
- Tschech, A. & Pfennig, N., 1984. Growth yield increase linked to caffeate reduction in *Acetobacterium woodii*. *Archives of Microbiology*, 137(2), pp.163–167.
- Vignais, P.M., Billoud, B. & Meyer, J., 2001. Classification and phylogeny of hydrogenases. *Fems Microbiology Reviews*, 25(4), pp.455–501.
- Weisburg, W.G. et al., 1991. 16s Ribosomal DNA Amplification for Phylogenetic Study. *Journal of Bacteriology*, 173(2), pp.697–703.
- Wheat, C.G., Feely, R.A. & Mottl, M.J., 1996. Phosphate removal by oceanic hydrothermal processes: an update of the phosphorus budget in the oceans. *Geochimica et Cosmochimica Acta*, 60(19), pp.3593–3608.
- White, A.K. & Metcalf, W.W., 2007. Microbial Metabolism of Reduced Phosphorus Compounds. *Annual Review of Microbiology*, 61(1), pp.379–400.
- White, A.K. & Metcalf, W.W., 2004a. The htx and ptx operons of *Pseudomonas stutzeri* WM88 are new members of the pho regulon. *Journal of Bacteriology*, 186(17), pp.5876–5882.
- White, A.K. & Metcalf, W.W., 2004b. Two C–P Lyase Operons in *Pseudomonas stutzeri* and Their Roles in the Oxidation of Phosphonates, Phosphite, and Hypophosphite. *Journal of Bacteriology*, 186(14), pp.4730–4739.
- Whitman, W.B., Coleman, D.C. & Wiebe, W.J., 1998. Prokaryotes: the unseen majority. *Proceedings of the National Academy of Sciences of the United States of America*, 95(12), pp.6578–6583.
- Wilson, M.M. & Metcalf, W.W., 2005. Genetic diversity and horizontal transfer of genes involved in oxidation of reduced phosphorus compounds by *Alcaligenes faecalis* WM2072. *Applied and Environmental Microbiology*, 71(1), pp.290–296.
- Yang, H.C. & Drake, H.L., 1990. Differential effects of sodium on hydrogen- and glucose-dependent growth of the acetogenic bacterium *Acetogenium kivui*. *Applied and Environmental Microbiology*, 56(1), pp.81–86.
- Yang, K., Metcalf, W.W. & Frey, P.A., 2004. A New Activity for an Old Enzyme: *Escherichia coli* Bacterial Alkaline Phosphatase Is a Phosphite-Dependent Hydrogenase. *Proceedings of the National Academy of Sciences of the United States of America*, 101(21), pp.7919–7924.

Yu, X. et al., 2015. Determination of phosphite in a full-scale municipal wastewater treatment plant. *Environmental Science-Processes & Impacts*, 17(2), pp.441–447.

Zhu, R. et al., 2006. Tropospheric phosphine and its sources in coastal Antarctica. *Environmental Science & Technology*, 40(24), pp.7656–7661.

Zhuang, W.Q. et al., 2014. Incomplete Wood-Ljungdahl pathway facilitates one-carbon metabolism in organohalide-respiring *Dehalococcoides mccartyi*. *Proceedings of the National Academy of Sciences of the United States of America*, 111(17), pp.6419–6424.

Appendix 2.1. Top genes upregulated under phosphite-fed vs. fumarate-fed conditions. Table includes all genes with p-value < 0.05 and log₂ fold change > 2. Genes are ranked based on log₂ fold change values. *Ptd* genes are highlighted in blue. RNA counts for each gene were determined by RNAseq and values shown are the average normalized counts of triplicate biological samples for each treatment. Statistical significance of differential expression between the two conditions for each gene was assessed using the DESeq software package. All cultures were grown in minimal media at 30°C with 1 mM phenylalanine and histidine, 10 mM sulfate, and 1 mM phosphate. All cultures were sampled for RNA extraction at mid-logarithmic growth phase (OD₆₀₀ = 0.3-0.4).

Rank	Gene	Log ₂ Fold Change	p-value
1	putative epimerase/dehydratase PtdF	6.90	3.63E-174
2	hypothetical protein	5.09	2.44E-27
3	putative transposase	3.58	4.25E-02
4	putative phosphite transporter PtdC	3.58	8.16E-231
5	glutathione transport system permease protein GsiD	3.42	1.05E-21
6	putative 4Fe-4S single cluster domain-containing protein	3.29	6.51E-44
7	hypothetical protein	3.23	1.97E-55
8	putative ABC transporter permease protein	3.19	2.45E-17
9	hypothetical protein	3.16	4.73E-04
10	TonB-dependent receptor	3.13	1.01E-21
11	B12-dependent radical SAM family protein PtdH	3.13	3.54E-76
12	inner membrane protein YhjX	3.13	1.66E-24
13	glutathione transport system permease protein GsiC	3.08	7.90E-16
14	NADPH-dependent 7-cyano-7-deazaguanine reductase QueF	3.07	7.67E-24
15	hypothetical protein, SHOCT family	3.05	1.49E-14
16	hypothetical protein	3.04	7.41E-33
17	cobalt transport system permease protein CbiN	3.01	1.24E-21
18	glutathione-binding protein GsiB	2.99	9.06E-18
19	hypothetical protein PtdI	2.97	3.95E-52
20	TonB-dependent receptor	2.96	1.71E-34
21	phosphomethylpyrimidine synthase ThiC	2.95	1.12E-24
22	antitoxin of toxin-antitoxin system VapB	2.92	3.94E-04
23	butyrate-CoA ligase YtcI	2.88	3.81E-16
24	UspA family protein PtdG	2.88	3.17E-90
25	phage Gp37Gp68 family protein	2.84	8.75E-03
26	hypothetical protein	2.81	9.46E-32
27	2-hydroxyglutaryl-CoA dehydratase D component HgdD	2.79	8.95E-15
28	hypothetical protein, DUF1858	2.77	1.42E-02
29	hypothetical protein	2.76	4.02E-13
30	formylmethanofuran dehydrogenase subunit FmdE	2.75	1.64E-30
31	putative glutathione ABC transporter ATP-binding protein	2.75	5.64E-12
32	putative ABC transporter, solute-binding protein	2.73	1.67E-21
33	7-cyano-7-deazaguanine synthase QueC	2.72	1.16E-14
34	queuosine biosynthesis protein QueE	2.69	5.28E-19
35	ABC transporter ATP-binding protein	2.59	5.16E-10
36	ABC-type glutathione transporter ATP-binding protein	2.58	1.85E-17
37	Na ⁺ /acetate symporter ActP	2.54	3.76E-15

38	hypothetical protein	2.52	5.59E-15
39	hypothetical protein, DUF4198	2.50	7.56E-15
40	hypothetical protein	2.47	1.39E-07
41	tetratricopeptide	2.44	7.16E-18
42	TonB-dependent receptor TonB	2.38	1.13E-36
43	hypothetical protein	2.36	6.71E-28
44	phosphonates transport ATP-binding protein PhnL	2.36	2.07E-02
45	putative nickel transport complex, NikM subunit, transmembrane	2.34	5.15E-14
46	nitrogen regulatory protein P-II	2.34	1.35E-04
47	bacteriophage protein gp37	2.29	1.54E-02
48	putative SAM-dependent methyltransferase	2.27	1.79E-09
49	hypothetical protein	2.26	1.89E-03
50	hypothetical protein	2.23	6.67E-03
51	PIN domain-containing protein	2.22	3.50E-02
52	4Fe-4S domain-containing protein	2.22	2.13E-23
53	GrpE protein HSP-70 cofactor	2.21	3.24E-12
54	molybdate-binding periplasmic protein ModA	2.20	7.28E-45
55	hypothetical protein	2.18	3.00E-13
56	cold-shock DNA-binding protein family	2.17	1.17E-30
57	hypothetical protein, DUF3450	2.14	8.82E-13
58	hypothetical protein	2.13	3.24E-05
59	Cu ²⁺ -exporting P-type ATPase CopB	2.12	5.26E-41
60	hypothetical protein	2.08	4.54E-11
61	hypothetical protein	2.07	7.76E-03
62	hypothetical protein	2.06	7.43E-13
63	cobalt/nickel transport system ATP-binding protein CbiO	2.05	1.15E-09
64	cobalt/nickel transport system permease protein CbiM	2.03	4.55E-12
65	6-pyruvoyltetrahydropterin synthase QueD	2.02	3.76E-12

Appendix 3.1. DNA sequence alignments of partial 16S rRNA genes belonging to OTU 21 (A) and Bin 2 (B) to the full 16S rRNA gene from clone Phox-21 (subject). The sequences were aligned using the BLASTN 2.3.1 algorithm (<http://blast.ncbi.nlm.nih.gov/Blast.cgi>).

A

Score	Expect	Identities	Gaps	Strand
331 bits(179)	4e-95	196/203(97%)	5/203(2%)	Plus/Plus
Query 1	GGGCGTAAAGAGCACGTAGGCCGATTGGTAAGTCAGGTGTGAAATCCCAGGGCTCAACTC	60		
Sbjct 595	GGGCGTAAAGAGCACGTAGGCCGATTGGTAAGTCAG--GTGAAATCCCAGGGCTCAACTC	652		
Query 61	CGGAACTGCATTTGATACTGCCAGTCTTGAGTGAGGTAGAGGGGAGTGGAAATCCCAGGTG	120		
Sbjct 653	CGGAACTGCATTTGATACTGCCAGTCTTGAGTGAGGTAAAGGGGAGTGGAAATCCCAGGTG	712		
Query 121	TAGAGGTGAAATTCGTAGATATCGGGAGGAACACCAGAGGCGAAGGCGACTCCCTGGGCC	180		
Sbjct 713	--GAGGTGAAATTCGTAGATATCGGGAGGAACACCAGAGG-GAAGGCGACTCCCTGGGCC	769		
Query 181	TCTACTGACGCTGAGGTGCGAAA	203		
Sbjct 770	TCTACTGACGCTGAGGTGCGAAA	792		

B

Score	Expect	Identities	Gaps	Strand
1797 bits(973)	0.0	1001/1013(99%)	8/1013(0%)	Plus/Plus
Query 10	AGAGTTTGATCCCAGGCTCAGAATGAACGCTGGCGGCGTGCCTAACACATGCAAGTCGAGC	69		
Sbjct 24	AGAGTTTGATCCTGGCTCAGAATGAACGCTGGCGGCGTGCCTAACACATGCAAGTCGAGC	83		
Query 70	GAGAAAGTCCCCTTCGGGGGGCGAGTAAAGCGGCGCACGGGTGAGTAACGCGTGGGTAAC	129		
Sbjct 84	GAGAAAGTCCCCTTCGGGGGGCGAGTAAAGCGGCGCACGGGTGAGTAACGCGTGGGTAAC	143		
Query 130	CTGCCCTAGAGTGGGGGATAAACCAGCCGAAAGGCTGACTAATCCCGCATAACGACCGGCAG	189		
Sbjct 144	CTGCCCTAGAGTGGGGGATAAACCAGCCGAAAGGCTGACTAATCCCGCATAACGACCGGCAG	203		
Query 190	ACACAAGTCTGCTGGGGAAAGATGGCCTCTGCTTGCAAGCTATCGCTCTTGATGGGCCT	249		
Sbjct 204	ACACAAGTCTGCTGGGGAAAGATGGCCTCTGCTTGCAAGCTATCGCTCTTGATGGGCCT	263		
Query 250	GCGTTGGATTAGCTAGTTGGTGAAGTAATGGCTCACCAAGGCTGCGATCCATAGCTGGTT	309		
Sbjct 264	GCGTTGGATTAGCTAGTTGGTGAAGTAATGGCTCACCAAGGCTGCGATCCATAGCTGGTT	323		
Query 310	TGAGAGGACGACCAGCCACACTGGAAGTGAAGACACGGTCCAGACTCCTACGGGAGGCAGC	369		
Sbjct 324	TGAGAGGACGACCAGCCACACTGGAAGTGAAGACACGGTCCAGACTCCTACGGGAGGCAGC	383		
Query 370	AGTGAGGAATATTGCGCAATGGGGGAAACCCTGACGCAGCGACCCGTGTGAGCGATGAA	429		
Sbjct 384	AGTGAGGAATATTGCGCAATGGGGGAAACCCTGACGCAGCGACCC--TGTGAGCGATGAA	442		

Query	430	GGCCTTCGGGTTCGTAAAGCTCTGTCAGAGGGAAAGAAAGGGCCGGAGGAATAATACCTT	489
Sbjct	443	GGCCTTCGGGTTCGTAAAGCTCTGTCAGAGGGAAAGAAAGGGCCGGAGGAATAATACCTT	502
Query	490	CGGCATTGACGGTACCCTCAGAGGAAGCACCGGCTAACTCCGTGCCAGCAGCCGCGGTAA	549
Sbjct	503	CGGCATTGACGGTACCCTCAGAGGAAGCACCGGCTAACTCCGTGCCAGCAGCCGCGGTAA	562
Query	550	TACGGAGGGTGCAAGTGTTATTTCGGAATCACTGGGCGTAAAGAGCACGTAGGCGGATTGG	609
Sbjct	563	TACGGAGGGTGCAAGTGTTATTTCGGAATCACTGGGCGTAAAGAGCACGTAGGCGGATTGG	622
Query	610	TAAGTCAGGTGTGAAATCCCGGGGCTCAACTCCGGAACTGCATTGATACTGCCAGTCTT	669
Sbjct	623	TAAGTCAG--GTGAAATCCCGGGGCTCAACTCCGGAACTGCATTGATACTGCCAGTCTT	680
Query	670	GAGTGAGGTAGAGGGGAGTGGAAATCCCGGTGTAGAGGTGAAATTCGTAGATATCGGGAG	729
Sbjct	681	GAGTGAGGTAAAGGGGAGTGGAACTCCCGGTG--GAGGTGAAATTCGTAGATATCGGGAG	738
Query	730	GAACACCAGAGGCGAAGGCGACTCCCTGGGCCTCTACTGACGCTGAGGTGCGAAAGCGTG	789
Sbjct	739	GAACACCAGAGG-GAAGGCGACTCCCTGGGCCTCTACTGACGCTGAGGTGCGAAAGCGTG	797
Query	790	GGGAGCAAACAGGATTAGATACCCTGGTAGTCCACGCCGTAAACGATGAGTACTAGGTGC	849
Sbjct	798	GGGAGCAAACAGGATTAGATACCCTGGTAGTCCACGCCGT-AACGATGAGTACTAGGTGC	856
Query	850	GGGGGTATAAACTCCTTCCGTGTCGCAGCTAACGCATTAAGTACTCCGCCTGGGAAGTA	909
Sbjct	857	GGGGGTATAAACTCCTTCCGTGTCGCAGCTAACGCATTAAGTACTCCGCCTGGGAAGTA	916
Query	910	CGGTCGCAAGGCTGAAACTCAAAGGAATTGACGGGGGCCCGCACAGCGGTGGAGCATGT	969
Sbjct	917	CGGTCGCAAGGCTGAAACTCAAAGGAATTGACGGGGGCCCGCACAGCGGTGGA-CATGT	975
Query	970	GGTTTAATTCGATGCTACGCGAAGAACCTTACCTGGACTTGACATCCTGAGAA	1022
Sbjct	976	GGTTTAATTTGATGCTACGCGAAGAACCTTACCTGGACTTGACATCCTGAGAA	1028

Appendix 3.2. List of organisms used to construct maximum likelihood 16S rRNA phylogenetic tree showing placement of Phox-21 (Figure 3.8). GenBank accession numbers and percent identities of each sequence to the Phox-21 16s rRNA gene are indicated. Sample sources for uncultured clones are indicated and are based on sequence metadata available on GenBank.

Organism	Accession	Identity (%)	Sample Source
Clone POMEbac42	KT167036.1	98	anaerobic food waste digester, Singapore
Clone De3155	HQ183995.1	97	landfill leachate sediment, China
Clone GW-28	EU407211.1	97	household biogas digester, China
Clone QEEB2BG06	CU918113.1	97	mesophilic anaerobic wastewater digester, Germany
Clone QEDN4AF12	CU924922.1	95	mesophilic anaerobic wastewater digester, France
Clone Er-LAYS-74	GU180168.1	94	anaerobic estuarine sediments, Taiwan
Clone DAB-3	KF550878.1	94	anaerobic food waste digester, China
Clone QEDN8BB03	CU927071.1	94	mesophilic anaerobic wastewater digester, France
Clone BSN045	AB364749.1	93	boreal oligotrophic peat wetlands, Japan
Clone CAR8MG52	FJ902368.1	93	biomat at 8m deep in Caracol sinkhole, Mexico
Clone FP H5	FJ769494.1	92	anaerobic wastewater digester, USA
Clone E32	JQ771480.1	91	octadecene degrading brackish sediment, France
Clone Z273MBM77	FJ485400.1	91	biomat at 273 m deep in El Zacaton sinkhole, Mexico
Clone MS12-1-F09	AM712336.1	90	Brothers Seamount hydrothermal vent, New Zealand
Clone GUAY_37enr_Bac71	FR682641.1	90	hydrothermal sediments at Guaymas Basin, Pacific Ocean
Clone BAC2_26	KJ569669.1	90	hydrothermal mat at Guaymas Basin, Pacific Ocean
Clone OTU-X3-1	JQ668576.1	86	oil reservoir, China
Clone OTU-X2-8	JQ668553.1	85	oil reservoir, China
<i>Syntrophus aciditrophicus</i> SB	NR_102776.1	85	N/A
<i>Desulfovibrio hydrothermalis</i> AM13	NR_102482.1	85	N/A
<i>Syntrophus gentianae</i> HQgoe1	NR_029295.1	85	N/A
<i>Desulfatibacillum alkenivorans</i> AK-01	NR_074962.1	85	N/A
<i>Desulfuromonas acetoxidans</i> DSM 684	NR_121678.1	85	N/A
<i>Desulfoluna spongiiphila</i> AA1	NR_115979.1	85	N/A
<i>Geobacter metallireducens</i> GS-15	NR_075011.1	85	N/A
<i>Desulfomonile tiedjei</i> DSM 6799	NR_074118.1	84	N/A
<i>Desulfatiferula olefinivorans</i> LM2801	NR_043971.1	84	N/A
<i>Desulfomicrobium baculatum</i> DSM 4028	NR_074900.1	84	N/A
<i>Desulfomonile limimaris</i> DCB-F	AF282177.1	84	N/A
<i>Anaeromyxobacter dehalogenans</i> 2CP-C	NR_074896.1	84	N/A
<i>Geobacter sulfurreducens</i> PCA	NR_075009.1	84	N/A
<i>Myxobacterium</i> KC	AF482687.1	84	N/A
<i>Desulfococcus oleovorans</i> Hxd3	NR_075012.1	84	N/A
<i>Pelobacter carbinolicus</i> DSM 2380	NR_075013.1	84	N/A

<i>Desulfonauticus autotrophicus DSM 4206</i>	NR_044591.1	84	N/A
<i>Desulfotignum phosphitoxidans FiPS-3</i>	AF420288.1	83	N/A
<i>Acidobacterium capsulatum ATCC 51196</i>	NR_074106.1	79	N/A
<i>Geothrix fermentans H5</i>	NR_036779.1	79	N/A
<i>Solibacter usitatus Ellin6076</i>	NR_074351.1	77	N/A

Appendix 4.1. Marker gene plot showing the degree of completeness, contamination, and strain heterogeneity of binned genomes. Each bar represents a lineage-specific, conserved marker gene expected to be present in single copy in the corresponding genome. CheckM calculates completeness based on the number of expected marker genes that are present in single copy in a given bin (green), contamination based on the number of marker genes that are present in multiple copies that have less than 90% amino acid identity to each other (yellow through red), and strain heterogeneity based on the number of marker genes that are present in multiple copies that have more than 90% amino acid identity to each other (light blue through dark blue). Plot was generated using CheckM v1.0.1.

